Logging Data Errors and their Propagation in Fluid Substitution

---

A Thesis

Presented to

the Faculty of the Department of Earth and Atmospheric Sciences

University of Houston

In Partial Fulfillment

of the Requirements for the Degree

Master of Science

By

Padmakar Deo

May 2012

Logging Data Errors and their Propagation in Fluid Substitution

_____

Padmakar Deo

APPROVED:

_____

Dr. John Castagna, Committee Chair, Advisor

_____

Dr. Christopher Liner, Committee Member

_____

Dr. Tad Smith, Outside Committee Member

_____

Dr. Mark A. Smith

Dean, College of Natural Sciences and Mathematics

Logging Data Errors and their Propagation in Fluid Substitution

---

An Abstract of Thesis

Presented to

the Faculty of the Department of Earth and Atmospheric Sciences

University of Houston

In Partial Fulfillment

of the Requirements for the Degree

Master of Science

By

Padmakar Deo

May 2012

Abstract

The sensitivity of the Gassmann fluid substitution technique to uncertainty in the input wireline measurements data has not been adequately studied (as per commonly available literature). This study describes the methodology to quantify errors present in the fluid substituted velocity by initially calculating the errors for petrophysical and the linearly elastic input parameters and then propagating the calculated input data errors throughout the fluid substitution process.

The synthetic pore fluid modeling technique commonly utilizes data from the wireline log measurements to model various pore fluid mixture scenarios that may give rise to the observed amplitude variation with offset (AVO) response. Each input parameter, whether directly measured or derived using a combination of measured parameters, is bound within an uncertainty range due to the inherent limitations of the measuring instrument or resulting from uncertainty in the empirical parameter estimation. By applying the theory of error propagation, the uncertainty is calculated at each step of the Gassmann fluid substitution process flow and the resultant uncertainty in the fluid substituted velocity is determined.

The uncertainty in the fluid substituted velocity can affect both the phase and the amplitude of synthetic traces generated for different offset angles and therefore, can produce anomalous AVO response in synthetic fluid substitution models. This uncertainty in the synthetic models can impact any direct comparisons with observations in order to determine the effect of different fluid scenarios. Additionally, the observed AVO data may be imprecise due to the anomalous AVO response resulting either from geologic uncertainty, data processing artifacts, or a combination of both thus increasing uncertainty in lithologic AVO interpretation.

Table of Contents

Chapter 1

1.1 Motivation of this study 1

1.2 Introduction 2

1.3 Literature review 3

1.4 Fluid substitution in shaley sediment and rock 5

1.5 Linearly elastic parameter estimation in mixed lithology 6

1.6 Petrophysical parameter estimation in shaley sediment 7

1.6.1 Wet shale anisotropic model 7

1.6.2 Wet shale isotropic model 8

1.7 Expected results from this study 9

1.8 Applications of the results of this study. 9

1.8.1 Limitations of this study for AVO synthetic modeling application 10

Chapter 2

2.1 Introduction 12

2.2 Types of data distributions 12

2.2.1 Binomial distribution 13

2.2.2 Poisson distribution 13

2.2.3 Gaussian distribution 14

2.2.4 Uniform distribution 14

2.3 Errors in logging measurements 14

2.3.1 Different approaches to assigning data uncertainty 15

2.3.2 Errors in nuclear measurements 16

2.3.3 Factors that impact accuracy of density measurements 17

2.3.4 Factors that impact accuracy of acoustic measurements 17

2.4 Logging data distribution and data quality control 18

2.4.1 Application of bivariate analysis to this study 23

2.4.2 Constructing error ellipses 24

2.4.3 Constructing confidence ellipses 24

2.4.4 Application of confidence ellipse to this study 24
2.5 Equations of error propagation 25
2.5.1 Uncertainty of a product: 26
2.5.2 Uncertainty of a ratio: 26
2.5.3 Sums and differences: 27
2.6 Interpreting data uncertainty 27
2.6.1 Uncertainty variation within the instrument measurement range 28

Chapter 3

3.1 Introduction 29
3.2 Description of terms used in this study 29
3.3 Description of the procedure used in this study 29
3.4 Process diagram 31
3.5 Method to compute uncertainty in the fluid substituted velocity 32
3.5.1 Clarification on the use of covariance term 35
3.6 Application of uncertainty calculation for fluid substituted velocity 36
3.6.1 Method to compute synthetic seismogram 37
3.7 Calculating reflection coefficients as function of incident angle 38
3.8 Constants used in the petrophysical and linearly elastic parameters 39
3.9 Parameter uncertainty assignments 40
3.10 Petrophysical cutoff values 41

Chapter 4

4.1 Introduction 43
4.2 Description of the terms used in the figures 44
4.3 Synthetic modeling 44
4.3.1 Synthetic model : Part 1 45
4.3.2 Synthetic model : Part 2 56
4.4 Determining RMS error in fluid substituted velocity on actual data set 62
4.4.1 Review of input data used in this study 62
4.4.2 Well logging data used in this study 63
4.4.3 Fluid properties for original and substituted fluid 63

4.4.4 Results of the uncrtainty calculation study on actual data set 63
4.4.5 Conclusions of uncertainty calculation on actual data set 67
4.5 Amplitude variation with offset 70
4.6 Limitation of the results from AVO modeling 71
4.6.1 Lack of equivalence between reflection coeff. and reflection amplitudes 71
4.6.2 Effect of anisotropy 72
4.7 Procedure to calculate synthetic AVO model 73
4.7.1 Calculating impedance curves 73
4.7.2 Application of Zoeppritz equations 73
4.7.3 Comparisons between synthetic AVO responses 74
4.8 Conclusions from this study 78
4.8.1 Estimating logging data accuracy requirements 79
4.8.2 Suggested future work 80

Appendix A - Chapter 5

5.1 Introduction 82
5.2 Calculating petrophysical parameters 83
5.2.1 Calculating porosity 83
5.2.2 Calculating volume of shale (V_{sh}) 85
5.2.3 Calculating water saturation (Sw) 86
5.3 Calculating linearly elastic parameters 87
5.3.1 Bulk modulus of saturated rock (K_{Sat}) 87
5.3.2 Shear modulus of rock (G or μ) 88
5.3.3 Bulk modulus of mineral matrix (K_0) 88
5.3.4 Bulk modulus of the porous rock frame (K*) 90
5.3.5 Bulk modulus of formation fluid (K_{fl}) 91
5.3.6 Calculating new saturated bulk modulus with substituted fluid (K_{sat2}) 93
5.3.7 Calculating velocities with substituted fluid (V_{p2} & V_{s2}) 94

Appendix B - Chapter 6

6.1 Introduction 96
6.2 Errors in petrophysical parameters 97

6.2.1 Error in bulk density 97
6.2.2 Error in porosity 98
6.2.3 Error in acoustic travel times (DTP, DTS) 99
6.2.4 Computing error in volume of shale (V_{sh}) 100
6.2.5 Error in water saturation (Sw) 101
6.3 Errors in linearly elastic parameters 103
6.3.1 Computing error in bulk modulus of mineral matrix (k_0) 103
6.3.2 Computing error in saturated bulk modulus (K_{sat}) 108
6.3.3 Computing error in bulk modulus of pore fluid (K_{fluid}) 109
6.3.4 Computing error in saturated bulk modulus with substituted fluid (K_{sat2}) .. 110
6.3.5 Computing error in bulk modulus of the porous rock frame (K*) 114
6.3.6 Computing error in shear modulus (G) 121
6.3.7 Computing error in fluid substituted bulk density 122
6.3.8 Computing error in fluid substituted velocity 123

Chapter 1

1.1 Motivation of this study

Fluid substitution is a commonly applied technique to predict elastic properties of a rock saturated with one fluid using the properties measured when the rock is saturated with another fluid. This technique is commonly used to model the various fluid scenarios that may give rise to an observed amplitude anomaly, AVO effect or 4D response. The rock elastic properties are typically obtained from measurements in a borehole using well logs. The key well logs that are used for this analysis are the gamma ray, formation density, neutron porosity, resistivity, and acoustic velocities. Formation bulk density and neutron porosity data are typically acquired using nuclear logging techniques, while the acoustic velocity data are acquired by using monopole/dipole/quadrupole logging technique. As with any kind of data, the individual well log measurements are subject to measurement errors. The quality of such data should therefore be quantified by its accuracy and precision. The accuracy and precision errors can be summarized into a single error term called *root mean square error* (RMS error). The RMS errors for individual measurements and instruments are published by logging companies. The instrument measurement errors are therefore propagated through any subsequent computation which utilizes the measured parameters as inputs. The motivation for this study is to quantify the amount of error that has been propagated from the individual measurements to the final predicted velocities, determined for the substituted fluid, by using the Gassmann fluid substitution relationship. The error present in the fluid substituted velocity will therefore impact any subsequent calculations or interpretations performed when using this velocity. This serves to assist any quantitative approach used in estimating the uncertainty in a lithologic AVO interpretation.

1.2 Introduction

Fluid substitution is a critical part of seismic modeling since it allows for simulation and quantification of various scenarios that may give rise to an observed seismic response. Gassmann (1951) derived an equation to calculate the bulk modulus of a fluid saturated porous medium using the known porosity and bulk moduli of the solid matrix, rock frame, and the pore fluid. The inputs into the equation are usually derived from well logging measurements of formation properties.

Gassmann's equations allows prediction of seismic velocities in a rock saturated with one fluid from the same saturated with a fluid of differing bulk modulus. This process is referred to as *fluid substitution*. When the rock is loaded under an increment of compression such as a passing seismic wave, an increment of pore pressure change is induced which resists the compression and therefore stiffens the rock. The low frequency Gassmann (1951)-limit of the more general Biot (1956) theory predicts the resulting increase in effective bulk modulus, K_{Sat}, of the saturated rock through the following equations

$$\frac{K_{Sat}}{K_0 - K_{Sat}} = \frac{K_{dry}}{K_0 - K_{dry}} + \frac{K_f}{\phi(K_0 - K_f)}, \qquad (1.1a)$$

$$\mu_{Sat} = \mu_{dry}. \qquad (1.1b)$$

where

K_{dry} = Effective bulk modulus of dry rock frame,

K_{sat} = Effective bulk modulus of rock fully saturated with pore fluid,

K_0 = Bulk modulus of solid material (matrix),

K_{fl} = Effective bulk modulus of pore fluid,

Φ = Porosity,

μ_{dry} = Effective shear modulus of dry rock (frame),

μ_{sat} = Effective shear modulus of rock fully saturated with pore fluid.

Although Gassmann's equations are derived for pure mineral and fluid components, in practice, the moduli are averages of differing components and are thus referred to as being "effective". Gassmann's equation assumes a homogenous mineral modulus and statistical isotropy of the pore space, but is free of assumptions of pore geometry and is valid only at sufficiently low frequencies such that the induced pore pressures are equilibrated throughout the work space. This limitation to low frequencies explains why Gassmann's relation works best for *in-situ* seismic data with frequencies (< 100 Hz) and does not typically perform as well at sonic logging (~10^4 Hz) and ultrasonic frequencies (~10^6 Hz) (Mavko et al., 2003). An implicit assumption is that there is no chemical interaction between porous rock and the fluid that affects the moduli. Several authors (Mavko et al., 2003) have pointed out that the Gassmann-Biot theory performs poorly when the measured very dry rock values are used for dry rock or dry frame. To avoid artifacts of ultra dry rocks it is often recommended to use samples that are at room conditions or that have been prepared in a constant humidity environment for the dry rock data. Smith et al., (2003) state that if completely dry samples are used the velocities computed can be too high as the first few monolayers of water may chemically weaken the rock frame.

1.3 Literature review

Previously published studies dealing with uncertainty analysis in fluid substitution have primarily concentrated on stochastic approaches. Paper by Samake et al. (2000) describes the stochastic simulation of the Gassmann's equations by randomly varying the

input parameters. The input parameters selected are assigned reasonable uncertainty values and simulation is performed by varying the input parameters over a large number of trials. Most of the published literature however, does not take into account errors propagated from the logging instrument. As a result, the value of inherent uncertainty present in the fluid substituted velocity due to the use of well logging data remains unknown.

Direct application of error propagation theory in fluid substitution was described in a paper by Broadhead (2005) and gives a deterministic approach to determining uncertainty in the fluid substituted velocity. This paper details the analytical formulae for determining the errors in applying the Gassmann fluid substitution. The paper however, does not address propagated errors in mineral or fluid bulk moduli computations when applying common mixing laws. Additionally the paper does not present an actual case history detailing with the final computed propagated error using real data. Wang (2005) presents the results of sensitivity of Gassmann's equation to analysis of the impact of assigning error ranges of a fixed value to the input parameters due to uncertainties in the input data.

To demonstrate the effect of error propagation, a methodology to calculate the impact of propagated error in the Gassmann's fluid substitution and resulting velocities and is derived and applied to seismic modeling. The error propagation equation differs in form depending on whether the variables used in the computation are dependent or independent. As an example, when an equation which contains the density and the porosity variables where the porosity term was previously computed from the density term using some transform, the porosity can be considered to be a dependent variable of density. The methodology described in this study involves determining the relationships between input parameters to determine

whether the variables can be considered to be dependent or independent in nature. Paper by Smith et al. (2003) is used for the basis for the computing the error propagation equation

Houck (2002) describes the uncertainty in AVO interpretation as a result of geologic uncertainty and measurement uncertainty. The measurement uncertainty in this case does not refer to uncertainties in the logging measurements but refers to uncertainties caused in AVO interpretation as a result of seismic data processing artifacts, noise or other interfering events that contribute to inaccurate information about the elastic properties of the rocks that produced the reflection.

While several authors describe the difficulties in applying Gassmann's fluid substitution equations in mixed lithologies, especially in sand-shale sequences, little literature has been published regarding the effects of error propagation from logging tool measurements on the final computed velocities or on any subsequent computations.

1.4 Fluid substitution in shaley sediment and rock

The traditional method of fluid substitution in porous rock requires the total porosity and the elastic modulus of the mineral phase as input and assumes that the fluid reaches instantaneous hydraulic equilibrium throughout the pore space. This assumption may not be appropriate for shaley sediment because of the low permeability of shale and the resulting immobility of water in it. To overcome the problem of lack of instantaneous equilibrium one of the approaches is to treat porous wet shale as part of the solid matrix material. This excludes the porosity within the shale from total porosity measurement and the new porosity is the effective porosity. (Dvorkin et al., 2007). The Gassmann equation implicitly assumes that the rock frame is composed of single mineral and therefore strictly speaking it cannot be used for multi-mineral rocks (Berryman et al., 1991). However for rocks whose minerals

have similar elastic constants, the accuracy of Gassmann fluid substitution may be adequate providing bulk modulus of the mineral matrix can be computed using one of the mixing laws to determine effective mineral moduli of the rock. In the case of using highly compressible porous shale as one of the solid components to be mixed, it is not clear that the approach of Dvorkin et al., (2007) will not introduce significant error.

1.5 Linearly elastic parameter estimation in mixed lithology

A rock is a naturally occurring mixture of minerals and is normally inhomogeneous both due to the mixed mineral content and also due to the presence of cracks and voids. When the rock is composed of two or more minerals, most mixing rules are based on volumetric fractions of the individual mineral constituents. To predict the effective elastic modulii of a mixture of grains and pores we need to specify: i) the volume fractions of the various phases, ii) the elastic modulii of the various phases, and iii) the geometric details of how the phases are arranged relative to each other (Mavko et al., 2003).

At any given volume fraction of the constituents, the effective modulus value will fall between upper and lower bounds but the precise value will depend on the geometric details. The exact geometric details of the mineral and pore arrangements are generally unknown and therefore an arithmetic mean of the upper and lower bounds is used as an estimate of the effective elastic moduli of the mixture of grains and pores. The two commonly used techniques for calculating the upper and lower bounds of the effective medium are the Hashin-Strickman and Voigt-Reuss bounds. The computation methodology for the two methods is described in detail in Appendix 5. The use of effective media bounds allows an

estimation of the range of average mineral modulus for a mixture of mineral grains and requires that both the rock as a whole and each constituent is isotropic and linearly elastic

1.6 Petrophysical parameter estimation in shaley sediment

Gassmann fluid substitution uses several petrophysical parameters as part of the fluid substitution work flow. The key parameter being the estimation of water saturation (and therefore hydrocarbon saturation), volumes of different mineral fractions, and porosity. The key parameter in petrophysical parameter estimation is the choice of a correct petrophysical model. There are several petrophysical models that may be used in the evaluation of shaley sand reservoirs. The key differentiator in the choice of model is whether the formation behaves as isotropic or anisotropic from the electrical conduction point of view. Two such models which have an impact on the petrophysical parameters computed for Gassmann fluid substitution are considered, isotropic and anisotropic wet shale. Both models use effective porosity (which is calculated by excluding bound water in shale). The bound water is of two kinds: i) shale *bound water*, generally associated with a double water layer associated with clay minerals, and ii) *capillary bound water*, held by electrically charged clay surfaces. Mollison et al. (2006) provide a description of various models in use for petrophysical analysis in shaley sands.

1.6.1 Wet shale anisotropic model

This model is used for formations exhibiting electrical anisotropy, with conductivity values depending on the direction in which they are measured. Electrical anisotropy appears primarily as a consequence of resistivity devices having vertical resolution insufficient to resolve individual layers or laminations. Under these conditions, the measurements provide

average values of the actual or intrinsic properties of the lamina, leading to measurement of macroscopic anisotropy. This type of model is generally applied to clastic sedimentary rocks (or shaley sand reservoirs) and requires measurement of a resistivity (or conductivity) tensor which is represented by its two main components R_V and R_H, which are the vertical and horizontal resistivities respectively. This model allows estimation of effective porosity and water saturations that are fundamental inputs to the Gassmann fluid substitution technique especially when applying fluid substitution to shaley sand reservoirs.

1.6.2 Wet shale isotropic model

The wet shale isotropic model is also an effective porosity model and can be used to characterize formations whose properties are represented solely by scalar quantities. This is the case where the electrical conductivity is independent of the direction in which it is measured. This model will generally apply to thick homogenous sands where we can expect to find rocks of complex mineralogy (but not necessarily layered) and to shaley sand formations containing mainly dispersed shale or authigenic structural clays.

An accurate estimate of uncertainty in petrophysical parameters would need a detailed reservoir study and would need to integrate data from several wells. Accurate estimation of petrophysical parameters has a direct impact in reducing errors in the petrophysical inputs to the Gassmann fluid substitution technique. This would however require measurements using advanced logging instruments coupled with inputs from other data such as measurements from core data. Lack of comprehensive data set presents a challenge. Inadequate data can lead to incorrect estimates of petrophysical parameters and therefore results in additional uncertainty in the fluid substituted velocity. In this study, I estimated uncertainty values are assigned to the petrophysical parameters based on

experience. However this serves to emphasize the difficulty of performing fluid substitution when faced with limited amount of petrophysical data. The choice of uncertainty values used for each petrophysical parameter is described later in this document.

1.7 Expected results from this study

The final computed velocity error value is not a completely random parameter but is a function of systematic errors present in the input data. While it is possible that some of the biases present in the input data will have opposite directions and will therefore tend to cancel each other, the maximum possible error that may occur given that the systematic errors act in the same direction and do not cancel each other is expected to be important. This would result in differences in reflection coefficients calculated by comparing the velocity curves with and without including the error term. The results of this study are expected to quantify the uncertainty bounds in the fluid substituted velocity resulting from standard set of instrument measurement errors. Following the calculation of uncertainty in the new velocity, it would also enable calculation of uncertainty error bounds for the reflection coefficient curves used in synthetic AVO modeling.

1.8 Applications of the results of this study.

The chief objective of this study was to quantify the amount of RMS error present in the fluid substituted velocity as a result of errors in the input measured data. Given the time and cost constraints on the tool design, operations, measurement conditions and the safety considerations it may be unfeasible to further reduce measurement errors in the logging instruments by a significant order of magnitude. While recognizing that the measurement errors will be reduced with new instrument designs and ongoing research, the reduction in the

measurement errors will not be of an order of magnitude that the impact on the calculated data, such as the Gassmann fluid substitution, would reduce to being negligible. In view of this limitation, the impact of uncertainty in the fluid substituted velocity on the reflection coefficients at various angular offsets will be determined. As mentioned earlier in this document, synthetic modeling for various fluid scenarios is a commonly applied AVO technique. By comparing the reflection coefficients at different incident angles between the fluid substituted velocity and its upper and lower velocity error bounds can be used to demonstrate the effect of measurement error on AVO studies. This by no means would indicate that the error in reflection coefficients exists but only points to the fact that it is entirely possible that the actual reflection coefficients may lie anywhere between the upper and lower bounds.

1.8.1 Limitations of this study for AVO synthetic modeling application

The application of this study is limited to the formations which are considered to be isotropic. An anisotropic rock has variations in its physical properties that depends upon the direction a property is measured. The Vertical Transverse Isotropy (or VTI anisotropy) is described when the axis of symmetry is vertical. The VTI anisotropy can either be the result of alternating thin layers that may be individually isotropic but may have significantly different P velocities or may be the result of layering in shales. The Horizontal Transverse Isotropy (or HTI anisotropy) on the other hand, is described when the axis of symmetry is horizontal and is caused by fractures or cracks present in the rock. The wireline compressional velocity data is typically measured using the monopole acoustic source and is unable to detect presence of VTI anisotropy and subsequently the vertical velocity is uncorrected for the effect of VTI anisotropy when the axis of symmetry is tilted from vertical.

i.e. dipping formations or in the presence of large relative dip Accounting for anisotropic effects in the seismic method was greatly advanced by the pioneering work of Thomsen (Hilterman, 2001). It has also been shown that the AVO gradients can be reversed by anisotropy and hence can significantly change the classification of the AVO anomaly. As shales are highly anisotropic this effect cannot be completely ignored.

One application of this study demonstrates the effect of error the fluid substituted velocity on reflection coefficients when analyzing synthetic models. However, it is limited by the fact that the effect of anisotropy on reflection curves is not accounted for. Therefore the synthetic data may show significantly different results when comparing with the actual data even when the systematic error in the measured data and the subsequent error in fluid substituted velocity is very well understood.

Chapter 2

2.1 Introduction

Geophysical data acquired by logging tools can be considered to be a subset of a continuous random variable measured as a function of distance. In the logging domain, we can consider the data curves that are generated to be sample values of a continuous curve at increments of the depth level spacing. In geophysical applications when the data are sampled with sufficient density and even though we may be looking at a subset of a very large data set, the variable (or measurement) may still resemble a continuous random variable over a fixed depth section. Although the available data set may contain only 4 data points / foot, the actual acquired data density may be much greater. As an example, wireline logging data may be acquired at a smaller depth interval which is then averaged out to either 4 or 2 samples per foot as per requirement. In another example, when the data are acquired during the course of drilling, the data density in regions of slow rates of penetration (ROP), may well exceed 4 data points per foot. With "while drilling" data acquisition, the sensor acquisition times are generally matched with expected ROP whereas with a wireline log, the number of data points per foot is controlled by the logging speed.

2.2 Types of data distributions

In geophysical applications, when the data are sampled with sufficient density, even though we may be recoding only a subset of a large data set, the variable (or measurement) will still resemble a continuous random variable. As an example, a thick reservoir section with constant properties which has been adequately sampled can be reconstructed to closely

resemble the continuous random variable with a mean value and distribution. Geophysical data can be defined by four common types of distributions as shown below.

2.2.1 Binomial distribution

The binomial distribution generally deals with data that have a fixed number of trials which are independent and each trial has two outcomes. In general, the binomial distribution is least suited to logging data simply because the random variable is discrete, which means that it can only have a finite number of values. This condition restricts us to use either integers or whole numbers for the data. This condition is easy to achieve by rounding off data values at the cost of data accuracy. The other condition requires that we restrict the number of trials to a fixed number and thereby limiting the possibilities. However there are cases where a binomial distribution can be used. An example of binomial distribution can be identifying sand/shale based on gamma ray log by using cut-off values. Therefore a formation is either identified as sand or as shale if the gamma ray value is either more or less than the cutoff value.

2.2.2 Poisson distribution

The Poisson distribution on the other hand deals with data that are random, independent, and occurs over some interval. The Poisson distribution can also approximate a binomial distribution when the number of data points is large and the probability of success is low. For example, the binomial distribution can be replaced by a Poisson distribution when we are looking at a large number of gamma log data points logged in a well and are interested only in determining the probability that the gamma ray counts occur over a small range.

2.2.3 Gaussian distribution

The Gaussian (or normal) distribution deals with a continuous random variable (or measurement) that has infinitely many values. The textbook on Elementary Statistics by Triola (2006) describes continuous variables as those recorded on a continuous scale with no gaps or interruptions. This definition comes close to the well log measurement where a large number of data points are collected over a continuous depth or time scale. Triola (2006) describes a normal distribution as a distribution of a continuous random variable that has a graph that is symmetric and bell shaped. Well logging data errors are best suited to be defined by normal distribution when the error can take infinitely different values and is not restricted to a integer value or only two trials as in the case of binomial distribution.

2.2.4 Uniform distribution

The Uniform distribution is used in cases where the value of the measured quantity has values spread evenly over range of possibilities. The graph of a uniform distribution will therefore be of rectangular shape. (Triola, 2006). For example, matrix or grain densities of minerals can be assumed to have values that fall within a specific density range. Therefore any density within the specified range is possible and also the probabilities of having any density value within the range are equal.

2.3 Errors in logging measurements

Without going into the detail of the instrument errors, we will focus on errors that result from measurement conditions. The errors in the measuring sensors are added up to generate an RMS error estimate for a reference measuring condition. Given below are some common sources of measurement errors that affect all logging instruments. Errors due to

measurements made outside the tool operational specifications, e.g. measurements in very high temperatures or pressures which are outside tool operating specifications are not considered. They include:

1. Tool calibration errors and tool biases,
2. Effect of borehole alteration or invasion in both space and time,
3. Human errors or incorrect applications of data correction algorithms,
4. Effect of varying logging speeds on data repeatability.

2.3.1 Different approaches to assigning data uncertainty

A sedimentary bed or layer may be composed of sub layers and may be heterogeneous at the well log scale. The individual layer thickness is generally much smaller than the seismic wavelength. Two approaches can therefore be taken while analyzing the data. The first approach would be to consider that the log values should remain constant within each sedimentary layer or sedimentary facies that are clearly identified by the seismic wavelet. Therefore, any variation in the measured data within a specified depth interval and within the tool measurement uncertainty range can be considered to be a result of measurement error and not due to variations in the measured property within the sedimentary facies. The other approach that is commonly used in petrophysical analysis is to block the data curve into zones for the discrimination of electrofacies. Doveton (1994) defines the electrofacies as the set of log responses which characterizes a bed and permits it to be distinguished from the others. The blocking process replaces the original data curve by a stepped function whose value can be considered as a discrete measurement representing the blocked zone and measured within a specified range of accuracy. Therefore a single sedimentary bed unit considered in the first approach may be further sub divided into several

zones in the second approach. For the second method to be effective it is important that the input curves are resolution matched and the matched vertical resolution is smaller than the bed thickness.

2.3.2 Errors in nuclear measurements

Formation bulk density, neutron porosity, and gamma ray curves are the primary curves generated using a radioactive source. While density and neutron porosity uses an external radioactive source, the gamma measurement measures natural radiation in the formation. The particles that are generated by radioactive decay are completely random events that are measured over a fixed interval of time. Since the generated particles are completely random events, any finite amount of counts over a fixed interval of times is subject to statistical fluctuations. It is important to note here that this is a fundamental property of radiation phenomenon and is not dependent on the nature and type of the instruments that measure the radiation.

The number of particle counts (N) that the detector observes over a fixed interval of time follows a Poisson distribution. The standard deviation of the counts that are observed over a fixed interval of time is given by $\sigma = \sqrt{N}$. However in nuclear logging instruments we are more concerned with the count rate (i.e. counts per unit time) rather than the number of counts by itself. The counting rate is given by N/t where 't' is the time of observation. In general, time is assumed to be measured with high degree of precision and therefore any error in time is generally ignored. Therefore the standard deviation of counting rate is given by

$$\sigma = \frac{\sqrt{N}}{t}. \tag{2.1}$$

The count rates observed at the detectors are transformed to bulk density or porosity value by a transfer function. Obviously, the statistical error from the random nature of these events in the observed count rate gets transferred to the computed bulk density or porosity value. This error is in addition to (and assumed to be independent of) the systematic errors arising from measurement conditions in a wellbore. The above described sources of errors affect all measurements, however I list below some of the specific factors that result in errors in density and acoustic measurements. I have limited the list of factors to density and acoustic measurements because these two data curves are primary measurements that are used in the Gassmann fluid substitution. Other important measurements include porosity, gamma and resistivity curves for which a separate list of factors is required.

2.3.3 Factors that impact accuracy of density measurements

1. Statistical errors which are function of radioactive source age and activity.
2. Effect of borehole conditions: washouts, rugose or elliptical boreholes.
3. Effect of logging bed boundaries in high angle boreholes.
4. Density contrast between the borehole fluid and the formation.
5. Impact of variable standoff (distance from sensor face to borehole wall). This variation is common to LWD density logging.
6. Borehole alteration and invasion.

2.3.4 Factors that impact accuracy of acoustic measurements

1. Borehole irregularities, tool tilt, and tool decentralization.
2. Velocity dispersion.
3. Effect of relative dip angle of the bed on measurement.

4. Formation anisotropy.

5. Cycle skipping.

6. Noise spike.

7. Borehole alteration and invasion.

2.4 Logging data distribution and data quality control

As stated earlier, logging data measures a continuous random variable and therefore can be described by the normal or Gaussian distribution. For a normal distribution, the probability of a measurement having a value between x and x+dx is given by the normal distribution function (Triola, 2006)

$$y = \frac{\exp\left[-\frac{1}{2}\left(\frac{(x-\mu)}{\sigma}\right)^2\right]}{\sigma\sqrt{2\prod}} \tag{2.2}$$

Where μ is the mean of the observed values (or also called the expected value) and is the mean that is used in the distribution. Thus, μ is the value we seek, however in reality with a limited number of measurements in the targeted formation, the measured mean value may be different from the actual mean value of the property that we seek. (Stein et al., 2003).

In order to analyze a collection of data pairs both of which are normally distributed, a bivariate normal distribution is defined by the means, variances and covariances of the two variables. The accuracies for the property being measured are often given in terms of Root Mean Squared (RMS) errors. When an accuracy of a measured property is stated, it generally encompasses both the accuracy and precision of the measurement. Accuracy can be defined as the difference between the measured value and the true value. Precision of a measurement refers to the repeatability of the measurement. In general, the precision of the logging tools

has greatly improved with the use of modern solid state electronic systems and therefore the electronic precision errors are generally very low as opposed to errors resulting from accuracy. The only key exception is the precision errors arising in measurements using the nuclear radiation which are prone to precision errors as a result of due to nuclear statistical errors.

If the variables x_1 and x_2 represent normally distributed errors in accuracy and precision of the measurement then the probability of having values with a specified accuracy and precision is given by Clifford (1973).

$$P(x_1, x_2) = \frac{1}{2\Pi\sigma_1\sigma_2\sqrt{1-\rho^2}} \exp\left\{-\frac{1}{2(1-\rho^2)}\left[\left(\frac{x_1-\mu_1}{\sigma_1}\right)^2 - 2\rho\left(\frac{x_1-\mu_1}{\sigma_1}\right)\left(\frac{x_2-\mu_2}{\sigma_2}\right) + \left(\frac{x_2-\mu_2}{\sigma_2}\right)^2\right]\right\} \quad (2.3)$$

where ρ is correlation coefficient given by $\rho = \frac{Cov(x_1 x_2)}{\sigma_1\sigma_2}$, where *Cov($x_1$, x_2)* represents the co-variance between x_1 and x_2 matrix. If ρ=0, it implies that the two error variables x_1 and x_2 are independent. This will be the case when we compare two independent error variables such as accuracy and precision. Therefore parameter measurement uncertainty, such as tool related errors, can be defined in two dimensions. Further, evaluation of electrofacies can be represented in three dimensional space bounded by minimum and maximum log values. As an example, bed of pure anhydrite should ideally be represented by a single point. In practice, combination of tool errors and mineral impurities will cause a constricted cloud to be focused on a the ideal anhydrite point. This uncertainty in either two or three dimensions can be geometrically represented in the form of error ellipses or ellipsoids. In two dimensions (or three dimensions) the error ellipses (or ellipsoids) are completely determined by their co-variance matrix. Thus the error ellipses measure the location and spread of Gaussian

distributions. As a special case with $\sigma_1 = 1, \sigma_2 = 1, \mu_1 = 0, \mu_2 = 0, \rho = 0$, the joint probability distribution on the x-y plane will look like a circle. When the standard deviations of the two variables are different, the joint probability function will look like an ellipse as shown in figure 2.1 below. This ellipse will be therefore a probability contour that represents a pair of values that have probability of $e^{½}$ times the maximum probability. It is important to note here that the axes of the ellipse coincide with graph axes, which indicates that the co-variance is zero (i.e. independent variables).

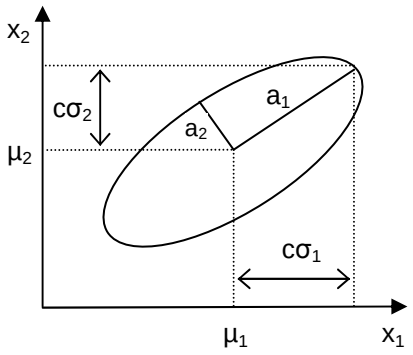

Figure 1 shows the error ellipse representation of two measurements. The semi- axes of the error ellipse are formed by standard deviations of the two measurements. The error ellipse allows for determination of data quality to isolate the data points which fall outside a given probability.

However when the two measurements or their errors are not completely independent, the axes of the ellipse will now be tilted. The co-variance matrix holds the key to determine the lengths of the axes of the ellipse and also the tilt of the ellipse. Computing the error ellipses allows us to determine if the data meets our required confidence level to be valid. Therefore we can compute ellipses of different confidence levels that can help us analyze the quality of the data. The probability contours of the ellipse can be determined by using the form below.

$$\frac{1}{1-\rho^2}\left[\left(\frac{x_1}{\sigma_1}\right)^2 - 2\rho\left(\frac{x_1}{\sigma_1}\right)\left(\frac{x_2}{\sigma_2}\right) + \left(\frac{x_2}{\sigma_2}\right)^2\right] = c^2 \tag{2.4}$$

In a matrix form the above equation can be given as

$$X^T K_{x_1 x_2}^{-1} X = c^2 \tag{2.5}$$

where $K_{x_1 x_2}^{-1}$ is the inverse of the co-variance matrix, and $X = \begin{bmatrix} x_1 \\ x_2 \end{bmatrix}$.

In general, the equation of the ellipse is of the commonly known form $ax^2 + 2kxy + by^2 = c$ provided $k^2 < ab$. Comparing the general equation of the ellipse with equation 2.4, we see that

$$a = \frac{1}{\sigma_1^2}, b = \frac{1}{\sigma_2^2}, k^2 = \frac{\rho^2}{\sigma_1^2 \sigma_2^2}.$$

Since the value of the correlation coefficient ρ lies between ± 1, the condition $k^2 < ab$ is satisfied. Therefore equation 2.4 represents the equation of an ellipse. For independent variables, correlation coefficient ρ=0 therefore the above equation reduces to the commonly known form of ellipse.

$$\left[\left(\frac{x_1}{\sigma_1}\right)^2 + \left(\frac{x_2}{\sigma_2}\right)^2\right] = c^2 \tag{2.6}$$

The co-variance matrix can be solved quadratically to determine the Eigen values. The square root of the Eigen values of the co-variance matrix gives the lengths of the ellipse while the Eigen vectors specify the ellipse axes directions.

$$\text{Semi - major axis} = \lambda_1 = \sqrt{\frac{\sigma_{x_1}^2 + \sigma_{x_2}^2 + \sqrt{\left(\sigma_{x_1}^2 - \sigma_{x_2}^2\right)^2 + 4\sigma_{xy}^2}}{2}}$$

$$\text{Semi - minor axis} = \lambda_2 = \sqrt{\frac{\sigma_{x_1}^2 + \sigma_{x_2}^2 - \sqrt{\left(\sigma_{x_1}^2 - \sigma_{x_2}^2\right)^2 + 4\sigma_{xy}^2}}{2}}$$

where λ_1 and λ_2 are the Eigen values. The direction in which the axes are pointing can be determined from the two solutions of

$$\tan 2\theta = \frac{2\sigma_{x_1 x_2}}{\sigma_{x_1}^2 - \sigma_{x_2}^2}. \tag{2.7}$$

Therefore the probability whether the data lies inside the ellipse as determined by bivariate distributions of stated standard deviations can be determined by:

$$\Pr obability(P) = 1 - \exp(-c^2/2) \tag{2.8}$$

If c=1, the confidence level is 39.3 % while for c=2 the confidence level is 86.4% and so on. When the true value (μ) and the co-variance matrix are known, the error ellipse contains the data estimates for variables x_1 and x_2 with a probability of P. Therefore we can construct error ellipses for pre-selected standard deviations of the data and determine if the data meets our quality specifications. The technique described can be expanded to three variables which will result in constructing the error ellipsoids instead of error ellipses.

The concentric ellipse represent contours of an ellipse for fixed standard deviation of the bivariate Gaussian distribution. However in some cases we may not know the true value of the parameter but we may have some knowledge about the co-variance matrix. In such cases the true value of the parameter can be estimated by sample mean μ. For independent variables, the equation 2.6 can also be written as

$$\left[\left(\frac{x_1}{\sigma_1}\right)^2 + \left(\frac{x_2}{\sigma_2}\right)^2\right] = \chi^2$$

or in the matrix form as $X^T K^{-1}_{x_1 x_2} X = \chi^2$. This indicates that the independent variables are distributed as chi-square distribution with 2 degrees of freedom. (Timm, 2002). Therefore the semi-major and semi-minor axis can now be computed as following.

$$\text{Semi - major axis} = \sqrt{\chi^2 \lambda_1}$$

$$\text{Semi - minor axis} = \sqrt{\chi^2 \lambda_2}$$

We can therefore construct confidence ellipses for unknown **μ**, corresponding to a specified probability as given in the chi-square (χ^2) table (Paradowski, 1997). The confidence ellipse will describe whether the data with unknown **μ** will lie inside or outside the ellipse. The chi-square distribution values for a stated probability value can be obtained from tables. A small table with commonly used values for 2 degrees of freedom is shown below.

χ^2	0.39	2.3	2.77	4.61	5.99	9.21
Probability (%)	50	68.3	75	90	95	99

In the above discussion, the primary intent was to describe a scheme to enable analysis of data quality and to visualize the distribution of measurement errors within the logging measurements. However the method is equally applicable when comparing distributions of any two variables as a quality control process.

2.4.1 Application of bivariate analysis to this study

The primary intent of this study is to quantify the amount of error present in the fluid substituted velocity as a result of measurement errors present in the input logging data. The result of this study will therefore determine the RMS error in the fluid substituted velocity given the presence of systematic error in the measured data and would therefore indicate the range of values between which the actual velocity may lie. The key application of bivariate

analysis to this study is to help determine appropriate methodology for parameter calculation by the use of probability contours. Bivariate analysis allows visualization of spatial distribution character of the data point cloud. This allows the user to select the appropriate parameter or the calculation method that reduces uncertainty by determining data points that either lie inside or outside the probability contours.

2.4.2 Constructing error ellipses

The error ellipses represent an area with a specified probability that the true value of the parameter lies within its bounds. Error ellipses can be constructed for a stated probability, however the requirement is that the true value of the parameter is known *priori*. In most cases the true parameter value is usually unknown when dealing with logging data and therefore it is difficult to compute error ellipses unless an alternate measurement such as core data which can be considered as close to the true value is available.

2.4.3 Constructing confidence ellipses

As a general case, this technique can be used to construct confidence ellipses when the true value is unknown but can be estimated by using the mean of the data. The confidence ellipses will therefore define confidence intervals for the unknown true value at a given value of probability.

2.4.4 Application of confidence ellipse to this study

The confidence ellipse generated about the data mean gives an indication of error distribution. As an example, comparison of confidence ellipses generated in different depth zones can indicate changes in error distributions. The calculation of Eigen values from the covariance matrix further allows calculating Eigen vectors. The semi-major axes coincide

with the direction of maximum variation in error and is also the principal component. The ratio of the eigen vectors indicates the contribution of the individual errors to the total variance in error.

Confidence ellipses (or ellipsoids when three dimensions are considered) can be useful when errors in velocities generated by applying two different estimates of uncertainty parameters. As an example, the error in water saturation calculation is dependent upon the methodology applied to compute the water saturation. Therefore creating error or confidence ellipse will allow comparison of the errors in the computed data as a result of using differing methodology.

2.5 Equations of error propagation

The error propagation equation allows determining the error associated with the dependent variable that has been propagated as a result of some transform using the independent variables. As an example, let U be the dependent variable where $U = f(x, y)$ and where *x* and *y* are the variables for which we define the individual variances as σ_x, σ_y, and σ_{xy}. The error propagation equation can therefore be written as

$$\sigma_u = \sqrt{\left(\frac{du}{dx}\right)^2 \sigma_x^2 + \left(\frac{du}{dy}\right)^2 \sigma_y^2 + 2\sigma_{xy}^2 \left(\frac{du}{dx}\right)\left(\frac{du}{dy}\right)} \qquad (2.9)$$

where

σ^2_x = Variance for variable x

σ^2_y = Variance for variable y

σ^2_{xy} = Co-variance between variables x and y.

The co-variance term σ^2_{xy} describes how fluctuations between the variables are correlated and is only required if the measurements are correlated in some way. The covariance term can be defined as

$$\sigma_{xy}^2 = \lim_{N\to\infty} \frac{1}{N} \sum_{i=1}^{N} (x_i - \bar{x})(y_i - \bar{y}).$$

(2.10

Equation 2.9 is called the error propagation equation which illustrates that the uncertainty in each variable contributes to the uncertainty in a function and depends on the partial derivative of the function with respect to that variable. If the variables x and y are completely independent (uncorrelated) then the above equation will reduce to the one shown below. For completely independent variables the co-variance term will eventually reduce to zero.

$$\sigma_u = \sqrt{\left(\frac{du}{dx}\right)^2 \sigma_x^2 + \left(\frac{du}{dy}\right)^2 \sigma_y^2} \qquad (2.11)$$

Therefore, as long as we have a quantity that is a function of independent variables, the above equation can be expanded appropriately for as many variables as long as the standard deviation of each of the variables is known. Since the uncertainties are independent they can therefore be added quadratically using some of the rules shown below.

2.5.1 Uncertainty of a product:

If $F = x \cdot y$ Then $\sigma_F = \sqrt{\left(\frac{dF}{dx}\right)^2 \sigma_x^2 + \left(\frac{dF}{dy}\right)^2 \sigma_y^2}$

2.5.2 Uncertainty of a ratio:

If $F = \frac{x}{y}$ Then $\sigma_F = \sqrt{\left(\frac{dF}{dx}\right)^2 \sigma_x^2 + \left(\frac{dF}{dy}\right)^2 \sigma_y^2} = \sqrt{\frac{\sigma_x^2}{y^2} + \frac{x^2}{y^4}\sigma_y^2}$

2.5.3 Sums and differences:

If $F = x \pm y$

Then $\frac{dF}{dx} = 1$ and $\frac{dF}{dy} = \pm 1$ $\qquad \sigma_F = \sqrt{\left(\frac{dF}{dx}\right)^2 \sigma_x^2 + \left(\frac{dF}{dy}\right)^2 \sigma_y^2} = \sqrt{(1)^2 \sigma_x^2 + (\pm 1)^2 \sigma_y^2}$

If we consider a data vector $\mathbf{x}_i = (x,y,z,\ldots)$ where x, y, z are independent variables, equation 2.11 can be written as shown below (Stein et al., 2003).

$$\sigma_u = \sqrt{\sum_{i=1}^{N} \sigma_i^2 \left(\frac{du}{dx_i}\right)^2} = \sqrt{\sum_{i=1}^{N} \sigma_i^2 \left(\frac{1}{N} \frac{\delta}{\delta x} \sum_{i=1}^{N} x_i\right)^2} = \sqrt{\frac{1}{N^2} \sum_{i=1}^{N} \sigma_{x_i}^2} \tag{2.12}$$

Therefore if all observations or measurements have equal uncertainties ($\sigma_{x_i}^2 = \sigma^2$) then

$$\sigma_u^2 = \frac{\sigma^2}{N}. \tag{2.13}$$

In the case of this study, this indicates that in sections of the borehole where the measurement conditions are constant, (i.e. no borehole washouts or other measurement issues) making N measurements reduces the standard deviation of the mean by $1/\sqrt{N}$. This points to the fact that acquiring higher data points per foot in a borehole can help reduce uncertainty in the mean value of the data. Higher data density can be achieved by reducing logging speeds and thereby achieving better estimates for true value of the formation property being measured.

2.6 Interpreting data uncertainty

The results of this study, as shown in chapter 4, quantified the amount of uncertainty in the fluid substituted velocity and stated the result as an RMS error value. It is important to understand that all the errors are not completely random and many of them (with the

exception of nuclear statistical errors) are simply the result of systematic error or bias. Therefore the final RMS error value does not indicate that the data would randomly lie anywhere between the upper and lower RMS error bounds. It does, however, indicate that given the systematic bias in the input data, it is possible that the computed data may be deviated from the true value by a maximum amount equal to the RMS error value. It is also possible that some of the errors may cancel each other and further reduce the total RMS error. One of the difficult problems in application of this study is to determine the direction (i.e. whether positive or negative) and the actual amount of systematic bias in the data since the true value of the parameter may be unknown. Determining the direction and the amount of systematic bias in the data is only possible with repeated measurements with different sets of instruments. Since all the input parameters specified the uncertainty have 1σ confidence, it is expected that the end result would also have similar confidence level.

2.6.1 Uncertainty variation within the instrument measurement range

Logging instrument literature generally quotes a single value for data uncertainty based on tests on a wide range of rock properties and at a given confidence level. This single uncertainty value does not indicate that the error value remains constant over the entire measurement range that the instrument is capable of measuring. In addition and apart from the measurement conditions the instrument accuracy is also a function of the rock property and will therefore vary with variations in the rock property. For example, the resistivity measuring devices are very accurate at low resistivity but are incapable of measuring formations with high resistivity with the same level of accuracy. In this study I have used a single value for a parameter uncertainty, however it is possible that this value may be lower or higher than the quoted value.

Chapter 3

3.1 Introduction

This chapter describes the procedure used in this study to estimate the uncertainty in fluid substituted velocity. This chapter also describes the input parameters, petrophysical and uncertainty constants used in this study, followed by a brief description of the process used to generate and compare synthetic traces and the calculation of amplitudes at different incidence angles.

3.2 Description of terms used in this study

The following methodology is used to describe the data mnemonics used in this document. The original data as recorded by the logging instrument do not use a numerical suffix, while similar data that have been computed using the original data as input use a numerical suffix. As an example, the input compressional velocity as recorded by the logging instrument is termed as V_P while the fluid substituted velocity obtained by computation is termed as $V_{p2.}$

Similarly, the initial bulk moduli value computed from original data do not carry the numerical suffix while the computed moduli terms use a suffix of "2". Therefore, the saturated bulk modulus calculated from the input data is termed as K_{Sat}, while the fluid substituted (or derived) bulk modulus is termed as K_{Sat2}. Suffix of 'Min' or 'Max' are also used to denote upper and lower bounds of the data with range of uncertainty.

3.3 Description of the procedure used in this study

This study involves calculation of new velocities by applying the Gassmann's fluid substitution process to the measured well logging data. I used the methodology as described

by Smith et al. (2003) to compute the new velocities for the substituted fluid. The data uncertainty for each parameter at each depth level is computed using the error propagation equation described earlier. Since the intent of this study is to determine the effect of error propagation from logging measurements on the computed velocities, other effects such as correlations between individual parameters in the field are not considered in this study. As an example, since velocity and density data are measured independently, they would be considered to be independent variables for the purpose of this study, and the velocity-density relationship is not required to be established to determine their inter-dependency. The result of applying the error propagation equation allows us to compute the uncertainty in the fluid substituted velocity, and therefore enables the calculation of the likely upper and lower bounds of the substituted velocity. The uncertainty bounds indicate the maximum and minimum values that the substituted velocity can fall within at a given confidence level.

Following the calculation of fluid substituted velocity and its RMS error, I compared the amplitudes of the synthetic seismic traces at different angular offsets up to a maximum of 30 deg between the computed velocity and its probable upper and lower velocity bounds. The synthetic traces were calculated using the Zoeppritz equations in order to determine the differences in reflectivity coefficients (or amplitudes) between the computed velocity and the probable velocity curve (which is calculated by adding or subtracting the RMS velocity error). The purpose of this comparison is to evaluate the impact of data uncertainty in the Gassmann fluid substitution process on synthetic amplitudes for AVO models that are commonly used in the AVO analysis and which can result in variations that are purely due to the tool measurement errors.

3.4 Process diagram

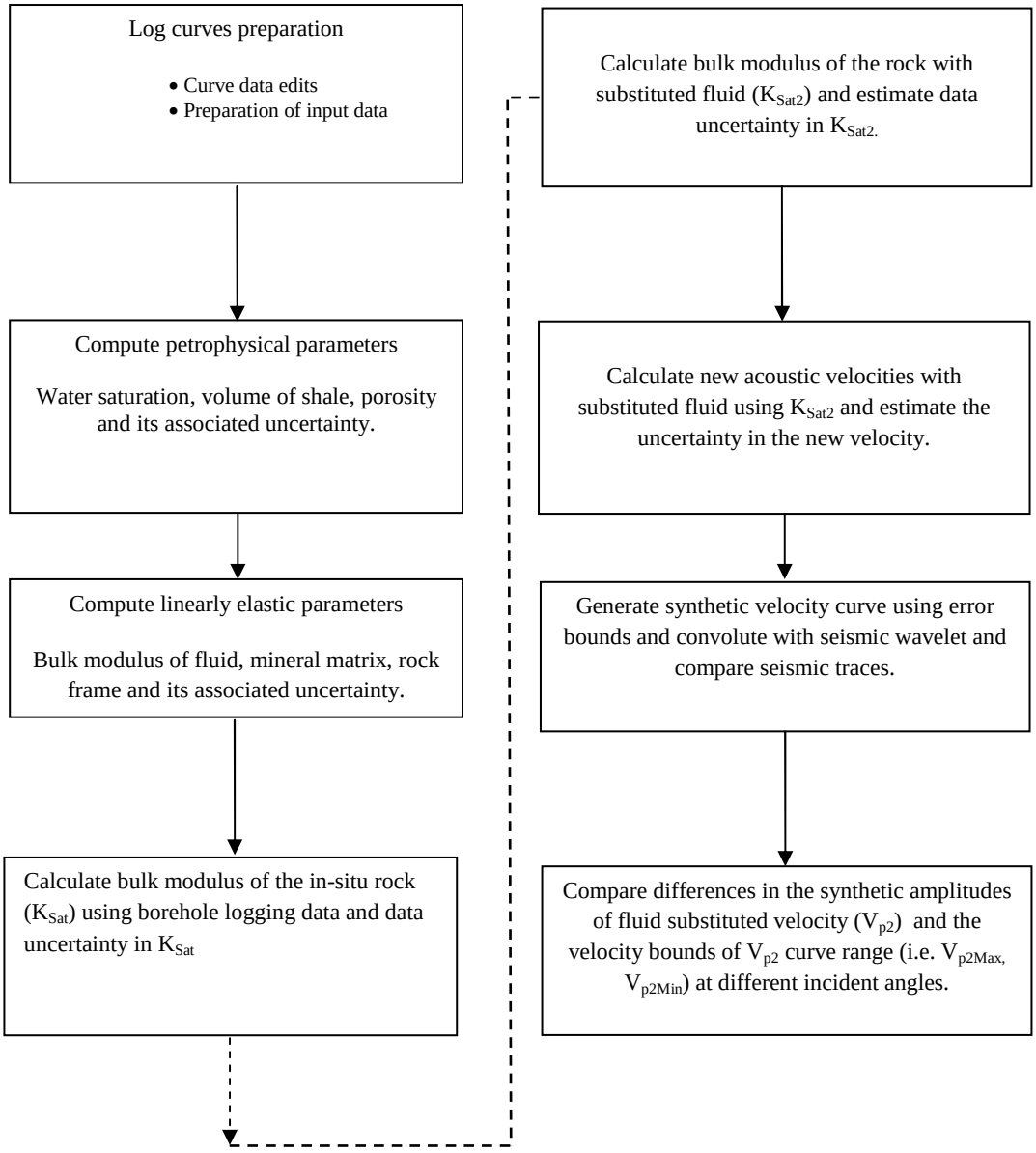

3.5 Method to compute uncertainty in the fluid substituted velocity

The paper by Smith et al. (2003) describes the methodology to perform fluid substitution in using the Gassmann fluid substitution methodology. The key equation relating saturated bulk modulus of the rock to its porosity, the bulk modulus of the porous rock frame, the bulk modulus of the mineral matrix and the bulk modulus of the pore filling fluids is shown below.

$$K_{Sat} = K^* + \frac{\left(1 - \frac{K^*}{K_o}\right)^2}{\frac{\phi}{K_{fl}} + \frac{(1-\phi)}{K_0} - \frac{K^*}{K_o^2}} \qquad (3.1)$$

where

ϕ = Porosity

K^* = Bulk modulus of porous rock frame

K_0 = Bulk modulus of the mineral matrix

K_{fl} = Bulk modulus of the pore fluid

K_{Sat} = Saturated bulk modulus of the in-situ rock

The saturated bulk modulus of the rock can also be computed using the log measurements namely compressional velocity, shear velocity and the formation bulk density through the following relationship.

$$K_{Sat} = \rho_b \left(V_p^2 - \frac{4}{3} V_s^2 \right) \qquad (3.2)$$

where

V_p = Compressional velocity of the rock

V_s = Shear velocity of the rock

ρ_b = Bulk density of the rock

The application of the equation 3.2 is a two part process where the bulk modulus of the porous rock frame (K^*) is determined in the first stage. Once the parameter K^* is computed it allows us to calculate the bulk modulus of the rock saturated with any desired fluid. Equation 3.1 can be rewritten in terms of K* as

$$K^* = \frac{K_{Sat}\left(\frac{\phi K_0}{K_{fl}} + 1 - \phi\right) - K_0}{\frac{\phi K_0}{K_{fl}} + \frac{K_{Sat}}{K_0} - 1 - \phi}. \tag{3.3}$$

The calculation of petrophysical parameters and the linear elastic parameters used in the above equation is described separately in Appendix A (Chapter 5) . The methodology used to determine the uncertainty in the petrophysical and the elastic parameters is also described in Appendix B (chapter 6).

In the equation 3.1, the porosity term has been obtained from the bulk density measurement and therefore both K_{Sat} and porosity are dependent functions of density. This implies that any error in bulk density measurement is propagated to the porosity and also to the computed K_{Sat} parameter as calculated using equation 3.1. If an independent measurement of porosity (using a separate instrument) was available, the K_{Sat} term would still be dependent on the density parameter however the porosity term would be completely independent from a measurement error perspective.

It is possible to determine propagated error in K* and then determine the uncertainty in the saturated bulk modulus with the substituted fluid (K_{Sat2}) as shown in equation 3.3. This method however is complicated since it would involve differentiating the new saturated bulk modulus (K_{Sat2}) with respect to K* parameter which itself has been computed previously

using equation 3.3 and is also a function of the original saturated bulk modulus (K_{Sat1}) and porosity. Another drawback of this method is the requirement to determine the relationship between K_{Sat} and porosity. This task is difficult due to the absence of core or any other additional data. If additional data was available that can help express K_{Sat} and porosity relationship, it would help simplify the differentiation of terms such as $\frac{dK^*}{dK_{Sat}}$ and $\frac{dK^*}{d\phi}$. Solving these terms involves determining solutions for inter-dependent variables K_{Sat} and porosity that are contained within in the term K* as per the equation 3.3.

An alternate methodology suggested by Brodhead (2005) simplifies the solution by eliminating the term K* in the calculation of the final saturated bulk modulus (K_{Sat2}) as shown below. The low frequency Gassmann-Biot theory relates the bulk moduli of the rock saturated with two different pore fluids as

$$\frac{K_{Sat1}}{K_0 - K_{Sat1}} - \frac{K_{fl1}}{\varphi(K_0 - K_{fl1})} = \frac{K_{Sat2}}{K_0 - K_{Sat2}} - \frac{K_{fl2}}{\varphi(K_0 - K_{fl2})}. \tag{3.4}$$

By rewriting the above equation in terms of K_{Sat2} we obtain

$$K_{Sat2} = K_0 \frac{\mathrm{X}}{(1+\mathrm{X})} \tag{3.5}$$

where $\mathrm{X} = \frac{K_{Sat1}}{K_0 - K_{Sat1}} - \frac{K_{fl1}}{\varphi(K_0 - K_{fl1})} + \frac{K_{fl2}}{\varphi(K_0 - K_{fl2})}.$

The above equation now allows calculation of error in K_{Sat2} term (σ_{KSat2}) without the need to determine error in the rock frame modulus (K*). I have applied the error propagation equation to initially determine errors in individual petrophysical and elastic parameters and then calculated the propagated error in the final computed velocities for the substituted fluid.

The uncertainty equation as stated by Broadhead (2005) is shown below and contains the covariance term $2\sigma_{Sat\phi}$, which is the covariance between the saturated bulk modulus and porosity.

$$\sigma_{Ksat2} = \sqrt{\left[\frac{dK_{Sat2}}{dK_0}\right]^2 * \sigma_{K0}^2 + \left[\frac{dK_{Sat2}}{d\phi}\right]^2 * \sigma_{\phi}^2 + \left[\frac{dK_{Sat2}}{dK_{Sat1}}\right]^2 * \sigma_{KSat1}^2 + \left[\frac{dK_{Sat2}}{dK_{fl2}}\right]^2 * \sigma_{K_{fl2}}^2 + \left[\frac{dK_{Sat2}}{dK_{fl1}}\right]^2 * \sigma_{fl1}^2 + 2\sigma_{KSat1\phi}^2 \left[\frac{dK_{Sat2}}{dK_{Sat1}}\right]\left[\frac{dK_{Sat2}}{d\phi}\right]} \quad (3.6)$$

Following the calculation of the error in the new saturated bulk modulus, the error in the new velocity is calculated by reapplying the error propagation equation to equation 3.2 which has been rearranged in the appropriate form to calculate new velocity. This is further described in Appendix B in section 6.3.8.

3.5.1 Clarification on the use of covariance term

It is necessary to clarify the application of covariance terms in the calculation of propagated error in this study. The objective of this study is to determine the uncertainty in the final computed velocities as a result of error propagated from the logging instruments. The logging measurements of density, velocities, resistivity, etc. are used to compute both petrophysical and linearly elastic parameters using the methodology as described by Smith et al. (2003).

The paper by Broadhead (2005) considers parameters such as bulk modulii of the mineral matrix and the fluid to be statistically independent, while considering the saturated bulk modulii of the rock and the porosity to show a strong negative correlation. While this consideration is accurate when all input parameters have been acquired independently (i.e. from core measurements or reservoir studies), it does not directly apply to this study. In this

study, I calculated both petrophysical and linearly elastic parameters using basic rock physical properties and also computed the propagated error for each calculated term. The input data for this study will show varying degrees of correlation between several sets of variables. As an example, several data pairs, such as density vs. velocity, K_0 vs. velocity, etc. (to name a few), may also show varying degrees of correlation. In such a case, covariance's for each data pair would then have to be included in the error propagation equation. For the purpose of this study, unless the calculated parameters have been derived from a common variable and therefore show direct dependence on each other, the covariance term for each data pair will not be calculated. As an example, terms such as porosity and K_{Sat1} are both calculated from the density measurement, where density is the independent variable measured by the logging instrument. Therefore when determining the solution to terms such as $\frac{dK_{Sat}}{d\phi}$ or $\frac{dK_{Sat2}}{dK_{Sat1}}$, the porosity term cannot be considered to be an independent variable for the purposes of error propagation from logging data measurements. If the total (or effective) porosity term was measured by an independent instrument (i.e. independent porosity instrument such as Neutron or NMR) the uncertainty in the porosity term can then be considered to be independent and will not require inclusion of the covariance term in the equation. This topic is discussed again in Appendix B (6.3.5 section) on calculating propagated error for the K* term where it has direct application.

3.6 Application of uncertainty calculation for fluid substituted velocity

One technique to determine the impact of the calculated error in the new velocity is by comparing the acoustic impedance curves and further transforming them into a reflection amplitude time-format. This allows comparison of the seismic traces generated by the fluid

substitution process both with and without considering the effect of uncertainty in the measured data set. The differences between the seismic traces would point to the minimum and maximum reflection coefficients (or amplitude) differences that can arise simply as a result of measured data uncertainty.

3.6.1 Method to compute synthetic seismogram

The process for converting the velocity-density curves to a synthetic seismic trace can be termed as forward synthetic. The basic assumption used in the generation of synthetic seismograms is that plane waves propagate vertically through a horizontally stratified medium and that reflectivity is governed solely by the acoustic impedance contrasts encountered within the layered medium. The reflection coefficient is then computed by taking the difference of the two acoustic impedances divided by their sum. The convolutional model of the seismic trace can be represented by $S_t = r_t * w_t + n_t$, where the symbol $*$ represents the convolution of the reflection coefficients 'r_t' with the wavelet 'w_t', and 'n_t' is the additive random noise. In this study, I did not consider the effect of additive noise, however the random noise would be a consideration for any serious study involving comparison of the synthetics with actual seismic traces. I have stated below some of the processing steps that I used to generate the synthetic seismogram. I have used Hampson-Russell software to convert the velocity - density data in depth domain to seismic traces in the time domain.

1. The sonic velocity and the density curves were digitized to a sample interval of 0.5 ft.
2. The curves can be 'blocked' to a larger sample interval taking care that the log values are not aliased in the process of creating the larger sample interval. I used a blocking interval of 2 feet which is greater than the highest wave number that can be sampled

i.e. Nyquist criteria would limit the highest wave number to 1 foot (2 x 0.5 ft.). Since the vertical resolution of the acoustic instrument is approximately 2 feet (or greater), the wavenumbers higher than value of 1 cannot be sampled due to the intrinsic resolution limit and therefore would not contribute to data aliasing.

3. The blocked acoustic impendence curve is then used to compute reflection coefficients at each interface between contrasting velocities using the equation $r_t = \frac{A_{t+1} - A_t}{A_{t+1} + A_t}$, where At is the acoustic impedance.
4. A wavelet is generally chosen that has frequency response and bandwidth similar to nearby seismic data. For this study I have chosen a Ricker wavelet with peak frequency of 70 Hz. This synthetic wavelet was convolved with the reflection series for the entire well data to generate a synthetic seismic trace.

3.7 Calculating reflection coefficients as function of incident angle

The P - wave reflection coefficient as a function of the incidence angle is defined as the ratio of the amplitude of the reflected P-wave to that of the incidence wave and is dimensionless because the respective amplitudes have been normalized (Hilterman, 2001).

At normal incidence, there is no mode conversion to S wave and the P-wave reflection coefficient is given by $R_P = \frac{I_{P2} - I_{P1}}{I_{P2} + I_{P1}}$ where I_{P2} and I_{P1} are the impedances of medium2 ($\rho_2 * V_{P2}$) and medium1($\rho_1 * V_{P1}$). The variation of reflection and transmission coefficients with incident angle (and corresponding increasing offset) is referred to as offset dependent reflectivity and is the basis for amplitude versus offset analysis. Knott (1899) and Zoeppritz (1919) invoked continuity of displacement and stress at the reflecting interface as boundary conditions to solve for the reflection and transmission coefficients as a function of

the incident angle and the media elastic properties (Castagna et al., 1993) The common incidence angles in exploration applications are, in general, less than 30 deg. Since the observed seismic data measure reflection coefficients but only reflection amplitudes with the assumption that there is an equivalence between reflection coefficients and the observed amplitudes, I have compared the amplitudes up to 30 degrees by using Zoeppritz equations and with the assistance of Hampson-Russel software. The intent of this analysis was to compare the differences in the amplitudes between fluid substituted impedance contrast and its upper and lower uncertainty bounds.

3.8 Constants used in the petrophysical and linearly elastic parameters

In the absence of additional data such as core, fluid, or reservoir data for use in this study, I used the following constants for the purposes of this study.

Constants used for calculating water saturation- (Archie's method)

- Resistivity of formation water : 0.075 ohm-m
- Cementation exponent (m) : 2.0
- Saturation Exponent (n) : 2.0

Constants used for density-porosity conversion

- Grain density of mineral matrix : 2.65 g/cc
- Density of formation water : 1.00 g/cc
- Density of dry clay : 2.60 g/cc

Constants used for calculating bulk modulus of the reservoir fluid:

- Sea water temperature at mudline : 40 deg F
- Formation temperature gradient : 1.1 deg/100 ft

- Formation pressure gradient :0.465 psi/ft
- API value of the hydrocarbon in the reservoir: -original fluid : 20
- Gas gravity of dissolved gas in the reservoir: - original fluid : 0.6
- API value of the hydrocarbon in the reservoir - substituted fluid : 45
- Gas gravity of dissolved gas in the reservoir: - substituted fluid : 0.6

Constants used for calculating bulk modulus of the mineral matrix

- Bulk modulus of quartz (K_{Quartz}) : 37 GPa
- Bulk modulus of clay (K_{Clay}) : 15 GPa
- Shear modulus of quartz(μ_{Quartz}) : 45 GPa
- Shear modulus of clay (μ_{Clay}) : 9 GPa

3.9 Parameter uncertainty assignments

The uncertainty assignments to the measured data that was used this study is shown in the table below. All measured parameters are typically quoted at one standard deviation confidence level by data acquisition companies. It is possible to use alternate values for data uncertainty for use in specific applications, however in view of no other tool or borehole quality information I used only published values for this study. The confidence levels for the calculated parameters are undetermined and would need additional study. The calculated parameters required assigning uncertainty values either due to limited data availability or complexity of determining the true data uncertainty. As an example, calculating the water saturation parameter in shaley sands requires the use of advanced interpretative tools and measuring instruments in order to reliably estimate the parameter and therefore required assigning uncertainty values based on expected uncertainty.

S/N	Parameter	Type	Description	Uncertainty
Measured Parameters				
1	Density	Measured	Formation Bulk Density	± 0.025 g/cc
2	DTP	Measured	Slowness- Compressional	± 5 % of measured value
3	DTS	Measured	Slowness- Shear	± 5 % of measured value
4	Res 90	Measured	Resistivity at 90" DOI	± 1 % of measured value
Calculated Parameters				
5	Sw (Archie)	Assigned	Water Saturation	± 20 % of calculated value
6	V_{Shale}	Assigned	Volume of Shale	± 5 % of calculated value
7	DenPor	Assigned	Porosity Calculated from Density	± 5 % of calculated value
8	Density 2	Assigned	Fluid Substituted	± 0.025 g/cc
9	K_{Water} / K_{Oil}	Assigned	Fluid Bulk Modulus (Water/Oil)	± 5 % of calculated value

3.10 Petrophysical cutoff values

Due to limited data availability, several petrophysical parameters required the use of cut-off values in order to constrain the solution to a meaningful value. If additional data is available the limits imposed by the cutoff values can either be loosened or eliminated by taking advantage of the additional information. The cutoff values are chosen such that there would not be any significant improvements to the derived results if the selected cutoff values were not applied.

Parameter	Cut off	Application
Volume of Shale (V_{Sh})	70 %	– V_{Sh} > 70 then rock type is regarded as shale – V_{Sh} > 70 then S_W = 1, disregard minor hydrocarbons in shale dominated rock. –V_{Sh} > 70 then porosity <= 0.05, improve porosity computation in shale dominated rock
Water Saturation (Sw)	70 %	– S_W > 0.7 then Sw=1.0, disregard negligible hydrocarbon saturation

Chapter 4

4.1 Introduction

Fluid substitution is widely used as a tool to model various scenarios which might give rise to an observed amplitude variation with offset or to model 4D response when *in-situ* hydrocarbons are replaced with water or brine during water flooding operations. Wireline logging data is the most common type of data available and is used to study the impact of fluid substitution. The primary intent of this study was to derive an estimate of the propagated error in the fluid substituted velocity as a result of uncertainty in the input data. In the first part of the study I calculated the impact of uncertainty in the various petrophysical parameters on the fluid substituted velocity by using synthetic data models. Following the use of synthetic data models, I performed similar computations on actual well log data set. To determine the consequence of the error in the fluid substituted velocity, I tested the impact of this uncertainty on amplitude variations by creating a synthetic AVO model by using approximations to the Zoeppritz equations. It must be understood that in the seismic datasets, the subsurface reflection coefficients are never directly measured. The reflection coefficients from seismic data can only be estimated using AVO inversion techniques which involves inverting the AVO data to estimate the subsurface elastic parameters. For the inversion process to be reliable, it is important that the seismic data processing output represents 'true amplitude' processing. Therefore when examining the impact of errors in the Gassmann fluid substitution output, I compared the impact of these errors on seismic amplitudes rather than on reflection coefficients. The results of this study are presented in this chapter.

4.2 Description of the terms used in the figures

V_p	=	P- Velocity - Measured
V_{p2}	=	New P- Velocity - Fluid substituted
V_s	=	S- Velocity - Measured
V_{s2}	=	New S - Velocity - Post fluid substitution
RHOB	=	Bulk Density -Measured
$RHOB_2$	=	New Bulk Density - Fluid substituted
RMS Error	=	Root Mean Square Error
Fl.Sub	=	Fluid substituted
Max	=	Subscript of 'Max' represents the parameter derived by adding the RMS error to the parameter value and represents the upper bound of the possible parameter value
Min	=	Subscript of 'Min' represents the parameter derived by subtracting the RMS error from parameter and represents the lower bound of the possible parameter value.

4.3 Synthetic modeling

The objective of synthetic modeling was to determine the error in the fluid substituted velocity as a result of uncertainty in the petrophysical input parameters using published rock property data. The results from the synthetic modeling can then be used to predict the major sources of error when applied to actual data sets. It is important to distinguish here that the measured data may have additional errors as a result of well bore conditions which may not be accounted for in the synthetic data modeling.

The synthetic modeling was performed in two parts . In the first part, I used constant rock properties for a high porosity water saturated sandstone, while for the second stage the computation was performed over range of velocities also for a water-saturated sandstone. In both cases the original fluid (brine) was substituted with hydrocarbon. The rock properties for both stages were derived from the Rock Physics Handbook (Mavco et al., 2003). The fluid properties for both original and substituted fluid were generic fluid properties and held constant since the exact pressure - temperature conditions of rock deposition are unknown.

4.3.1 Synthetic model : Part 1

Objective of synthetic modeling for the first part was to compute error curves for final velocity when the errors in the input petrophysical parameters are varied. Therefore, by varying the uncertainty in the petrophysical parameters a set of curves representing errors in final velocity were computed. When determining the effect of error for a specific petrophysical parameter, the errors from other input petrophysical parameters have been ignored. As an example, when determining impact of error in Sw, the uncertainty in other petrophysical parameters (such as V_{sh}) have been assumed to be zero. In some cases two different properties for sandstone were used in the synthetic modeling. The rock properties for high porosity sandstone and medium porosity sandstone used in the synthetic model are shown below.

High Porosity Sandstone	
Vp (Km/s) = 3.80	Bulk Modulus of Brine (GPa) = 3.35 (Original Fluid)
Vs (Km/s) = 2.16	Bulk Modulus of Oil (GPa) = 1.50 (Sub. Fluid)
Porosity (frac) = 0.20	Volume of Shale = 20% (Assumed)
Bulk Density (g/cc) = 2.33	Density of Orig. / Sub. Fluid (g/cc)= 1.00 / 0.85
Medium Porosity Sandstone	
Vp (Km/s) = 4.09	Bulk Modulus of Brine (GPa) = 3.35 (Original Fluid)

Vs (Km/s) = 2.41	Bulk Modulus of Oil (GPa) = 1.50 (Sub. Fluid)
Porosity (frac) = 0.16	Volume of Shale = 20% (Assumed)
Bulk Density (g/cc) = 2.37	Density of Orig. / Sub. Fluid (g/cc)= 1.00 / 0.85

The values for the bulk moduli of brine and hydrocarbon were assumed for the purposes of this modeling study. The fluid substitution modeling assumed replacement of the entire original fluid with the substituted fluid . Results of the first part of the synthetic are given shown below.

4.3.1.1 Effect of error from water saturation (Sw) on fluid substituted velocity

As described above, the original rock is assumed to be completely saturated with water (Sw=1) and therefore the error in the input water saturation (Sw-Original) is assumed to be zero. Additionally, the error in the bulk density of the original fluid is considered to be zero. When determining errors in the new velocity when the original fluid is saturated with two (or more) fluids, the errors in water saturation for both the original and the new fluid would have to be considered. In this case I have only accounted for the error in water saturation after substituting the original fluid.

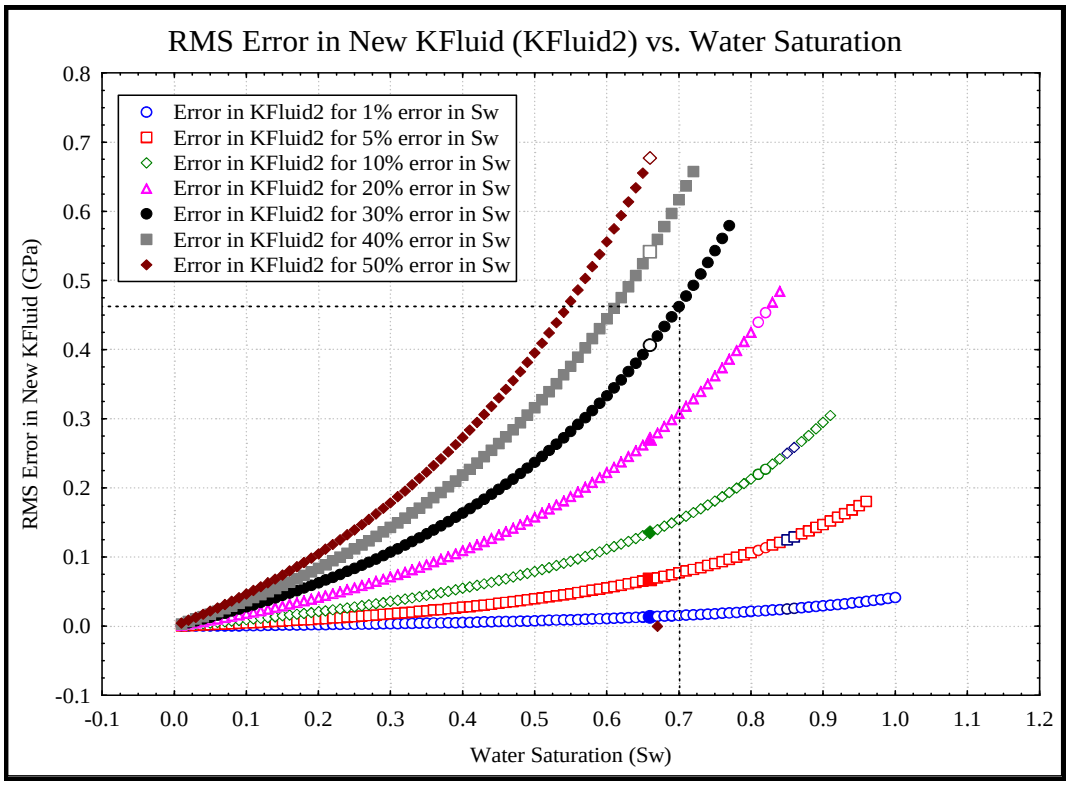

Figure 2 shows the error in the bulk modulus of new fluid vs. water saturation. The individual curves show the percent error in the water saturation. As an example, the dotted black line shows the error in Kfluid of ~0.45 GPa for Sw=0.7 and when uncertainty in Sw estimated at 30%. This indicates that after replacing 30% of the original fluid with hydrocarbon (Sw reduced from 1.0 to 0.7) and assuming 30% error in Sw calculation, the error in the bulk modulus of the new fluid is ~0.45 GPa.

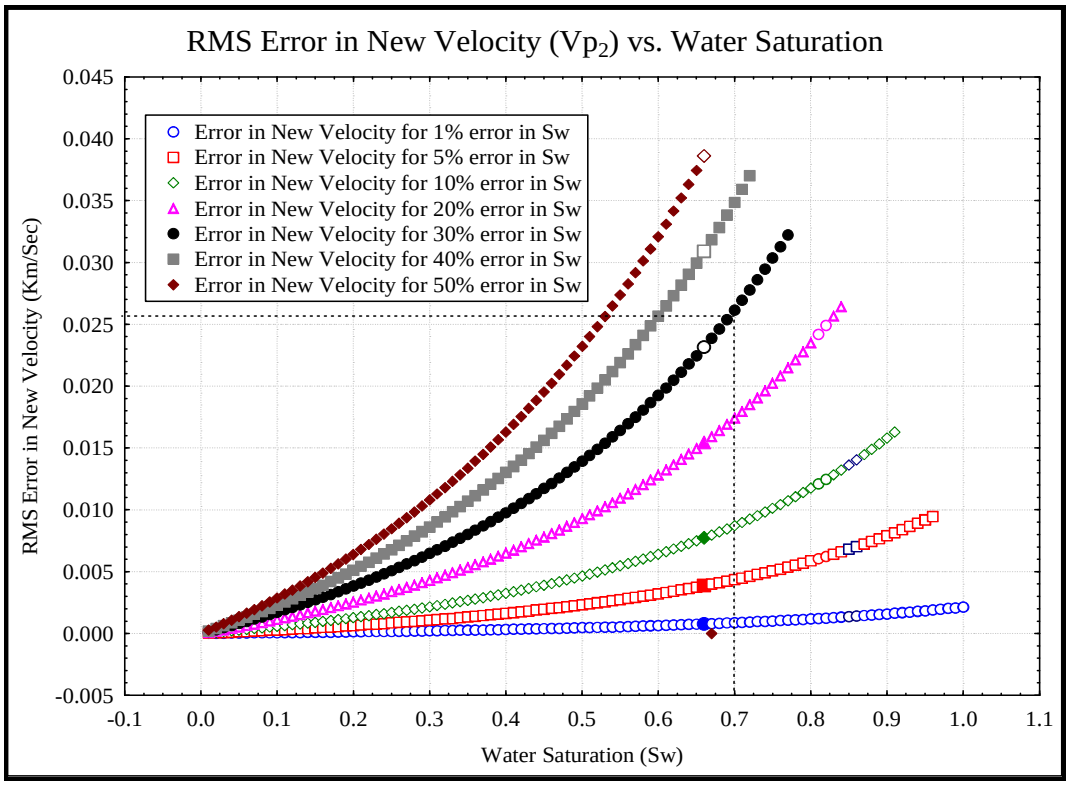

Figure 3 shows velocity errors for errors in water saturation. The dotted black line shows the error in velocity of 0.026 Km/s for the water saturation of 0.7 and for uncertainty in Sw at 30%. As seen in the plot, the error in the new velocity is large when substituting partial fractions of the original fluid with the substituted fluid. To restate, the original rock was assumed to be completely saturated with brine and therefore the error in the original Sw is considered to be zero.

4.3.1.2 Effect of error from volume of shale (Vsh) on fluid substituted velocity

The clean high porosity sandstone was assumed to have recorded 1%, 5%, 10%, and 20% volume of shale for the purposes of this modeling study. Since this study is conducted for a fixed lithology, the impact of error for increasing fractions of Vsh beyond 20% could not be modeled, since any incremental increase in Vsh would also affect other input parameters (i.e. density, porosity, velocity, etc.) which are also dependent on the Vsh. Values for other input parameters would also have to be known priori for each incremental value of Vsh.

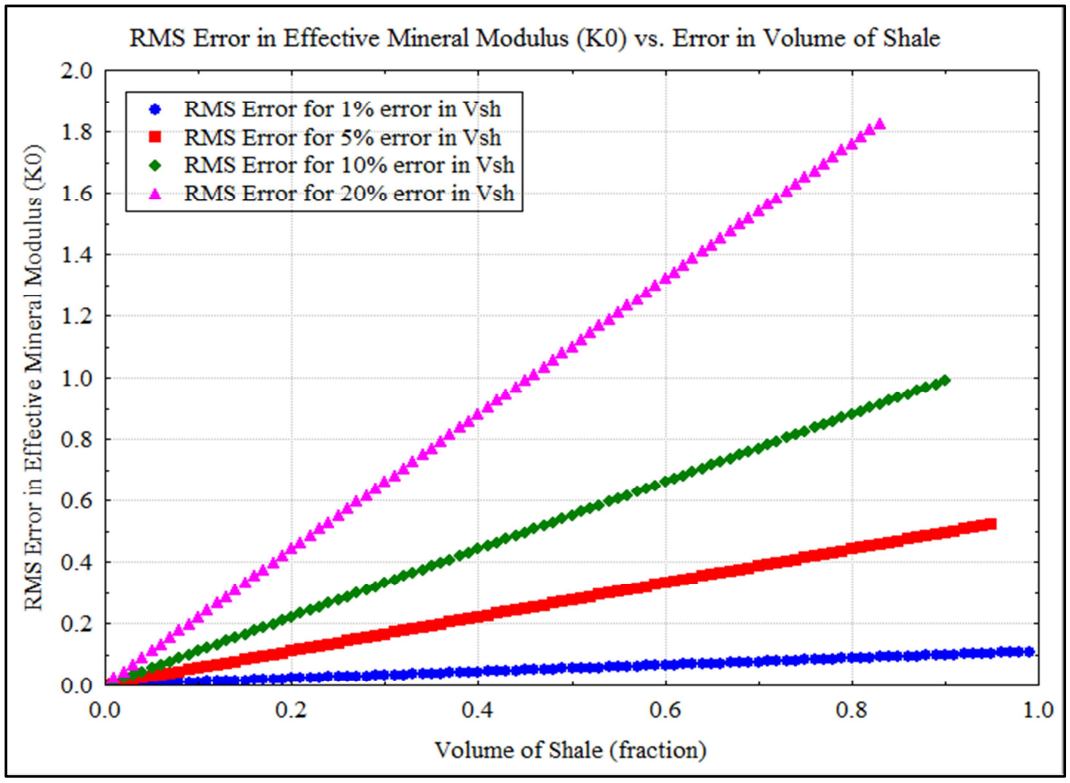

Figure 4 shows effect of uncertainty in volume of shale (Vsh) on the effective mineral modulus for different fractional shale volume up to a maximum volume of 20%.

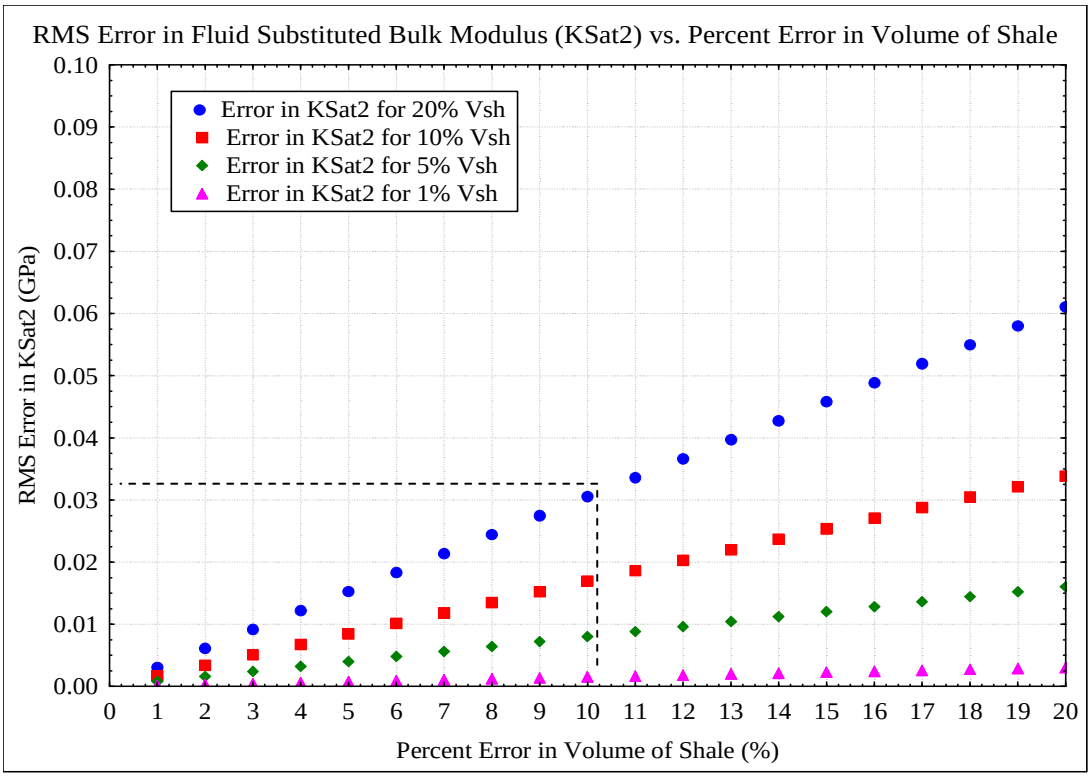

Figure 5 shows effect of uncertainty in volume of shale on the new saturated bulk modulus. The dotted line shows the error in KSat2 to be ~±0.032 GPa for 10% error in volume of shale for the volume of shale of 20%. The error in KSat2 is directly a result of error in the effective bulk modulus shown in figure 4.

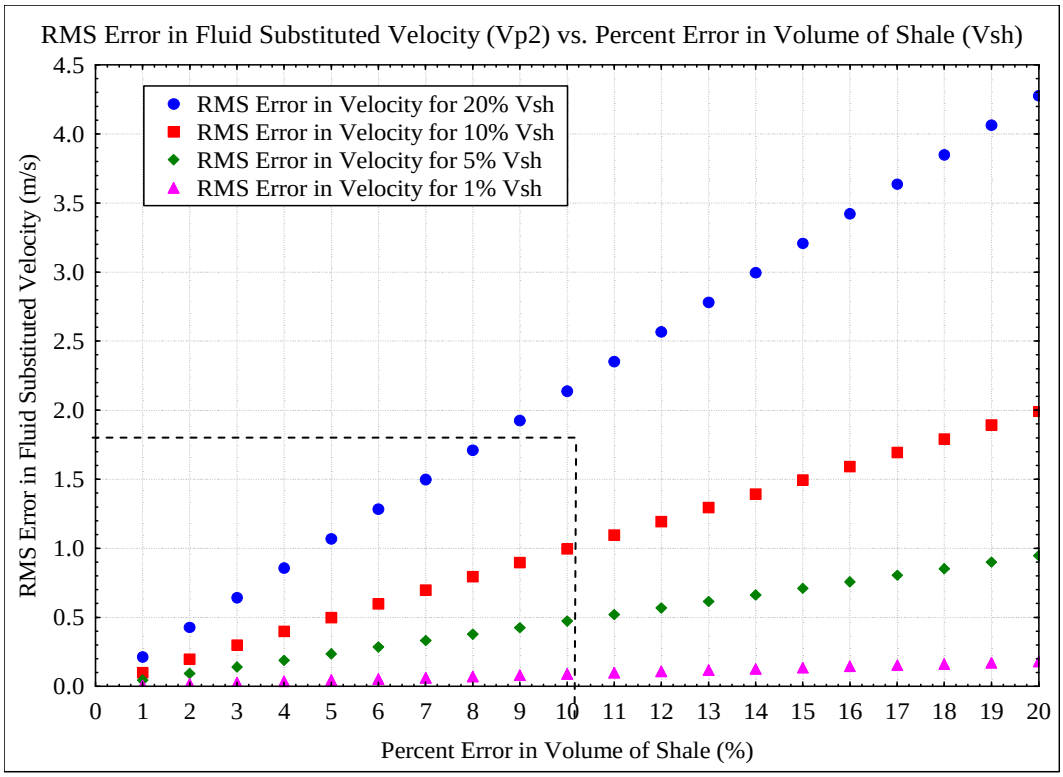

Figure 6 shows effect of error in volume of shale on the new velocity. The dotted line shows the error in new velocity to be ~±2.2 m/s for 10% error in volume of shale for the volume of shale value of 20%. The error in Vsh is a minor contributor to the error in new velocity for relatively cleaner sands.

4.3.1.3 Effect of error from travel time (delta T) on fluid substituted velocity

The error in the measured value of delta T can impact the substituted velocity results. The delta T measurement can be affected by anisotropic effects as a result of large relative dips as well as operational factors such as resulting from hole enlargement and drilling fluid substitution. Shown below is the effect of uncertainty in both compressional and shear Delta T measurements on the final substituted velocity.

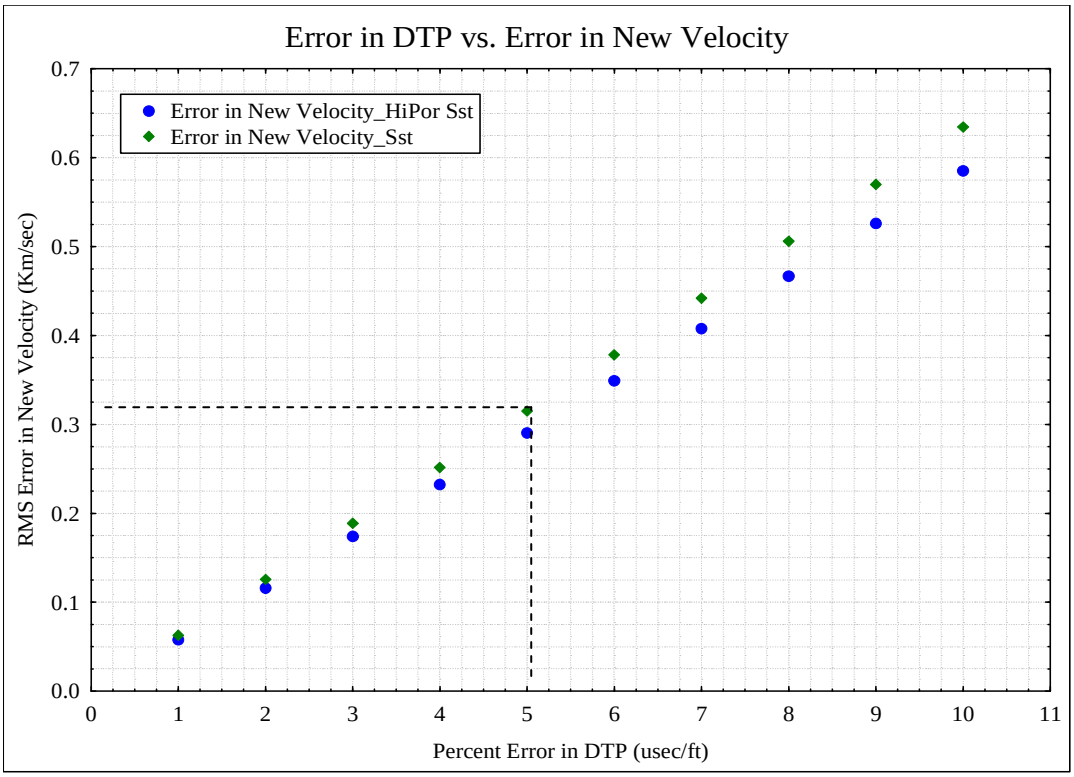

Figure 7 shows effect of error in delta T (measured) on the new velocity. As indicated by the dotted black line, for 5% error in delta T value for the compressional velocity can result in a erroneous fluid substituted velocity of ~0.32 Km/Sec for the medium porosity sandstone. All other input parameters have been kept constant throughout the calculation.

4.3.1.4 Effect of error from measured bulk density on fluid substituted velocity

The high porosity sandstone used in this modeling study had a bulk density of 2.33 g/cc. I calculated the error in saturated bulk modulus as a result of the error in bulk density. Following the calculation of error in the saturated bulk modulus of the in-situ rock, the error in the new saturated modulus using the substituted fluid was calculated. The porosity value used in the fluid substitution process is often derived from the bulk density measurement and in this study is termed as the dependent porosity. Any error in the measured bulk density is therefore propagated to the calculated porosity. I computed the error in the new velocity by

considering the porosity term to be either dependent or an independent variable. When the porosity term was derived from density, the error propagation equation was used to calculate the error in the to the porosity term. For the purposes of this calculation, the error in matrix density and the fluid density was assumed to be 2% and 1% respectively. When porosity was considered to be an independent variable a constant error value of 5% was assigned to the porosity variable.

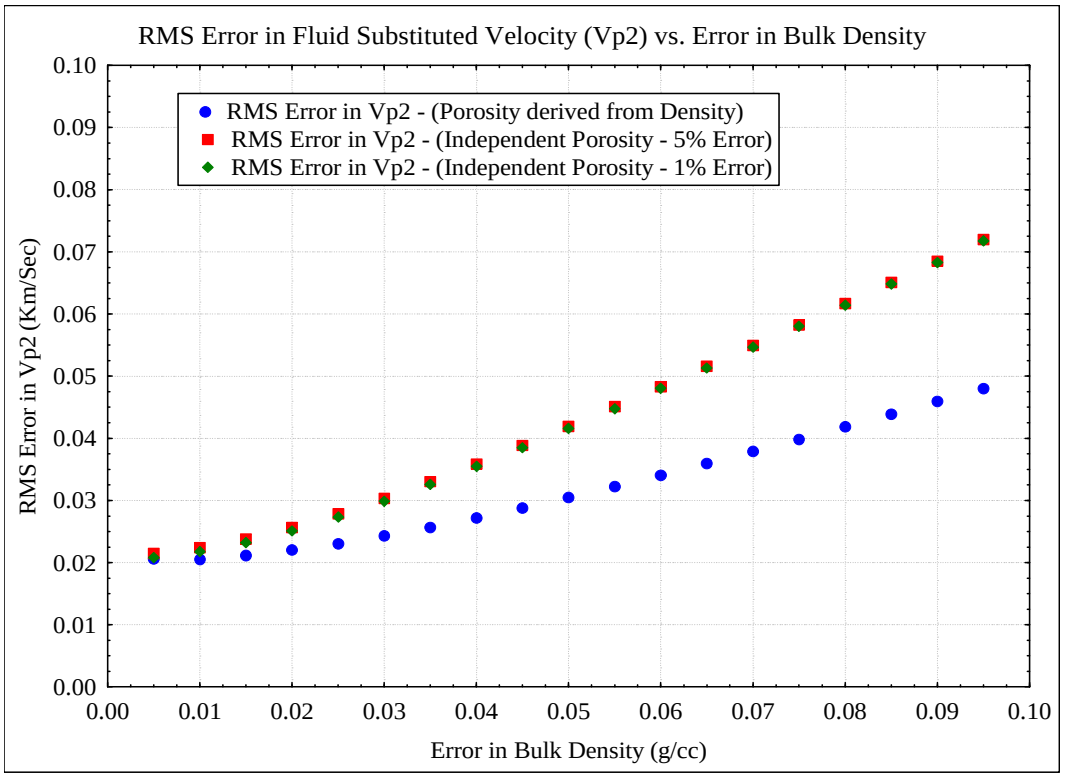

Figure 8 shows effect of error in the bulk density on the new velocity. The blue curve shows the error when porosity is derived from the density measurement. In this figure, both density and porosity instrument errors are considered to operate simultaneously which results in errors in the new velocity. It is seen that the contribution of the error in porosity is minor especially for clean formations.

4.3.1.5 Effect of error in independently measured porosity on fluid substituted velocity

The modeling was conducted for both medium and high porosity sandstones with porosity of 16% and 20% respectively. The error in the measured porosity term directly affects the calculation of new saturated bulk modulus. Following the calculation of the error in the new saturated bulk modulus, the error in the new bulk density was calculated. Finally the errors in new saturated bulk modulus and the new bulk density were combined to calculate the error in the new velocity. In this case. the errors in all other measurements were considered to be zero.

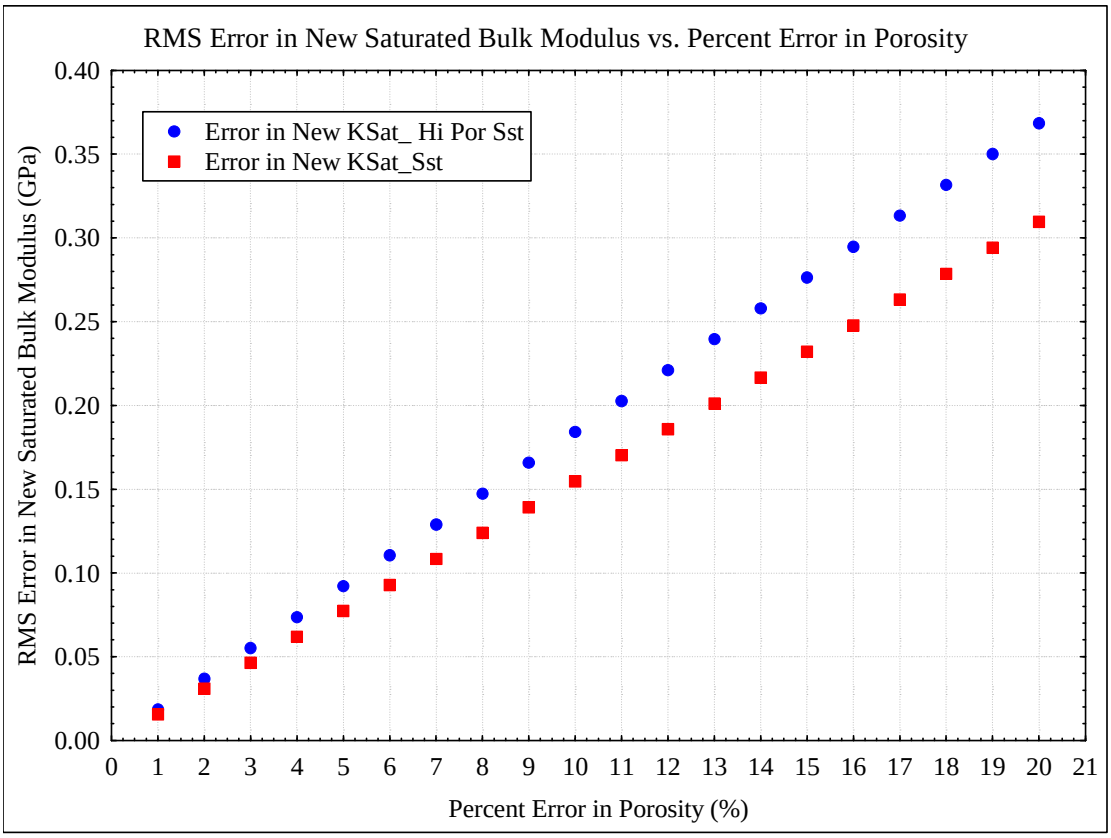

Figure 9 shows the effect of error in the porosity instrument on the error in new saturated bulk modulus. Uncertainities in all other measurements have been assumed to be zero.

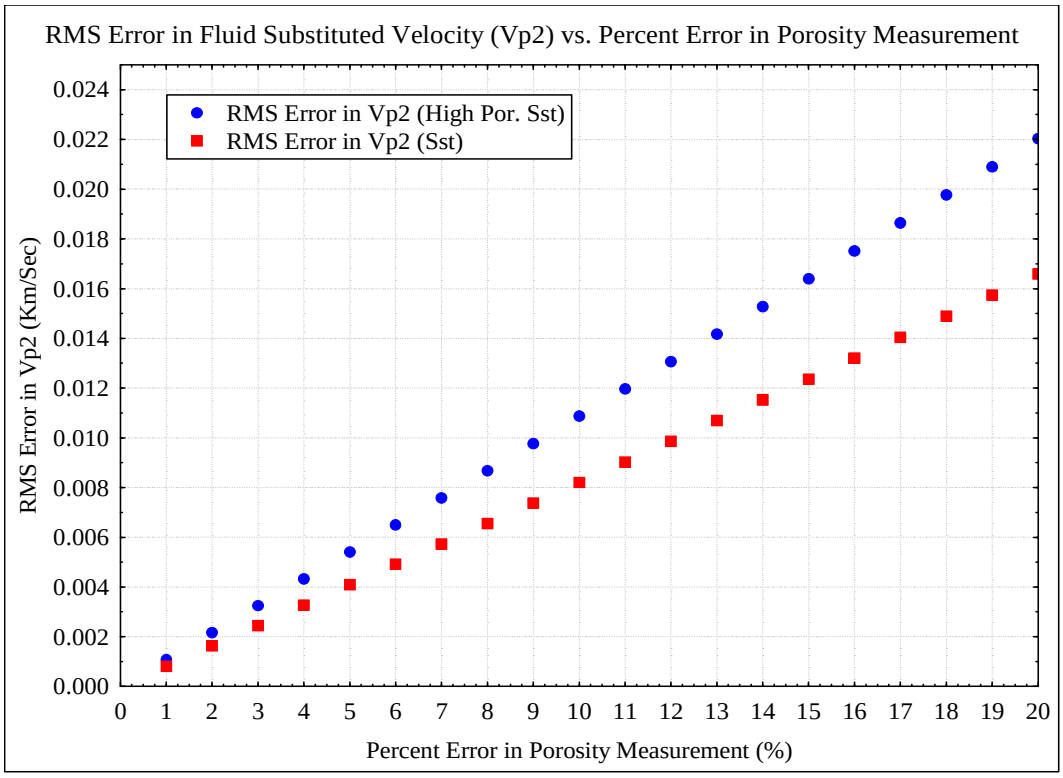

Figure 10 shows the effect of error in the measured porosity on the error in the new velocity. It must be understood that the volume of shale in this modeling study is low, however higher shale fraction tends to increase the uncertainty in the porosity measurement.

4.3.1.6 Conclusions from Part 1 Modeling

Using the parameter uncertainty assignments stated in section 3.9 and which can be considered to be generic error ranges present in the measured data, the table below gives the RMS error in the final velocity for the high porosity sandstone.

Petrophysical Parameter	RMS Error in Petrophysical Parameter	RMS Error in Final Velocity (Km/s)
Sw	±20%	±0.01
Density	±0.025 (g/cc)	±0.02
Travel Time (DTP)	± 5%	±0.32
Volume of shale	±10%	±0.002
Porosity	±5%	±0.005

Following conclusions can be drawn from the results of the modeling from part 1.

1. The largest source of error in the fluid substitution process is the error in the input travel time measurement. Therefore any attempt to improve accuracy of the fluid substituted velocity should focus on improving the quality of the measured travel time by the logging instrument. This improvement includes anisotropic corrections for relative dip angles and the compensation for drilling fluid substitution effects.

2. The second major contributor to the error in final velocity is the error in density measurement.

3. Error in water saturation has a larger impact when substituting partial fractions of the original fluid with the new fluid. This is especially true when the substituting fluid remains a minor component (less than 50% by volume) of the final fluid. Therefore when substituting original fluid containing two or more components, improving the accuracy of Sw estimates is a key step in reducing error in total error in final velocity.

4. Uncertainty in porosity measurement (when using an independent instrument) and the uncertainty in volume of shale are minor contributors to the total error in final velocity.

4.3.2 Synthetic Model : Part 2

The objective of part 2 of synthetic modeling was to determine the variation in the error curves over a range of velocities (or over a range of velocity-density trend) . The rock type used for the synthetic model was water-saturated sandstone with following rock properties.

	Minimum	Maximum
Vp (Km/s)	3.13	5.52
Vs (Km/s)	1.73	3.6
Density	2.09	2.64

The volume of shale for this sandstone was assumed to be 10% to account for presence of minor quantities of shaley material in the rock matrix.

A linear velocity-density relationship was established using the values shown in the table to create set of 240 data points covering the range defined by minimum and maximum values. This water saturated sandstone was subject to fluid substitution with the constraint that 90 % of the original fluid is substituted . The fluid properties used in this substitution are given below.

	Brine (Original fluid)	Hydrocarbon (Sub. Fluid)
Bulk Modulus (GPa)	3.35	1.50
Density (g/cc)	1.00	0.80
Error in Bulk Modulus (%)	5.00	5.00

The results of the synthetic model over a velocity-density range are given below. A fixed uncertainty range for the petrophysical parameters was used as given in section 3.9 for the entire velocity-density range.

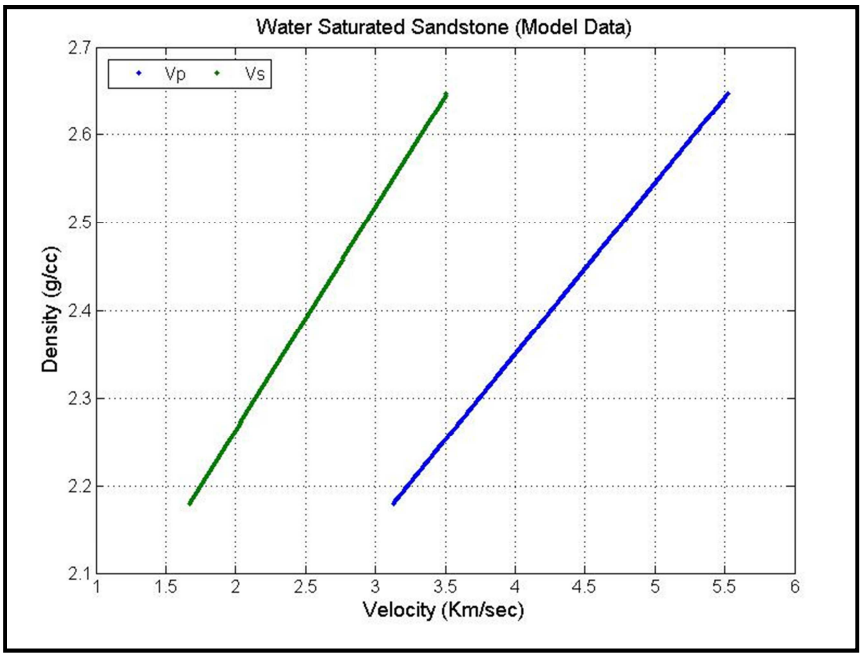

Figure 11 shows the linear velocity-density relationship used for synthetic fluid substitution model.

4.3.2.1 Effect of error from travel time (delta T) on fluid substituted velocity

As observed from the results from the first part of the synthetic modeling, the RMS error in measured travel time is the largest contributor to the total RMS error in the fluid substituted velocity. Using a fixed RMS error value of ± 5% in the travel time over the range of velocities, the error in the new saturated bulk modulus was initially calculated. This was followed by propagating the error in the new saturated bulk modulus to the velocity calculation to compute the RMS error in the new fluid substituted velocity. Figure 12 below shows the error curves for the new saturated bulk modulus.

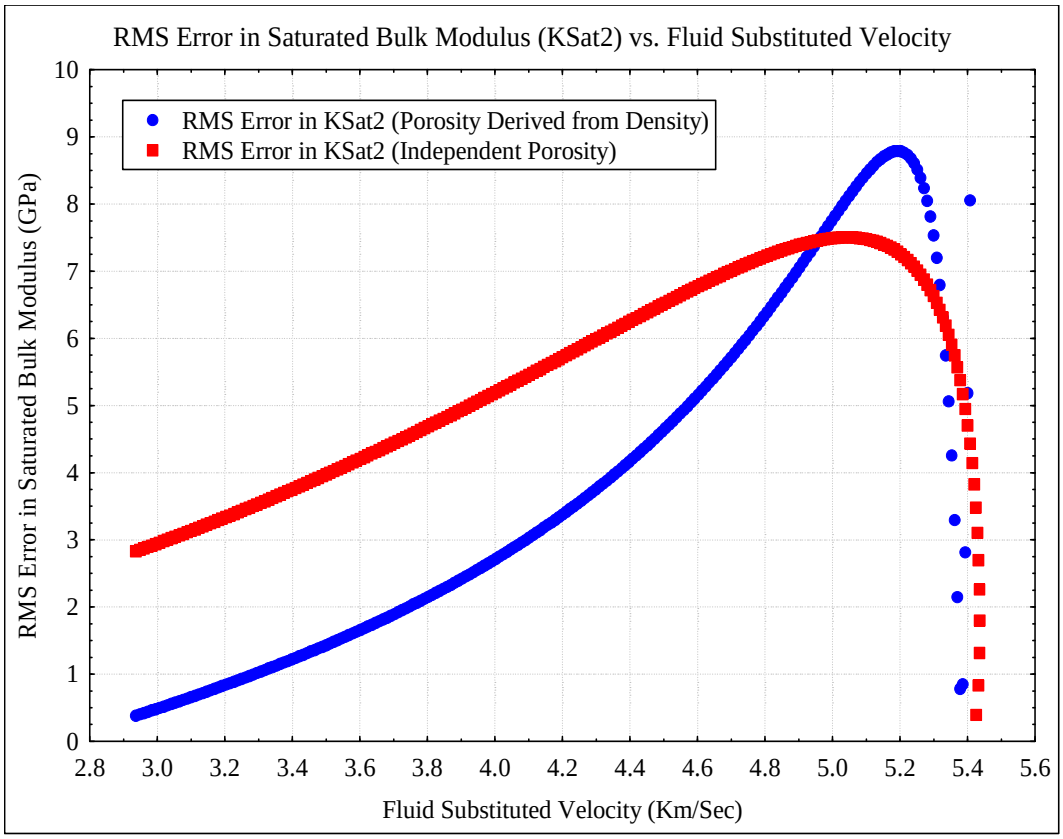

Figure 12 shows the errors in the saturated bulk modulii over the fluid substituted velocity range. The variation in the errors in the saturated bulk modulus over the entire velocity range is shown for two cases. i.e. when the porosity is derived from the density measurement and when an independent porosity measurement is available.

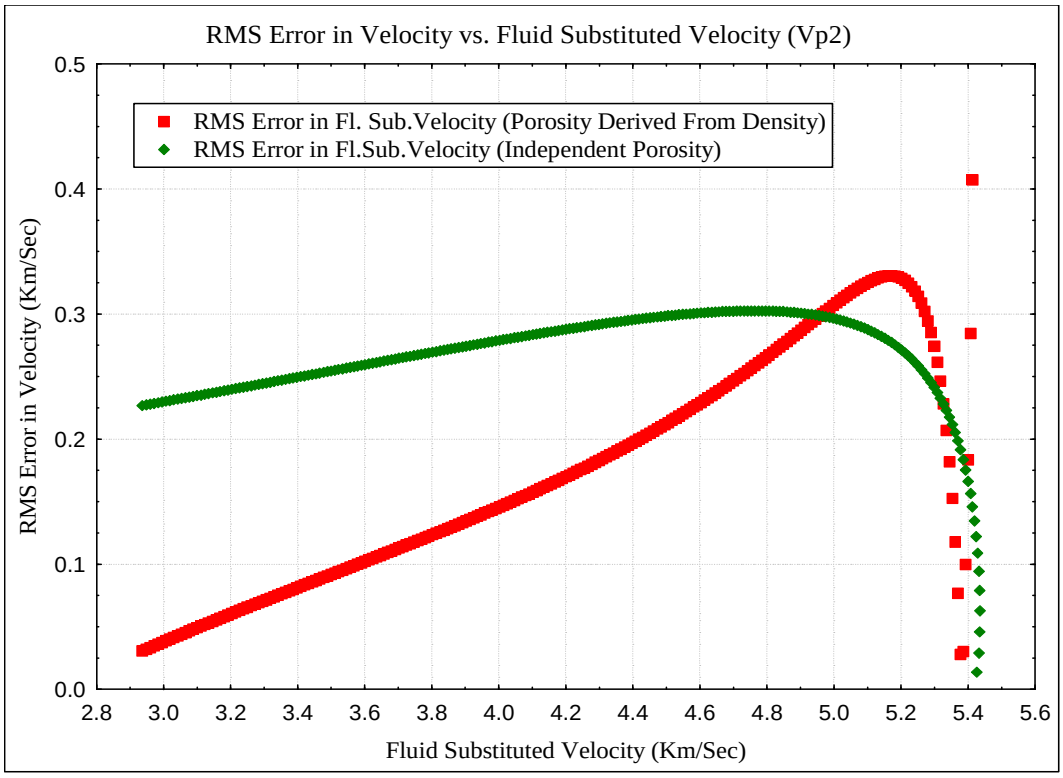

Figure 13 shows the RMS error in the new velocity for the two cases i.e. when the porosity is derived from the density measurement and when an independent porosity measurement is available.

4.3.2.2 Effect of error from bulk density (RHOB), volume of shale (Vsh) and water saturation (Sw) on fluid substituted velocity

RMS error in the new velocity was calculated for each of the petrophysical parameters described above. In this calculation only single parameter error was applied for a single iteration while keeping the errors for remainder of the parameters at zero. This process for repeated for each of the petrophysical parameters. A combined graph of the RMS error contribution from each of the petrophysical parameters is shown in figure 14.

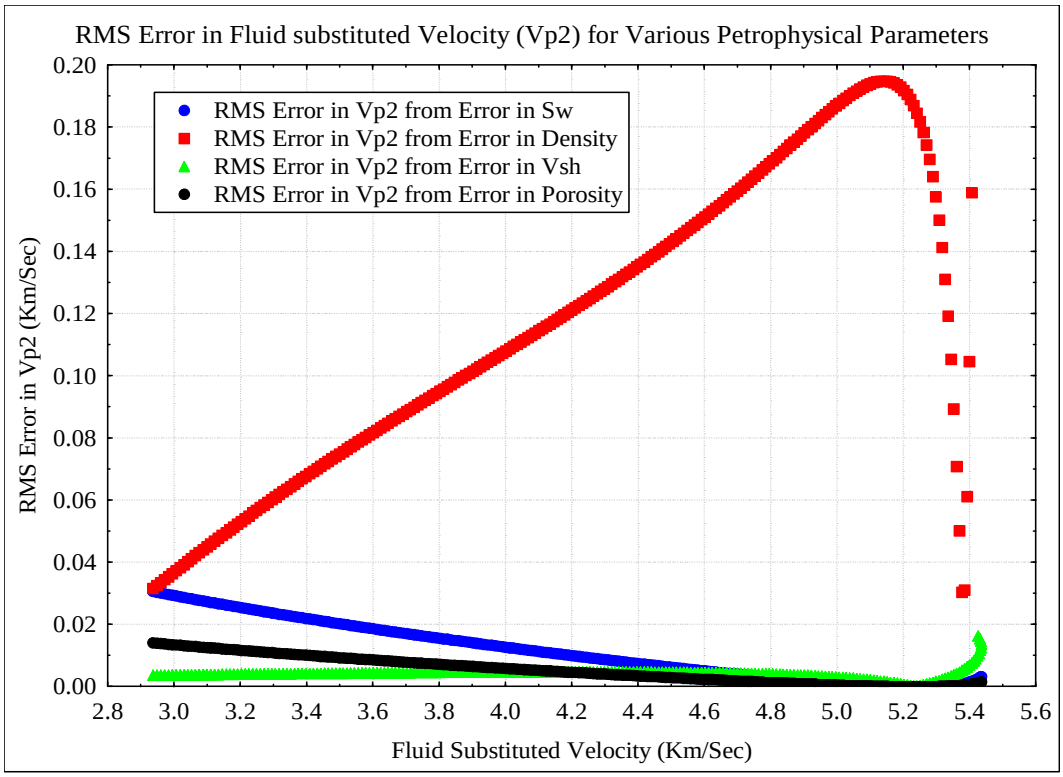

Figure 14 shows the RMS errors in the new velocity which have been calculated for each of the input petrophysical parameters. In addition to the RMS error curves resulting from errors in Sw and Vsh, the two other cases are presented for errors in density measurement (i.e. porosity has been derived from density) and for the combined contribution of density and porosity (i.e. when the porosity is an independent measurement. The two cases represents instances when the porosity is derived from the density measurement and when an independent porosity measurement is available.

Following conclusions can be drawn from the results of the modeling from part 2.

1. In general, the total RMS error in the new velocity increases with increase in the new velocity. Although this increase in the RMS error could be attributed to using a constant uncertainty value for the measurement over the entire velocity (and density) range, in reality this is unavoidable. Parameter uncertainty values tied to the measured data value are rarely available. Therefore in most cases it is only possible to utilize a single value for parameter uncertainty which is applicable over a large range of measurements.

2. This model assumes that at high velocities (and high density) the porosity value is proportionally reduced as derived from the Wyllie's equation. This would be a reasonable assumption in most cases. As a result, the calculation of errors in new velocity becomes unstable at very high velocities (and low porosities) especially when the new saturated bulk modulii value equals or exceeds the effective mineral modulii.
3. The primary contributors to the total error in the new velocity is the delta T and the density measurement. It is important to predetermine the density-porosity relationship as accurately as possible in order to reduce propagated errors in the final velocity. As an example, if an independent porosity measurement is available, it should be used in lieu of generic porosity estimation the density measurement.
4. RMS errors in Sw and Vsh generally have a lower contribution in the overall RMS errors in the new velocity. This is especially true for Sw when dealing with reservoir properties having low porosity. RMS errors in Sw may have a higher effect when dealing pores that are partially saturated with gas and liquid hydrocarbons.

4.4 Determining RMS error in fluid substituted velocity on actual data set

4.4.1 Review of input data used in this study

Detailed description of petrophysical and elastic parameters used in this study is given in chapter 3. I briefly state the data that was used in this study for the purposes of demonstration of the results.

4.4.2 Well logging data used in this study

The methodology as developed in this study was tested on logging data from the two wells drilled in the Gulf of Mexico and have been identified below.

S/N	Well Name	API Number	Depth Interval (ft)		Water Depth (ft)	Data available
			From	To		
1	GC 782-1	608114026100	17095	20268	4423	Den,Res,GR,DTP,DTS
2	GC 782-1 ST03BP00	608114026103	14596	20362	4420	Den,Res,GR,DTP,DTS

4.4.3 Fluid properties for original and substituted fluid

The hydrocarbon-bearing sands were targeted for determining the errors in the fluid substituted velocity using the Gassmann's equation. The API value and the gas gravity for the hydrocarbon was assumed to be 45 and 0.6 respectively. It was assumed that over 90% of the original hydrocarbon fluid was substituted with brine. This allowed assigning errors in water saturation for both the original and the substituted fluid.

4.4.4 Results of the uncertainty calculation study on actual data set

The total RMS error in the fluid substituted velocity was calculated for the two wells using individual parameter uncertainties as shown in section 3.9. The uncertainties in the section 3.9 represents a common set of uncertainty values that can be assigned to petrophysical parameters for most cases and can therefore be considered to be standard set of errors. Individual parameter error may be greater or lower than the stated value depending on the specific cases. The mean RMS error in the new velocity for all depth levels was computed to be around ~190 m/s with an standard deviation of ± ~20 m/s. It is important to remember

here that the uncertainty value for each input petrophysical parameter was kept constant during the entire calculation. This assumption may not always be true and therefore the resultant errors in the fluid substituted velocity may show a larger variation than that observed in this study.

The RMS error in the new S velocity value as a result of the fluid substitution process is very small to negligible and can be ignored in most cases. The S velocity is only affected by the changes to the rock bulk density as a result of the changes in the density of the pore fluid. Therefore unless the fluid substitution process involves replacement of gas, the impact on new rock bulk density is small which in turn has a minimal effect on the new S velocity .

As mentioned earlier, the final RMS error value at each depth level does not indicate that the data would randomly lie anywhere between the upper and lower RMS error bounds for that depth level. It does however indicate that given the systematic bias in the input data, it is possible that the computed data may be deviated from the true value by a maximum amount equal to the RMS error value. One of the difficult problems in application of this study is to determine the direction and the actual amount of systematic bias in the data and this is only possible with repeated data measurements using with different sets of instruments in order to determine the direction and the amount of bias in the data.

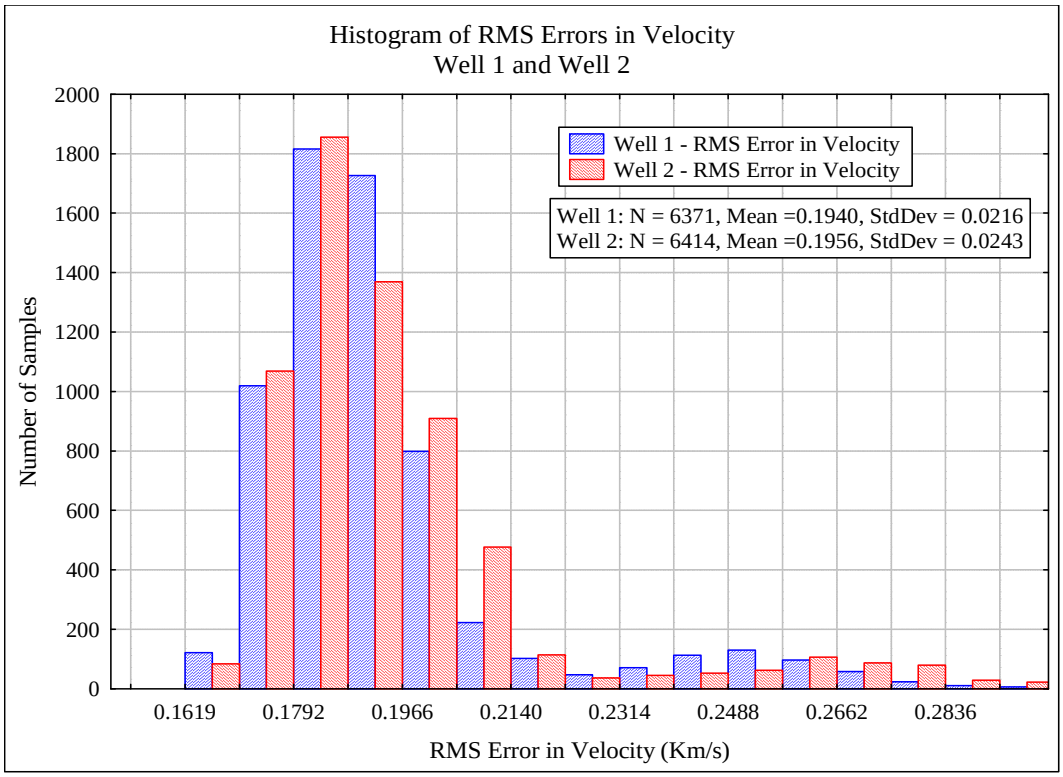

Figure 15 shows the histogram of RMS errors calculated at all depth levels for well 1 and well 2.

Following the calculation of total RMS error in the new velocity, error contribution from each petrophysical parameter was calculated for the hydrocarbon-bearing depth intervals. The intent behind selecting only the hydrocarbon-bearing intervals was to allow estimation of error contribution from the water saturation parameter. Figures 16 and 17 illustrate the contributions of individual petrophysical parameters for the two wells.

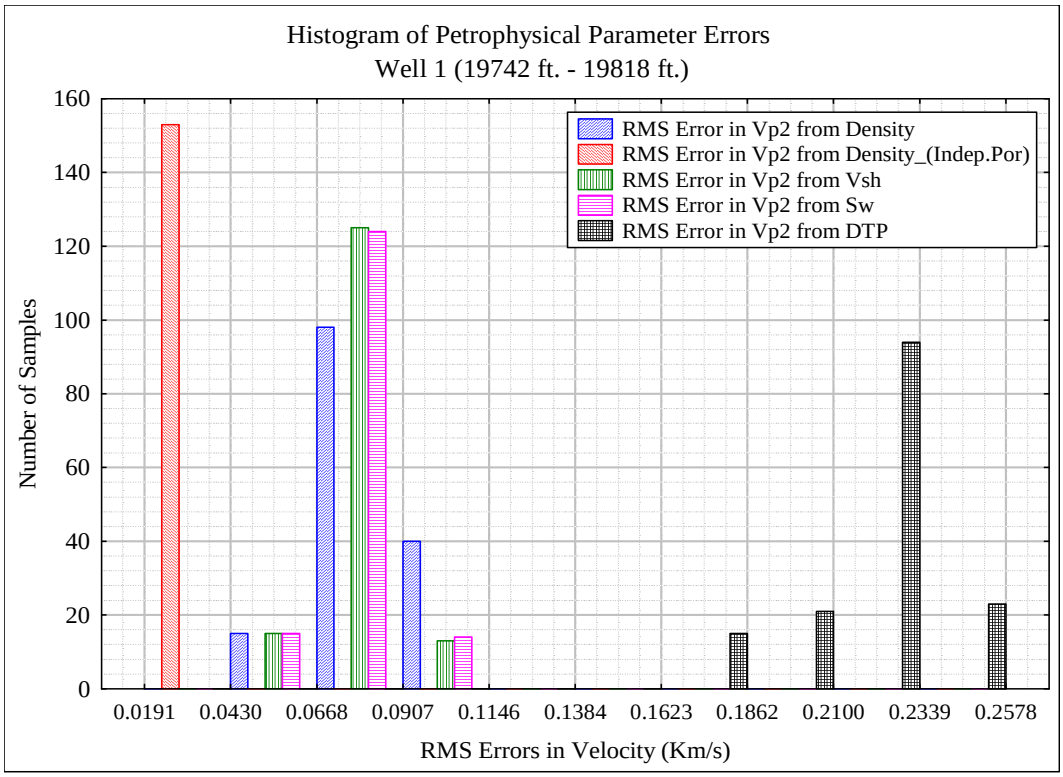

Figure 16 shows the histogram of error contribution from individual petrophysical parameter for the hydrocarbon-bearing interval for well 1. The error term for "Indep.Por" within brackets indicates that the error for the porosity term was separately assigned and kept independent of error propagation from the density term.

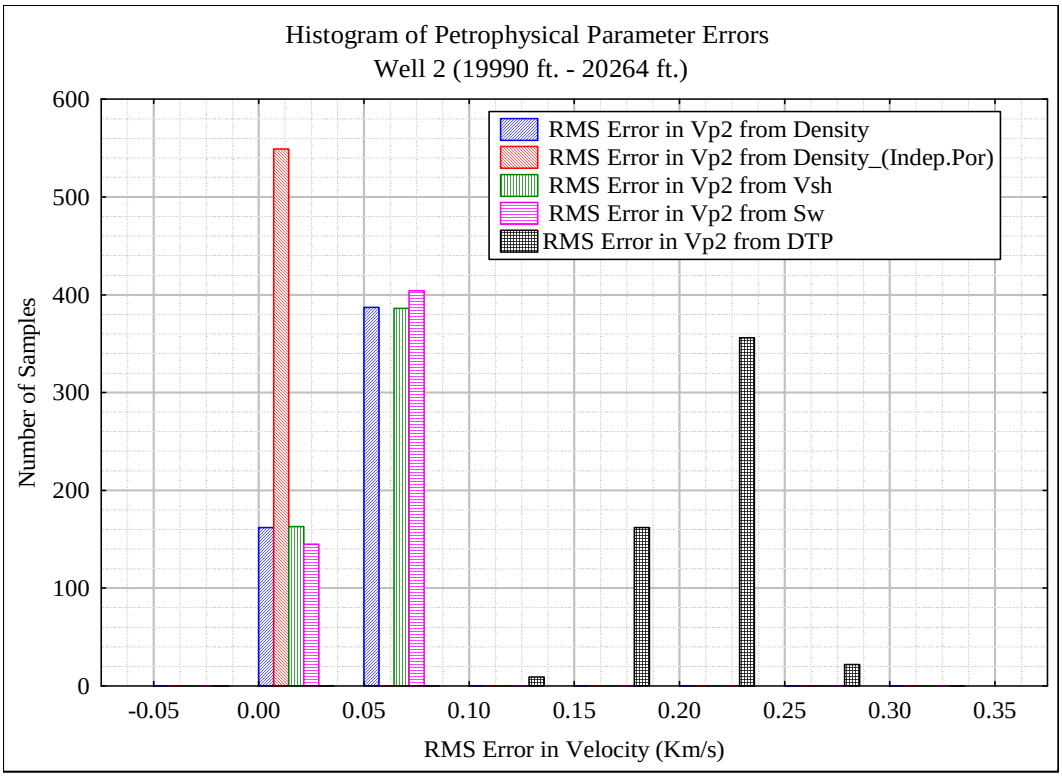

Figure 17 shows the histogram of error contribution from individual petrophysical parameter for the hydrocarbon-bearing interval for well 2.

4.4.5 Conclusions of uncertainty calculation on actual data set

The following conclusions can be drawn from the uncertainty calculation performed using an actual data set.

1. As would be expected, the uncertainty in the original velocity can be the largest contributor of uncertainty in the fluid substituted velocity. In this study, the measured travel time curve has been assigned an uncertainty value of ± 5% at 1σ confidence. If the study area has multiple measurements of velocity, it is possible to reduce the uncertainty value of the velocity and thereby significantly reduce the RMS error in the new velocity. Any edits or corrections that can be applied to the measured travel

time measurements will therefore have the largest effect in lowering the uncertainty in the fluid substituted velocity.

2. The velocity errors from density, porosity, water saturation, and volume of shale overlap each other. This makes it difficult to determine the causes of errors in new velocity and attribute the causes to a specific parameter.
3. Uncertainty values for parameters such as water saturation are difficult to determine. This is especially true for mixed lithologies such as shaley sands. In this study, I have used an uncertainty of 20% for the water saturation for both the original and the substituted fluid. However in the presence of gas, the uncertainty value assigned to Sw may not correctly account for the error in the new velocity. In such cases, the uncertainty value for oil saturation would have to be separately assigned in addition to the uncertainty in water saturation while calculating the uncertainty in the fluid modulus. Additionally confidence ellipses can be calculated to determine quality of a parameter can be used. Use of confidence ellipse has been previously described in section 2.4.3. Figure 18 shows confidence ellipses drawn for Sw curves calculated using two different methods and using two sets of porosities for the same depth interval. Both ellipses have been drawn at 95% confidence levels. From the figure it is apparent that the Sw calculation using mixture shaley sand model is better constrained than the Sw calculation using Archie's method. Therefore choosing the Sw curve calculated from the former model would have lower parameter uncertainty than the latter.

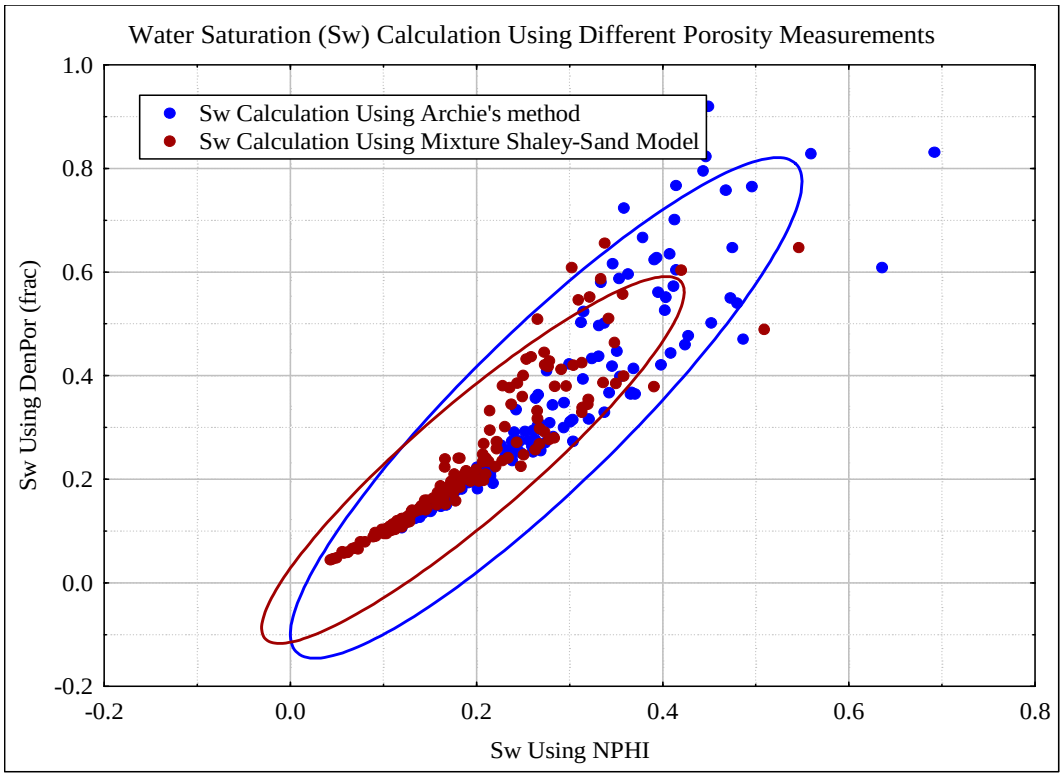

Figure 18 shows water saturation (Sw) calculation using two models calculated using two separate porosity curves. The calculation was performed for well1 in the hydrocarbon-bearing section from 19742 - 19818 ft. The confidence ellipses constructed for the two data sets are for 95% confidence level. The Sw calculation using the mixture shaley sand model is better constrained.

4. Using an independent measurement of porosity can help in reducing the total RMS error in the velocity calculation. In this study, and due to limited data availability, I did not use a independent porosity measurement. I however assigned a separate uncertainty value of ± 5% for porosity term derived from the density measurement. Similar to the uncertainty in the water saturation calculation, the uncertainty in the porosity parameter can also be difficult to determine in mixed lithology. Better constraining the porosity parameter may help in reducing the uncertainty value assigned to the porosity term by ignoring the porosity component resulting from clay-bound water. A combination of different methods of porosity measurements may

help in determining effective porosity which can used in lieu of total porosity especially in mixed lithologies.

4.5 Amplitude variation with offset

The complete solution for the amplitudes of transmitted and reflected P and S waves for both incident P and S waves is given by Zoeppritz (1919) equations (Castagna, 1993). Although Zoeppritz equations can be evaluated numerically, it is useful to use simpler approximations. Several authors have presented approximations to the Zoeppritz equations. The isotropic form of the AVO technique stems from the study of Ostrander (1984) who showed that the P-wave data could be used to detect changes in the velocity ratio at an interface. The classical AVO equation for two isotropic media with elastic properties and moderate incidence angles can be written as

$$R_{PP}(\theta) \approx R_{P0} + B \sin^2\theta + C(tan^2\theta - sin^2\theta)$$

where

$$A \approx \frac{1}{2}\left(\frac{\Delta V_P}{V_P} + \frac{\Delta\rho}{\rho}\right), B \approx \frac{1}{2}\left(\frac{\Delta V_P}{V_P} - 2\frac{V_S^2}{V_P^2}\left(\frac{\Delta\rho}{\rho} + 2\frac{\Delta V_S}{V_S}\right)\right), \quad C = \frac{1}{2}\frac{\Delta V_P}{V_P}$$

$\Delta V_P = V_{P2} - V_{P1}, \quad \Delta V_S = V_{S2} - V_{S1}, \quad \Delta\rho = \rho_2 - \rho_1,$ and $\theta = (\theta_2 + \theta_{1)}/2,$ but θ is often approximated by θ_1.

This form of the equation can be interpreted in terms of different angular ranges (Castagna, 1993). In the above equation R_{P0} is the normal incidence reflection coefficient expressed by

$$R_{p0} = \frac{I_{P2} - I_{P1}}{I_{P2} + I_{P1}} \approx \frac{\Delta I_P}{2I_P} \approx \frac{1}{2}\left(\frac{\Delta V_P}{V_P} + \frac{\Delta\rho}{\rho}\right) \qquad -6.1$$

The parameter B describes the variation at intermediate offsets and is often called the AVO gradient and the parameter C dominates at far offsets near the critical angle. As mentioned

earlier, I compared the effects of errors in the fluid substitution results on the amplitudes of synthetic traces with the assumption that there is a good equivalence between the reflection coefficients and the observed amplitudes.

4.6 Limitation of the results from AVO modeling

Comparison of observed AVO signature with synthetically modeled data can be useful in distinguishing between real and artificial AVO responses. In this study I calculated the uncertainty in the fluid substituted velocity which in turn introduces error in the synthetic AVO model. In addition to the errors in synthetic models, the observed data may also be imperfect as a result of acquisition and processing errors. I therefore state two potential limitations of using synthetic AVO models to directly compare the results of the synthetic models to observed data.

4.6.1 Lack of equivalence between reflection coefficient and reflection amplitudes

Although reflection coefficients are dependent upon contrasts of physical properties across isolated subsurface reflectors however the reflection amplitudes depend on wide range of factors. Castagna et al., (1993) lists several factors affecting seismic amplitudes . Some of the key factors that distort reflection amplitudes are coupling and random noise, divergence and transmission losses of seismic energy, inelastic attenuation, interference by neighboring reflections, multiples, etc. Presence of these factors add to the complexity of AVO processing. As a result of these factors, the seismic reflection amplitudes observed on real data may not be directly equivalent to the reflection coefficients.

4.6.2 Effect of anisotropy

Thomsen (1988) demonstrated the effects of VTI anisotropy on AVO. The AVO gradient (parameter B) can be reversed by anisotropy and hence can significantly change the classification of AVO anomaly. If the overburden consists predominantly of shales or clay, then VTI anisotropy also means that the phase angle (necessary for calculating reflectivity) and group angle (for geometric ray path) are not identical (Macbeth, 2002). The P-wave reflection coefficient for weakly anisotropic VTI media in the limit of small impedance contrast is given by (Thomsen, 1993)

$$R_{pp}(\theta) = R_{pp\ Iso}(\theta) + R_{pp\ Aniso}(\theta).$$

The reflection coefficient for isotropic media remains unchanged as shown in the equation 6.1, however the reflection coefficient for anisotropic media is now controlled by the Thomsen parameters namely δ and ε is as shown in equation 6.2

$$R_{pp\ Aniso}(\theta) \approx \frac{\Delta\delta}{2} sin^2(\theta) + \frac{\Delta\varepsilon}{2} sin^2(\theta) tan^2(\theta). \quad -6.2$$

The parameter delta controls the AVO behavior at small to moderate angles and can take both positive and negative values.

Therefore even if the systematic errors in the input data and its effect on fluid substituted velocity is completely understood, the differences between the actual and modeled AVO curves cannot be attributed only to the presence of systematic errors in the input data. Therefore presence of VTI anisotropy may either work in masking or in enhancing the errors when comparing modeled versus actual reflection coefficients even in cases when the systematic errors are well understood and accounted for.

4.7 Procedure to calculate synthetic AVO model

This section describes the procedure to build the synthetic AVO models for the fluid substituted impedance curve and its upper and lower bounds. This would allow an comparison of the amplitudes of the traces in order to confirm the impact of error present in the wireline data set that is commonly used for fluid substitution modeling. I used the following steps to calculate the synthetic AVO models.

4.7.1 Calculating impedance curves

The computed error in the fluid substituted velocity for each of the wells was used to determine its impact on synthetic AVO modeling. To do this, I computed the impedance curves and the reflectivity series for three cases, namely the fluid substituted impedance and its upper and lower bound. I used the following parameters and naming convention to identify impedance curves for the three cases. The three cases represent the worst cases wherein the contributions of all errors act in the direction so as to add to the total error.

Case 1 : Fl.Sub_Impedance = $V_{p2} \times RHOB_2$

Case 2 : Fl.Sub_Impedance_Min = $V_{p2\_Min} \times RHOB_{2\_Min}$

Case 3 : Fl.Sub_Impedance_Max = $V_{p2\_Max} \times RHOB_{2\_Max}$

4.7.2 Application of Zoeppritz equations

Following the computation of impedance curves, the amplitudes at different angles of incidence (up to a maximum of 30 deg) was determined by using the Zoeppritz equations. For this study I used the Hampson-Rusell software to compute the synthetic traces for incidence angles up to 30 deg by convolving the reflectivity series with a 70 Hz Ricker wavelet. To determine the impact of errors in synthetic AVO modeling, I compared the differences in the

amplitudes of the synthetic traces created from the fluid substitution process and its upper and lower bound. As indicated earlier in this document, the data error bounds do not indicate that the data will randomly lie anywhere within the upper and lower bounds but it does point to the possibility that the synthetics generated using the logging data may produce an anomalous AVO response and should be taken into consideration when comparing it to the observed data.

4.7.3 Comparisons between synthetic AVO responses

For purposes of this comparison I selected a hydrocarbon-bearing sand section of sufficient thickness that showed a strong impedance contrast and also shows a reflection from both top and bottom of the reservoir. The presence of hydrocarbon was notionally interpreted using the resistivity log.

I show the differences in the amplitudes for the synthetic AVO models created for the impedance contrast and its upper and lower bounds using equations shown in 4.5.1. Also shown in figures 20 and 22 are the differences in amplitudes for the hydrocarbon-bearing sands in the two wells.

Example 1: Hydrocarbon-bearing sand from well 1

I have compared the variation in AVO response in a hydrocarbon-bearing sand at nominal depth of 20000 ft and which is clearly marked by a strong impedance contrast at the top and the base of sand. The synthetic traces shows a peak on top of the hydrocarbon-bearing sand followed by a trough at the bottom of the sand as is expected. The marked dotted lines in figure 19 were used as depth markers in order to compute and compare the amplitudes of the synthetic traces. The amplitudes of the synthetic traces have not been corrected for normal moveout.

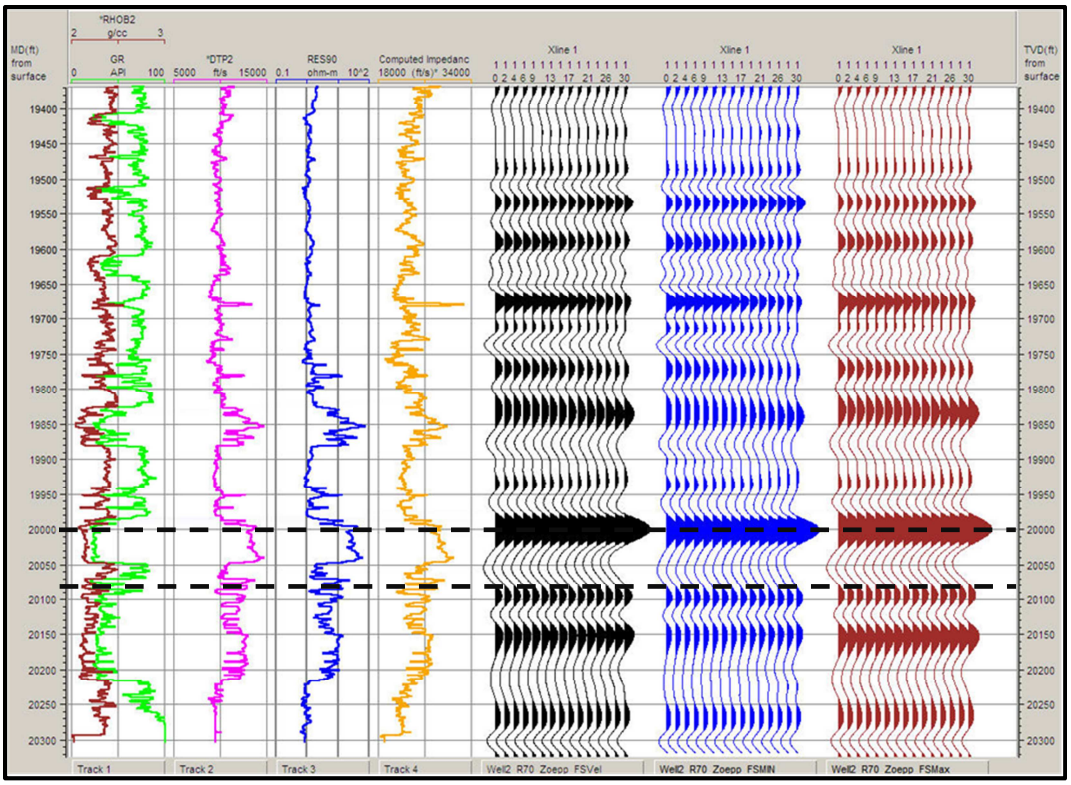

Gamma Ray & Density | Delta T (New) | Res | Impedance | AVO Synthetics. Fl. Sub Vel. | AVO Synthetics Lower Bound | AVO Synthetics Upper Bound

Figure 19 shows the synthetic AVO model with synthetic traces created for incidence angles up to 30 degrees using the Zoeppritz equations. The hydrocarbon-bearing reservoir at 19990 ft (indicated by dotted lines) shows a strong impedance contrast and is therefore chosen to compare differences in AVO response resulting from errors in the fluid substituted velocity. The suffix of upper and lower bound indicates AVO synthetic traces created using velocity and density bounds as indicated in figure 20.

Figure 20 shows the amplitude variations with angle of incidence for the three synthetic traces seen in figure 19.

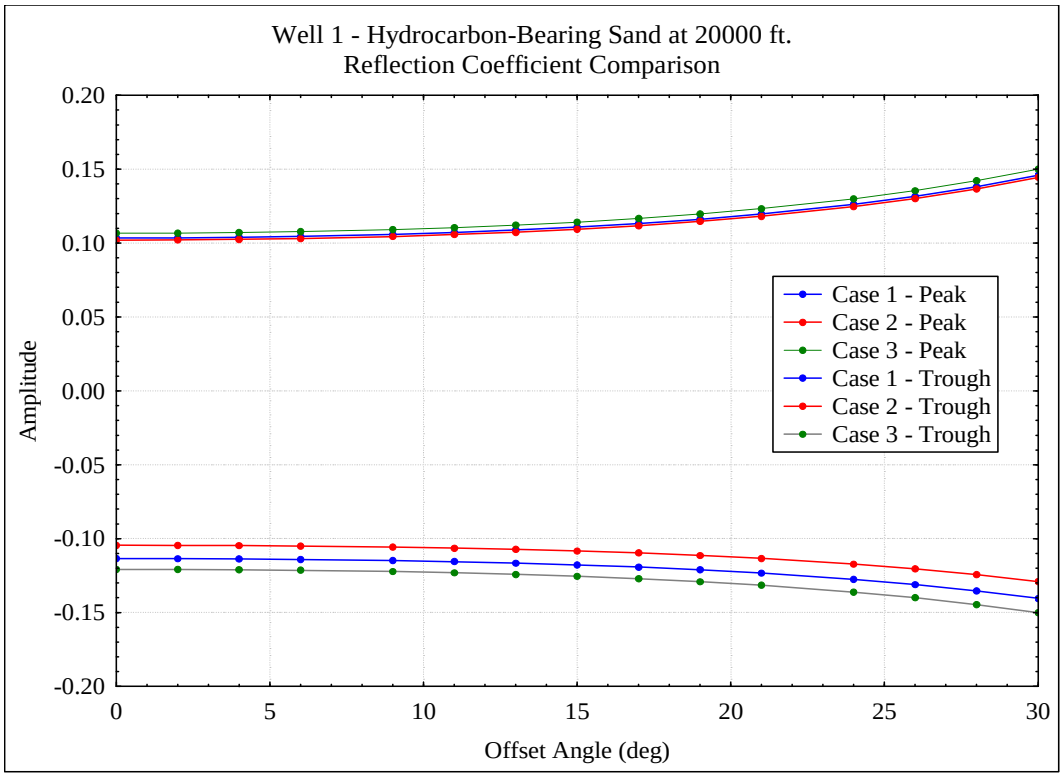

Figure 20 shows the differences in amplitudes in the synthetic AVO models for the new impedance contrast and its upper and lower bounds for the top and bottom of the hydrocarbon-bearing. The amplitude curves for the top of the hydrocarbon-bearing interval which represents the peak of the seismic wavelet shows a smaller range of uncertainty bounds in reflection amplitudes as compared to the range of uncertainty bounds for the trough of the seismic wavelet at the base of the hydrocarbon-bearing interval. The cause of this difference may be attributed to a relatively strong impedance contrast at the base of the reservoir as compared with the top of the reservoir.

Example 2: Hydrocarbon-bearing sand from well 2

Similar to the first example for well 1, I have compared the variation in AVO response in a hydrocarbon-bearing sand at nominal depth of 19850 ft and is marked by a strong impedance contrast at the top and base of sand. While the first example serves as a good indicator of the impact of the errors in the new velocity determined by Gassmann fluid

substitution on the AVO synthetics, the second example confirms the results for a similar hydrocarbon-bearing interval and is presented here for completeness.

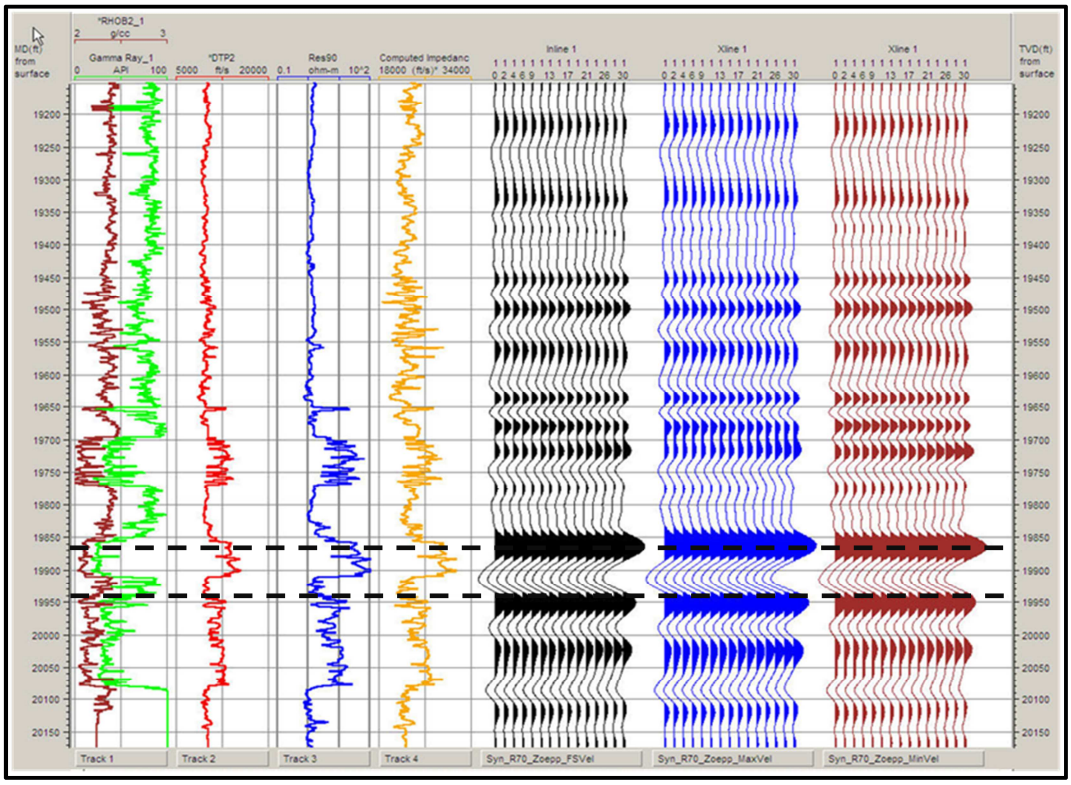

Figure 21 shows the synthetic AVO model with traces created for incidence angles up to 30 degrees using the Zoeppritz equations. The hydrocarbon-bearing reservoir at 19850 ft (indicated by dotted lines) shows a strong impedance contrast and is similar to the first example from well 1.

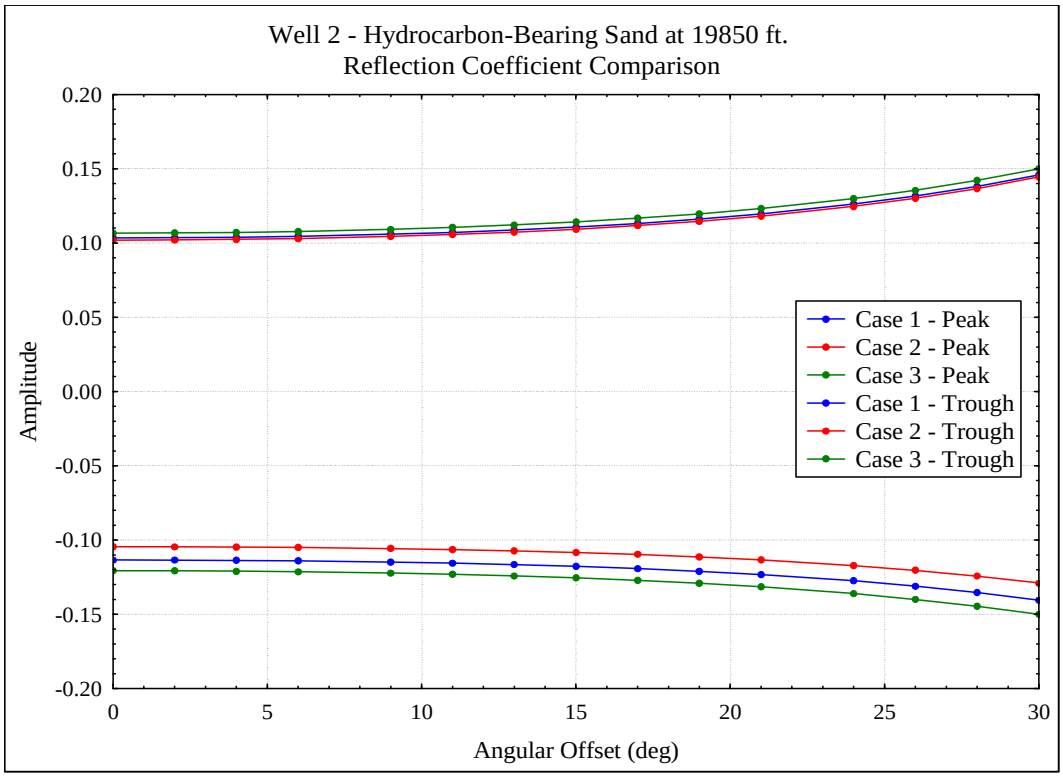

Figure 22 also shows the differences in amplitudes in the synthetic AVO models for the new impedance contrast and its upper and lower bounds for the top and bottom of the hydrocarbon-bearing for well 2.

4.8 Conclusions from this study

The synthetic modeling and calculation using actual data demonstrates the impact of propagation of errors from the petrophysical parameters to the fluid substituted velocity and on the synthetic AVO modeling. While it is possible to quantify the RMS errors in the velocity by using reasonable estimates of parameter uncertainty, the determination of the direction of systematic biases in the input data remains a difficult problem. For some inputs, it is possible to generate a parameter uncertainty curve over the logging interval. Using depth based uncertainty data should be encouraged rather than using a single uncertainty value over the entire depth range. The results of this study emphasizes the role of quality control during

the data acquisition phase, selection of appropriate petrophysical models, data correction, and during subsequent data processing. This is especially important when determining the petrophysical parameters that are used in the fluid substitution modeling. When comparing synthetic AVO models with observed AVO data it is possible that the perfect match between the two could be a result of a false positive match (or lack thereof) which could be a result of combination of uncertainties in the synthetic model as well as in the processing of the observed data set. By calculating the uncertainty curves for reflection coefficients can be helpful in improving the confidence in the AVO response comparison study. This study also serves to reiterate the importance of petrophysical data integration and data quality control into the fluid substitution processes in order to assist with interpretation.

4.8.1 Estimating logging data accuracy requirements

The results derived above show considerable influence of logging data error propagation in the Gassmann's fluid substitution. Although in some cases the errors may appear to be exaggerated and may not seem to be significant observation, it is important to note that some of the differences between predicted and actual velocities may come from errors in the logging data. The question now arises is, whether it is possible to estimate the required logging data accuracy to reduce uncertainty in the predicted velocities. This would actually be a reverse of the process that has been described above. To explain this further, if we knew the maximum standard deviation of the K_{Sat} parameter that can be tolerated, what would be the maximum RMS error of the logging data that would be required. Yardley Beers (1958) quotes the following formulas that can be used to make this calculation.

Suppose the value of σ_{KSat} (standard deviation of K_{Sat}) has been computed by using average data from 10 measurements for bulk density and velocities in a formation. By simple

averaging the 10 measurements we assumed that the contribution of each of the individual measurement is equal. This implies that all 10 measurements were conducted in similar logging environment where the hole or logging conditions were similar and therefore their error contributions are equal. To obtain the required standard deviation in K_{sat}, the standard deviation for bulk density and the acoustic velocities can be computed as follows.

$$\sigma_{\rho_b} = \frac{\sigma_k}{\sqrt{N}\frac{\delta K_{sat}}{\delta \rho_b}},\ \sigma_{V_p} = \frac{\sigma_k}{\sqrt{N}\frac{\delta K_{sat}}{\delta V_p}},\ \sigma_{V_S} = \frac{\sigma_k}{\sqrt{N}\frac{\delta K_{sat}}{\delta V_S}}$$

Therefore by reducing the error in the original computation of saturated bulk modulus can help reduce the propagation of error throughout the Gassmann's fluid substitution process.

4.8.2 Suggested future work

While it is well known that the uncertainties in the input parameters can have a impact on subsequent computed results, the contribution of the individual error component in the final error value still needs additional study using large data set. Additionally, the integration of petrophysical models for shaley sand analysis in the fluid substitution is much less understood outside the petrophysical community. This however has a direct impact on rock physics modeling. Most of the current literature on the Gassmann fluid substitution refers to fairly simple models to in order to determine the input parameters used in the calculation. As an example, most literature limits the calculation of water saturation calculation to the Archie's equation or using simple transforms for porosity which may not give accurate results in mixed lithology. Additional deterministic studies using are required to understand the variation in the fluid substituted velocities as a result of varying data

uncertainty values and lithology over the logging interval. Rapidly changing parameter uncertainty values may result in variation in the phase of the synthetic traces generated in AVO modeling. Deterministic error calculation using partial fluid saturation or in multi fluid phases with partial gas saturation would be another area of interest. Additional statistical methods to identify the parameter(s) that play a major role in the overall uncertainty in the result with changing parameter uncertainties would also be an area of interest. Additionally this analytical study can also be performed using Monte Carlo statistical technique which would be an additional area of interest.

Appendix A - Chapter 5

5.1 Introduction

Appendix A describes the procedure used to compute the petrophysical and the linearly elastic parameters. Materials are called linear elastic when stress is proportional to strain and are related by Hooke's law. As an example, bulk and shear modulii can be described for linear elastic materials. Bulk modulus 'K' is defined as the ratio of hydrostatic stress to volumetric strain while the shear modulus 'μ' is defined as the ratio of shear stress to shear strain. Mavko et al. (2003) gives a detailed explanation of the moduli in terms of stress and strain tensors.

The logging data set contained gamma ray, bulk density, acoustic travel time, and resistivity data curves. These data were used to calculate the petrophysical parameters, namely porosity, volume of shale, and water saturation, which were followed by calculation of linearly elastic parameters such as the bulk and shear moduli of the saturated rock, bulk modulii for the mineral matrix, porous rock frame, and the pore fluid. I have described the methodology used to compute each of the individual parameters and are stated here as a table for quick reference.

No	Type	Parameter	No	Type	Parameter
5.2.1	Petrophysical	Porosity (φ)	5.3.3	Elastic	Bulk Modulus of Mineral Matrix(K_0)
5.2.2	Petrophysical	Volume of Shale (V_{Sh})	5.3.4	Elastic	Bulk Modulus of Porous Rock Frame(K*)
5.2.3	Petrophysical	Water Saturation(S_W)	5.3.5	Elastic	Bulk Modulus of Formation Fluid(K_{fl})
5.3.1	Elastic	Bulk Modulus of Saturated Rock (K_{sat})	5.3.6	Elastic	Bulk Modulus of Saturated Rock(K_{Sat2})
5.3.2	Elastic	Shear Modulus of Rock(G or μ)	5.3.7	Base	Velocity (Vp or Vs)

5.2 Calculating petrophysical parameters

This section describes the methodology used to compute the petrophysical parameters such as porosity, volume of shale, and water saturation.

5.2.1 Calculating porosity

Porosity was calculated from the density measurement. Independent porosity curves from neutron porosity measurements were available for two wells. However, neutron porosity measurements require a wide variety of environmental corrections for lithology matrix, borehole size, mud weight, salinity to name a few, in order to arrive at the final porosity value. This additional information related to type and nature of environmental corrections applied to the measurement was unavailable and therefore in order to maintain consistency, I used the density data at each depth point to arrive at the porosity measurement using the standard porosity equation stated below.

$$\phi = \frac{\rho_{grain} - \rho_{bulk}}{\rho_{grain} - \rho_{fluid}}. \qquad (5.1)$$

where

Φ = Porosity in fractions

ρ_{grain} = Matrix grain density (ρ_{grain})

ρ_{fluid} = Density of the pore fluid

ρ_{bulk} = Density of the rock as measured by the logging instrument

When the shale is present in the rock, using the above equation will result in calculation of either additional or reduced porosity. This error in porosity is a result of presence of shale with bulk density either lower or higher than the density of the dominant

mineral matrix . Presence of shale should therefore be accounted for in the bulk density of the mineral matrix (ρ_{grain}) used in the porosity calculation. This can be done by subtracting the erroneous porosity contribution by using the shale density and the shale volume fraction. This method is, however, subject to errors since it assumes that the density of shale is constant throughout the well and that the correction for erroneous porosity may not be linear as a function of the shale volume and it also depends on the type of shale. The structural shale, for example, can only be present as a replacement of the sand grains, while laminar shale replaces the sandstone portion of the rock and does not occupy or alter the intergranular sand porosity. Therefore knowledge of type of shale is required for true determination of effective porosity and is therefore a much more complex problem than that can be addressed simply by adjusting the total porosity for presence of shale.

The total porosity equation shown above, also assumes that the total porosity is the effective porosity and does not account for fluids contained in the clay mineral structure or the capillary bound water both of which are constituent of the total porosity but are termed as non-movable fluids. Presence of non-movable fluids violates the key assumption of Gassmann's fluid substitution which requires that the propagating stress wave must equilibrate instantaneously in the pore space.

One of the methods suggested by Dvorkin et al., (2010) considers porous wet shale as part of the solid grain material and excludes porosity within the shale from total porosity. However the computation of effective porosity as suggested in the above paper requires availability of data from advanced porosity instruments such as NMR and requires the determination of the porosity of clay term (φ_{clay}) for the calculation of effective porosity. This data was unavailable for the purposes of this study and hence I considered total porosity as

effective porosity and adjusted the effective porosity with cutoff values to account for errors in porosity due to the presence of shale.

5.2.2 Calculating volume of shale (V_{sh})

Natural Gamma ray measurement can be used as a basic clay indicator. It is important to note here that the terms clay and shale have been used interchangeably. The term clay is used for clastic rocks having particle size less than 1/256 mm while the term shale represents sedimentary rock showing laminations and fissile nature. Therefore a shale is a sedimentary rock composed of clay minerals and the term V_{sh} is used interchangeably to represent volumetric fraction of either clay or shale.

The volume of shale was computed using the gamma ray log which responds to the natural radiation of the formation. In the derivation of shale content, the assumption is that the radioactive component of the formation is shale. Thus increasing natural radiation implies increasing shale content. The presence of other radioactive minerals such as present in radioactive sands will cause the shale volume to be too high.

$$V_{sh} = \frac{GR_{\log} - GR_{\min}}{GR_{\max} - GR_{\min}} \tag{5.2}$$

where

GR_{log}= Gamma ray measurement

GR_{min}= Gamma ray measurement in a clean sand line

GR_{max}= Gamma ray measurement in a thick shale

The volume of shale computed using equation above is a linear approximation. However the gamma ray measurement may sometimes have a non-linear response to the clay

content of the rock. The volume of shale can therefore be corrected using the Steiber relationship for miocine-pliocine rocks (Hearst et al., 2000). The Steiber relationship for shale volume, adjusted for the age of the rock can be stated as

$$Vol.OfShale = \frac{Vol.OfShale}{a - b * Vol.OfShale}. \qquad (5.3)$$

Where, a = 3 and b = 2 for miocene-pliocene rocks.

Application of the Steiber relationship in order to determine the volume of shale would require reservoir level knowledge in order to assign accurate values for the 'a' and 'b' coefficients. I have therefore used the linear approximation for calculating the volume of shale.

5.2.3 Calculating water saturation (Sw)

Water saturation was computed using the standard Archie equation. The Archie equation is a total porosity - total water saturation relationship and is given by the equation

$$S_w = \left[\frac{aR_w}{\phi^m R_t} \right]^{\frac{1}{n}} \qquad (5.4)$$

where

R_w = Resistivity of water in filling the pores of the rock

R_t = True resistivity of the rock

Φ = Porosity (v/v)

a, m, n = Constants based on empirical data.

For well consolidated sandstones the typical values for 'a', 'm', and 'n' are 1, 2, and 2 respectively. Actual values of 'a', 'm', and 'n' are typically derived from core measurements. A wide variety of formulations have been used to model resistivity-water saturation relationships in shaley sands. Worthington (1985) describes over thirty shaley sand models

used to compute water saturation. The correct methodology to compute water saturation would involve defining the type of shaley sand model. The advantage of using a specific equation suitable in a particular field is to reduce the error in estimates of water saturation. Application of a specific shaley sand model would require additional information that is normally obtained from core data. In the absence of any core data, I have restricted the calculation of water saturation to using Archie's equation. While this restriction may increase the uncertainty in the value of water saturation, the exact computation using any of the other methods may not necessarily help reducing the uncertainty due to a large number of variables used and the complexity of the calculation. This topic is further explained in chapter 6.

5.3 Calculating linearly elastic parameters

This section describes the methodology used to compute the linearly elastic parameters such as the bulk modulii of the saturated rock, mineral matrix, fluids and the rock frame.

5.3.1 Bulk modulus of saturated rock (K_{Sat})

The bulk modulus of the rock was calculated using wireline data for the *in-situ* rock that is undrained of pore fluids. The well log data can be used to relate bulk modulus of a rock (K_{Sat}) to its compressional, shear velocity and bulk density through the following relationship which is simple to implement.

$$K_{Sat} = \rho_b \left(V_p^2 - \frac{4}{3} V_s^2 \right). \qquad (5.5)$$

where

ρ_b = Bulk density in g/cc

V_p = Compressional velocity in Km/sec

V_s = Shear velocity in Km/sec

K_{Sat} = Saturated bulk modulus in Gigapascals (GPa)

5.3.2 Shear modulus of rock (G or μ)

The shear modulus can be calculated from the form given by

$$G = \rho_b * V_S^2 . \tag{5.6}$$

where

G = Shear modulus in GPa

ρ_b = Bulk density of the rock (g/cc)

V_s = Shear velocity (Km/sec)

Berryman (1999) states that for purely mechanical effects, the shear modulus for the case with trapped fluids (undrained) is the same as that for the case with no fluid (drained).

$$\mu(undrained) = \mu(dry)$$

Therefore monitoring any changes in shear modulus with changes of fluid content provides a test of both Gassmann's assumptions and results. Throughout the process of fluid substitution the value of shear modulus of the rock (G) is kept constant.

5.3.3 Bulk modulus of mineral matrix (K_0)

To predict the effective elastic moduli of a mixture of grains and pores theoretically, we need to specify the volume fractions, elastic moduli of various phases and the geometric details of how the phases are arranged with respect to each other. If we specify only the volume fractions and the constituent moduli the best we can do is predict the upper and the

lower bounds (Mavko et al,2003). In order to predict the bulk modulus of mineral matrix, information about the composition of the rock must be available (Smith et al., 2003). The rock composition may be determined by various techniques such as thin section analysis of core samples or X-ray diffraction etc. Alternately, specialized wireline logs may be available which measure the elemental composition of the rock.

The actual rock composition data was not available for this study and hence I assumed a two mineral rock composition consisting of quartz and clay. To calculate the effective moduli I used the average of upper and lower bound value at a given volume fraction of clay. I used two approaches to calculate the upper and lower bounds, the first approach is the Hashin - Shtrikman bound and the other Voigt- Reuss bound. The Hashin-Shtrikman bounds for two phases are given by

$$K^{HS\pm} = K_1 + \frac{f_2}{(K_2 - K_1)^{-1} + f_1(K_1 + \frac{4}{3}\mu_1)^{-1}} \tag{5.7}$$

where

K_1, K_2 = bulk moduli of individual phases

$\mu_1, \mu_2,$ = shear moduli of individual phases

f_1, f_2 = volume fractions of individual phases

The above expression gives upper bound when stiffest material is termed '1' and lower bound when the softest material is termed '1'. The Voigt upper bound is defined as

$$M_V = \sum_{i=1}^{N} f_i M_i$$

where

f_i = Volume fraction of the i^{th} medium

M_i = Elastic modulus of the i^{th} medium.

The Reuss lower bound of the effective elastic modulus, M_R is given by

$$\frac{1}{M_R} = \sum_{i=1}^{N} \frac{f_i}{M_i}.$$

I have used the following constants for calculating the upper and lower bounds using both methods described above.

K_{quartz} = 37 GPa, μ_{quartz} = 45 GPa

K_{clay} = 15 GPa, μ_{clay} = 9 GPa

I have calculated the effective elastic modulii using both Hashin-Shtrikman and Voigt-Reuss methods, in the final computation I have only used the Voigt-Reuss method to compute the average effective modulii.

5.3.4 Bulk modulus of the porous rock frame (K*)

Prior to applying the Gassmann's relationship it is necessary to determine the bulk modulus of the porous rock frame. Bulk modulus of porous rock frame (K^*) can be computed using the equation shown below:

$$K^* = \frac{K_{Sat}\left(\frac{\phi K_0}{K_{fl}} + 1 - \phi\right) - K_0}{\frac{\phi K_0}{K_{fl}} + \frac{K_{Sat}}{K_0} - 1 - \phi}. \qquad (5.8)$$

where

ϕ = Porosity

K_0 = Bulk modulus of the mineral matrix

K_{fl} = Bulk modulus of the pore fluid

K_{Sat} = Saturated bulk modulus of the in-situ rock

The K* term is derived either from (i) velocity measurements on controlled humidity dried cores or (ii) application of empirical relationships or effective medium theory or (iii) from direct calculation from log data. (Smith et al, 2002). In the absence of core analysis data I calculated K* term directly from the log measurements. The implication of this calculation is that existing uncertainties in the log data are now propagated through the K* calculation.

The porous rock frame modulus is sometimes also termed as 'dry' rock modulus. This refers to the incremental bulk deformation resulting from an increment of applied confining pressure with pore pressure held constant. This corresponds to a drained experiment in which the pore fluids can flow freely in and out of the sample to ensure constant pore pressure. (Mavko, et al., 2003) As a note of caution, laboratory measurements on very dry rock can give incorrect results by lowering the frame moduli as a result of disrupting surface forces acting on pore surfaces. In view of this, slightly wet or drained measurement of K* should be used. (Smith et al,2002). This observation will assume importance when an independent value of K* obtained from core measurements is used rather than calculating this from the logging measurements. In this study, I have not directly used the parameter K* for uncertainty calculation because of the complexity of its dependence on several variables. The calculation of the parameter has been described for completeness.

5.3.5 Bulk modulus of formation fluid (K_{fl})

The bulk modulus of individual fluid phases can be calculated using the Reuss average. Since the fluids do not have shear moduli, the Hashin-Shtrikman lower bound is the

same as the Reuss bound (Mavko et al., 2003). I have assumed that the reservoir fluids consist of only two phases namely brine and oil. Volumetric fractions of the two reservoir fluids was determined by calculating the water saturation using the Archie's equation as described earlier. To calculate the bulk modulus of the reservoir fluid, information about the reservoir temperature, pressure, salinity and fluid type is required. In the absence of well specific information I used the following methodology to compute these parameters.

Reservoir fluid : The API value of the hydrocarbon component in the reservoir fluid was nominally set at 45 grade. If the density of the reservoir fluid is available the API value can be calculated using the API conversion formula given as $API = \frac{141.5}{\rho} - 131.5$, where ρ is density of oil measured at 15.6 deg C and at atmospheric pressure. The gas density was also nominally set at 0.6. These values were used to calculated the bulk moduli of the hydrocarbon used in the calculation.

Formation pressure: I used a hydrostatic pressure gradient of 0.465 psi/ft which is typical for offshore Gulf of Mexico (Dutta, 2002) to compute the properties of fluid bulk modulus.

Formation temperature: In the absence of formation temperature data from the wells, I used a temperature gradient of 1.1 deg F/100 feet. The temperature at the mudline for each of the wells was assumed to be 40 deg F.

Salinity of Brine: The salinity of the brine can be estimated by evaluating the resistivity of the brine at 100 percent water saturation. This is accomplished by using the Pickett plot method. (Hearst et al., 2000) Accurate estimates of formation temperature and pressure are required to be able to convert the water resistivity to the salinity of formation water. In the absence of formation temperature and pressure data value I assumed salinity value of 80000 ppm @ 77 deg F which is a typical value for the Gulf of Mexico (Dutta, 2002).

The fluid bulk modulus was calculated using the following equation

$$K = \rho_{fluid} * v^2 / 1000 \tag{5.9}$$

where

K = Bulk modulus of the fluid, mPa

P = Bulk density of the fluid, g/cc

ν = Acoustic velocity of the fluid, m/s

The factor of 1000 in the velocity calculation is due to the fact that bulk density unit is in the CGS system while the other quantities are expressed in the MKS system. The exact equations for calculating the acoustic velocity and bulk density of the fluid as a function of pressure and temperature are given by Batzle et al. (1992) and are not reproduced here.

5.3.6 Calculating new saturated bulk modulus with substituted fluid(K_{sat2})

The new saturated bulk modulus for substituted fluid can be computed using the equation 5.10 as described by Smith et al. (2003). This equation was unsuitable for the purposes of determining the uncertainty in the fluid substituted velocity primarily because of the presence of K* term. The nature of complexity as a result of K* term is further explained in section 5.10

$$K_{Sat} = K^* + \frac{\left(1 - \frac{K^*}{K_o}\right)^2}{\frac{\varphi}{K_{fl}} + \frac{(1-\varphi)}{K_0} - \frac{K^*}{K_o^2}} \tag{5.10}$$

An alternate form for calculating the saturated bulk modulus is shown below in equation 5.11 and involves eliminating the K* term shown in the equation 5.10.

$$K_{Sat2} = K_0 \frac{\mathrm{X}}{(1+\mathrm{X})}, \text{ where, } \mathrm{X} = \frac{K_{Sat1}}{K_0 - K_{Sat1}} - \frac{K_{fl1}}{\varphi(K_0 - K_{fl1})} + \frac{K_{fl2}}{\varphi(K_0 - K_{fl2})} \quad (5.11)$$

All parameters in the above equation can be easily calculated from the logging measurements as described earlier in this chapter. For the calculation involving bulk modulus of the new fluid (K_{fl2}) I used the cutoff value of 0.7 for water saturation term (Sw) in order to delineate the hydrocarbon and water-bearing zones. The cutoff value implies that any minor hydrocarbons present in zones having water saturation greater than 0.7 are effectively ignored.

5.3.7 Calculating velocities with substituted fluid (V_{p2} & V_{s2})

The new velocities using the substituted fluid can be easily computed using the equations stated below

$$Vp = \sqrt{\frac{K_{Sat2} + \frac{4}{3}G}{\rho_b}} \quad \text{and} \quad Vs = \sqrt{\frac{G}{\rho_b}} \quad (5.12)$$

The equations are relatively simple to implement, however the only requirement is to recalculate the bulk density parameter when using the substituted fluid. The initial step to calculate the new bulk density is to first compute the apparent grain density of the matrix using the measured bulk density and then keeping the grain density and the porosity terms constant substitute the density of the substituted fluid in the standard porosity equation.

$$\rho_b = \rho_g(1 - \varphi) + \rho_{fl}\varphi$$

The apparent grain density was initially calculated using the equation

$$AGD = \frac{(DenMat*(1 - Porosity - Vsh) + DenShale*Vsh}{1 - Porosity} \quad (5.13)$$

where

AGD = Apparent grain density (g/cc) or (ρ_g in the standard porosity equation)

DenMat = Matrix grain density (constant : 2.65 g/cc)

Vsh = Volume of shale in fractions

DenShale = Density of dry shale (constant : 2.60 g/cc)

In the absence of any additional data, I have assumed the density of dry shale to be 2.6 g/cc. The cutoff values for porosity and V_{sh} have been selected such that if the volume of shale is greater than 0.7 the porosity value is constrained at 5%. This porosity cutoff is required to limit the spurious calculation of apparent grain density when the majority of the mineral constituent of the rock is shale. While it is possible to assign an uncertainty value to each of the terms used in the above equation and then calculate the uncertainty in the new bulk density, I used an uncertainty value of ±0.025 g/cc for the recomputed bulk density parameter which is similar to the uncertainty in the measured density. This assigned uncertainty value has been kept constant to ensure that the data is not unnecessarily biased due to inherent assumptions due to limited data availability. By replacing the grain density and the bulk density of the substituted fluid in the standard porosity equation, the new bulk density can be calculated. Other input parameters in the velocity calculation have been computed previously and are used to compute new velocities using the substituted fluid.

Appendix B - Chapter 6

6.1 Introduction

Appendix B describes the methodology used to calculate the error for each of the petrophysical and linearly elastic parameters that have been described in the previous chapter. The error in each individual input component was calculated using the error propagation equations described in section 3.

Errors in petrophysical parameters: I describe the methodology used to determine errors for the petrophysical parameters namely errors in bulk density(ρ), porosity(φ), volume of shale(Vsh) and water saturation(Sw). One of the limitations to petrophysical data analysis is that each instrument uses different principles of measurement and has its own depth of investigation. It will therefore respond differently to various formation properties. The combined effects of measurement principles, source-receiver spacing and measurement conditions will produce a different sensitive volume for each measurement. The key assumption that is commonly applied is that all measurements respond to almost the same volume of investigation and this assumption may not be true in most cases.

Errors in linearly elastic parameters: Most of the elastic parameter calculation requires petrophysical parameters as the input and therefore requires the calculation of uncertainty in the petrophysical parameters *a priori*, before the calculation of errors in linearly elastic parameters. The errors in some input parameters such as bulk moduli of a specific mineral is considered to be a constant and therefore assigned a value of zero. The methodology describing the error computation for each of the parameters is given below and their section numbers are given here as a table for quick reference.

No	Type	Parameter	No	Type	Parameter
6.2.1	Petrophysical	Error in Density (ρ)	6.3.2	Elastic	Error in Saturated Bulk Modulus(KSat)
6.2.2	Petrophysical	Error in Porosity (φ)	6.3.3	Elastic	Error in Bulk Modulus of Pore Fluid(K_{fl})
6.2.3	Petrophysical	Error in Acoustic Velocity (Vp, Vs)	6.3.4	Elastic	Error in Saturated Bulk Modulus (substituted fluid) (K_{Sat2})
6.2.4	Petrophysical	Error in Volume of Shale (V_{Sh})	6.3.5	Elastic	Error in Bulk Modulus of Porous Rock Frame(K*)
6.2.5	Petrophysical	Error in Water Saturation (S_W)	6.3.6	Elastic	Error in Shear Modulus (G)
6.3.1	Elastic	Error in Bulk Modulus of Mineral Matrix(K_0)	6.3.7	Elastic	Error in Computed Velocity (V_{p2},V_{s2})

6.2 Errors in petrophysical parameters

6.2.1 Error in bulk density

Formation density instruments using radioactive sources relate electronic density (i.e. number of electrons per cubic centimeter) to formation density. Several factors affect accuracy and precision of the measurement resulting in data uncertainty. The primary factors are internal to instrument design and calibration errors. However in addition to these systematic errors, the measurement conditions that also contribute to errors in density measurements are described below.

1. Statistical errors which are function of radioactive source age and activity.
2. Effect of borehole conditions: washouts, rugose or elliptical boreholes.
3. Effect of logging bed boundaries in high angle boreholes.
4. Density contrast between the borehole fluid and the formation.

5. Impact of variable standoff (distance from sensor face to borehole wall). This variation is common to LWD density logging.

I used an RMS error value of ± 0.025 g/cc at 1σ confidence as the error in density measurement. This value is typically used in technical brochures provided by instrument manufacturers. In reality the uncertainty value is not a constant and varies with changing formation properties as well as wellbore conditions. If an independent density uncertainty curve with depth is available it can be used instead of a constant value. However this type of data is generally not available and hence a constant value for uncertainty has been used.

6.2.2 Error in porosity

Porosity can be obtained independently by the logging instrument such as nuclear magnetic resonance or neutron porosity measurement. If the porosity has been obtained independently then the error in porosity as published by the instrument manufacturer can be used directly. For this study I derived the porosity from the density measurement. The error in porosity can be determined from the density measurement using the error propagation equation shown below.

$$\sigma_\phi = \sqrt{\left(\frac{\partial\phi}{\partial\rho_{ma}}\right)^2 * \sigma^2_{\rho_{ma}} + \left(\frac{\partial\phi}{\partial\rho_{fl}}\right)^2 * \sigma^2_{\rho_{fl}} + \left(\frac{\partial\phi}{\partial\rho_{ma}}\right)^2 * \sigma^2_{\rho_{\log}}} \qquad (6.1)$$

The above equation is solved as shown below.

$$\sigma_\phi = \sqrt{\left(\frac{\rho_{\log} - \rho_{fl}}{(\rho_{ma} - \rho_{fl})^2}\right)^2 * \sigma^2_{\rho_{ma}} + \left(\frac{\rho_{ma} - \rho_{\log}}{(\rho_{ma} - \rho_{fl})^2}\right)^2 * \sigma^2_{\rho_{fl}} + \left(\frac{1}{(\rho_{ma} - \rho_{fl})^2}\right)^2 * \sigma^2_{\rho_{\log}}}$$

where

ρ_{ma} = Density of the mineral matrix

ρ_{fl} = Density of the fluid in the pore space

ρ_{log} = Density of the formation as measured by the logging instrument.

As seen from the above equation, the accurate computation of error in porosity would require some knowledge of the uncertainty in the matrix density and the density of the fluid. The errors caused by incorrect values of ρ_{fl} can be large if there is partial gas saturation instead of assuming completely fluid-filled pore space. Since the uncertainty values for ρ_{ma} and ρ_{fl} are unknown the solution would require assigning best estimates of uncertainty based on empirical data or field experience. Further, the uncertainty values used for the density of matrix would also be dependent on volume of shale. In general the error in matrix density would increase with increase in the shale fraction. The only parameter which is available is the error in density measurement as published by the instrument manufacturer and is assumed to be constant for a range of densities and borehole conditions. In view of the uncertainties in the input parameters, I used a constant uncertainty value of, $\sigma_{\varphi} = 0.05 * porosity$, for the porosity term. This value is not a unreasonable assumption since several porosity instruments typically quote a uncertainty value of 5% at ± 1σ confidence level.

6.2.3 Error in acoustic travel times (DTP, DTS)

Logging instruments measure formation slowness in microseconds/foot rather than in direct velocity units. In addition to borehole conditions that affect the measurement, acoustic travel time data also suffers from anisotropic effects related to micro-anisotropy of shales and thin bed laminations of sand-shale sequences in the presence of large relative dip angles (Vernik, 2007). The large relative dip angles may simply result due to well deviation even in areas of relatively low formation dip. The main factors that affect accuracy of acoustic velocity are given below.

1. Borehole irregularities, tool tilt and logging instrument decentralization.
2. Velocity dispersion.
3. Effect of relative dip angle of the bed on measurement.
4. Formation anisotropy as a result of large relative dip angle.
5. Cycle skipping.
6. Noise spikes.

Instrument manufacturers generally state measurement uncertainties for slowness rather than in direct velocity terms. I have used an uncertainty of 5% at ± 1σ confidence level for slowness value and converted the uncertainty in slowness to uncertainty in velocity for each data point.

6.2.4 Computing error in volume of shale (V_{sh})

Volume of shale was computed using the gamma ray log which responds to the natural radiation of the formation as shown in equation 6.2.

$$V_{sh} = \frac{GR_{\log} - GR_{\min}}{GR_{\max} - GR_{\min}} \tag{6.2}$$

where

GR_{log} = Gamma ray measurement

GR_{min} = Gamma ray measurement in a clean sand line

GR_{max} = Gamma ray measurement in a thick shale

The number of nuclear particle counts (N) that the detector observes over a fixed interval of time follows a Poisson distribution. The standard deviation of the counts that are observed over a fixed interval of time is given by $\sigma = \sqrt{N}$. However in nuclear logging instruments we are more concerned with the count rate (i.e. counts per unit time) rather than

the number of counts by itself. In general, time is assumed to be measured with high degree of precision and therefore any error or variation in time is generally ignored. Therefore the standard deviation of counting rate is given by

$$\sigma = \frac{\sqrt{N}}{t}. \tag{6.3}$$

The count rates observed at the detectors are transformed to Gamma ray API value by means of a transfer function. The statistical error from the random nature of these events in the observed count rate gets transferred to the computed API value. This error is in addition (and independent) to the systematic errors arising from measurement conditions in a wellbore. Since the actual logging tool instrumentation technical parameters are confidential to the manufacturer and are therefore unknown, I used a generic value of 5 % error in the volume of shale computation. By inference, similar value of 5 % error was used for volume of sand fraction which is directly computed from the volume of shale.

6.2.5 Error in water saturation (Sw)

I calculated water saturation using the Archie's equation as shown below.

$$S_w = \left[\frac{aR_w}{\phi^m R_t} \right]^{\frac{1}{n}} \tag{6.4}$$

where

R_w = Resistivity of water in filling the pores of the rock

R_t = True resistivity of the rock

Φ = Porosity (v/v)

The a, m, n= constants are based on empirical data. For well consolidated sandstones the values are 'a'=1, 'm' and 'n'=2. Actual values of 'a', 'm', and 'n' are typically derived from core measurements and were not available for this study.

As is apparent from the equation above, one of the key inputs to the equation is the true resistivity of the rocks. While it is possible to apply the error propagation equation to compute the uncertainty in the water saturation using any of the shaley sand models, the actual computation is difficult since it would require accurate knowledge of resistivity tool response functions at various vertical resolutions and at varying formation resistivity.

Numerous authors have described the challenges associated with the evaluation of a low resistivity, low contrast laminated sand-shale reservoir. When the thickness of the laminations is significantly less than the vertical resolution of conventional logging instruments, the formation displays a macroscopic anisotropy with respect to properties such as conductivity and permeability. These properties will have different values depending on the directionality of the measurements with maximum anisotropy occurring when measured parallel and perpendicular to the bedding planes. The petrophysical model for interpreting sand-shale reservoirs is based on the concepts of the volumetric shale distribution model (Thomas and Stieber, 1975) and a tensor resistivity model to determine laminar shale volume and laminar sand resistivity (Mollison, et al., 1999, 2000; Schoen et al., 1999). The resistivity tensor utilizes macroscopic electrical anisotropy defined by the combination of the horizontal parallel and vertical series resistivity equations (Hagiwara, 1997, 1998; Klein, 1996; Klein et al., 1997; and Herrick and Kennedy, 1996; Mezzatesta et al., 2002; Popta et al., 2004).

While several methods of calculation of water saturation are described in the literature, the use of Archie's method seems to be the most common used. The primary reason

for this seems to be the ease of use and the availability of published empirical data. As a note of caution, using Archie's methods for Sw estimation is prone to errors especially in shaley sand lithology and therefore the uncertainty value for Sw may have a much wider range than for other petrophysical parameters.

6.3 Errors in linearly elastic parameters

Propagated error from logging data was used to compute uncertainty in each of the linearly elastic parameters. I have described the methodology used to compute errors for each of the elastic parameter used in Gassmann fluid substitution.

6.3.1 Computing error in bulk modulus of mineral matrix (K0)

The error in bulk modulus of mineral matrix was calculated using both methods of estimating effective elastic moduli. The two methods were Hashin-Shtrikman bounds and Voigt-Reuss bounds. The methodology for calculating the effective elastic moduli for both methods is described below. While only the Voigt-Reuss method was used in the computation of the error in the K_0 parameter for this study, I have described the methodology to compute the error in the Hashin-Shtrikman method for completeness.

For the Hashin-Shtrikman bounds, the error in K_0 can be calculated from the equation shown below. The elastic constants of individual minerals are considered to be constants and it is therefore assumed that the only source of error is in the volumetric fractions of the minerals. The volumetric fractions have been computed using the gamma ray log, which in turn is computed from the natural radioactivity of the minerals and is therefore a function of statistical precision of the natural radioactivity and the tool calibration constants. It is difficult to comprehensively compute the error in the volumetric fractions in the absence of other

information such as radioactive count rates or tool measurement errors, etc., to name the few error sources, and therefore a constant volumetric error value of 5% is assumed.

$$K_{0(Avg)} = \frac{1}{2}\left(K_0^{HS^+} + K_0^{HS^-}\right) \tag{6.5}$$

The expression which computes the error in K_0 is given as

$$\sigma_{K_0}^2 = \left\{\left[\frac{\partial K_0}{\partial K_{HS^+}}\right]^2 * \sigma_{K_{HS^+}}^2 + \left[\frac{\partial K_0}{\partial K_{HS^-}}\right]^2 * \sigma_{K_{HS^-}}^2\right\}, \tag{6.6}$$

$$\sigma_{K_0}^2 = \frac{1}{4}\left\{\sigma_{K_{HS^+}}^2 + \sigma_{K_{HS^-}}^2\right\}.$$

The upper and the lower bounds of the mineral modulus is a function of several variables such as bulk and shear modulii of the individual minerals and their volumetric fractions.

$$K_0^{HS^\pm} = f(K_1, K_2, \mu_1, \mu_2, f_1, f_2)$$

As mentioned earlier, only the error in mineral volumetric fractions is considered and the elastic constants for the minerals are considered to be constants and therefore the error is zero. The equation for Hashin-Shtrikman bounds can therefore be written as

$$K^{HS\pm} = K_1 + \frac{f_2}{C_1 + C_2 f_1}. \tag{6.7}$$

where C_1,C_2 are constants and can be expressed as

$$C_1 = (K_2 - K_1)^{-1}, C_2 = (K_1 + \frac{4}{3}\mu_1)^{-1}.$$

It is noted here that the upper and lower bounds are computed by interchanging which material is termed 1 and which is termed as 2. The constants C_1 and C_2 are used when the stiffest material (quartz) is termed as 1. However in order to improve clarity, new constants

C_3 and C_4 are used so that the material indices can remain unchanged. Therefore quartz will continue to be termed as material 1 and clay as material 2 when computing the lower bound. Therefore the equation 5.6 for lower bound is stated as

$$K^{HS-} = K_2 + \frac{f_1}{C_3 + C_4 f_2}.$$

where

$$C_3 = (K_1 - K_2)^{-1}, C_4 = (K_2 + \frac{4}{3}\mu_2)^{-1}.$$

Using the error propagation equation, the error in Hashin-Shtrikman bounds can be defined as

$$\sigma^2_{K_{HS}\pm} = \left[\frac{\partial K_{HS}}{\partial f_1}\right]^2 * \sigma^2_{f_1} + \left[\frac{\partial K_{HS}}{\partial f_2}\right]^2 * \sigma^2_{f_2}. \quad (6.8)$$

σ_{f1} and σ_{f2} in the above equation are the error in volumetric fractions of quartz and clay components respectively.

Additionally,

$$\sigma^2_{K_{HS}^+} = \frac{-C_2 f_2}{(C_1 + C_2 f_1)^2} * \sigma^2_{f_1} + \frac{1}{C_1 + C_2 f_1}\sigma^2_{f_2},$$

and similarly

$$\sigma^2_{K_{HS}^-} = \frac{1}{C_3 + C_4 f_2} * \sigma^2_{f_1} + \frac{-C_4 f_1}{(C_3 + C_4 f_2)^2} * \sigma^2_{f_2}.$$

In the above equations, the materials termed as 1 and 2 remained unchanged giving the equation as

$$\sigma_{K_0}^2 = \frac{1}{4}\left\{\left(\frac{-C_2 f_2}{(C_1 + C_2 f_1)^2}\right)^2 * \sigma_{f_1}^2 + \left(\frac{1}{C_1 + C_2 f_1}\right)^2 * \sigma_{f_2}^2 + \left(\frac{1}{C_3 + C_4 f_2}\right)^2 * \sigma_{f_1}^2 + \left(\frac{-C_4 f_1}{(C_3 + C_4 f_2)^2}\right)^2 * \sigma_{f_2}^2\right\}.$$

Substituting error value for volume fractions (σ_{f1} and σ_{f2}) as 5% in the above equation we obtain.

$$\sigma_{K_0}^2 = 0.00625 * \left\{\left(\frac{-C_2 f_2}{(C_1 + C_2 f_1)^2}\right)^2 + \left(\frac{1}{C_1 + C_2 f_1}\right)^2 + \left(\frac{1}{C_3 + C_4 f_2}\right)^2 + \left(\frac{-C_4 f_1}{(C_3 + C_4 f_2)^2}\right)^2\right\} \tag{6.9}$$

The second approach for calculating the effective elastic moduli is the Voigt-Reuss bounds. The Voigt upper bound of the effective elastic modulus Mv of 'N' phases is given by

$$M_V = \sum_{i=1}^{N} f_i M_{i.} \tag{6.10}$$

The Reuss lower bound of the effective elastic modulus is given by

$$\frac{1}{M_R} = \sum_{i=1}^{N} \frac{f_i}{M_i} \tag{6.11}$$

where

f_i = Volume fraction of the i^{th} medium.

M_i = Elastic moduli of the i^{th} medium.

$$K_0 = \frac{1}{2}\left[M_v + M_R\right]$$

$$\sigma_{K_0}^2 = \frac{1}{4}\left\{\left[\frac{\partial K_0}{\partial M_v}\right]^2 * \sigma_{M_v}^2 + \left[\frac{\partial K_0}{\partial M_R}\right]^2 * \sigma_{M_R}^2\right\} \tag{6.12}$$

$$\sigma_{K_0}^2 = \frac{1}{4}\left\{\sigma_{M_v}^2 + \sigma_{M_R}^2\right\}$$

where

$$\sigma_{Mv}^2 = \left(\frac{\partial f_1 M_1}{\partial f_1}\right)^2 \sigma_{f_1}^2 + \left(\frac{\partial f_2 M_2}{\partial f_2}\right)^2 \sigma_{f_2}^2$$

Since we consider the error in volumetric fractions (f_1 and f_2) to be 5% we obtain

$$\sigma_{Mv}^2 = 0.0025 * (M_1^2 + M_2^2).$$

Similarly

$$\sigma_{M_R}^2 = \left(\frac{\partial M_R}{\partial f_1}\right)^2 \sigma_{f_1}^2 + \left(\frac{\partial M_R}{\partial f_2}\right)^2 \sigma_{f_2}^2$$

where

$$M_R = \left(\frac{f_1}{M_1} + \frac{f_2}{M_2}\right)^{-1}$$

$$\sigma_{M_R}^2 = \left(\frac{-M_R^2}{M_1}\right)^2 \sigma_{f_1}^2 + \left(\frac{-M_R^2}{M_2}\right)^2 \sigma_{f_2}^2$$

Substituting error value for volume fractions (σ_{f1} and σ_{f2}) as 0.05 in the above equation we obtain.

$$\sigma_{M_R}^2 = 0.0025 * \left[\left(\frac{-M_R^2}{M_1}\right)^2 + \left(\frac{-M_R^2}{M_2}\right)^2\right]$$

Substituting into equation 6.12 we get

$$\sigma_{K_0}^2 = \frac{0.0025}{4} * \left\{ (M_1^2 + M_2^2) + \left(\frac{-M_R^2}{M_1} \right)^2 + \left(\frac{-M_R^2}{M_2} \right)^2 \right\} \quad (6.13)$$

6.3.2 Computing error in saturated bulk modulus (K_{sat})

I used formation bulk density and acoustic velocities measured by the logging instruments to calculate bulk modulus of the in-situ rock (K_{Sat}) using the relationship

$$K_{Sat} = \rho_b \left(V_p^2 - \frac{4}{3} V_s^2 \right) \quad (6.14)$$

where

ρ_b = Bulk density in g/cc

V_p = Compressional velocity in Km/sec

V_s = Shear velocity in Km/sec

K_{Sat} = Saturated bulk modulus in Gigapascals (GPa)

By applying the error propagation equation, I calculated the error in the saturated bulk modulus for each data point. Since the data are independent, the error propagation equation for error in K_{Sat} is as shown below.

$$\sigma_{K_{Sat}} = \sqrt{\left(\frac{dK_{Sat}}{d\rho_b} \right)^2 * \sigma^2_{\rho_b} + \left(\frac{dK_{Sat}}{dV_p} \right)^2 \sigma^2_{V_p} + \left(\frac{dK_{Sat}}{dV_s} \right)^2 * \sigma^2_{Vs}}$$

$$\sigma_{K_{Sat}} = \sqrt{\left(V_p^2 - \frac{4}{3} V_S^2 \right)^2 * \sigma^2_{\rho_b} + \left[2\rho_b V_p \right]^2 \sigma^2_{V_p} + \left(-\frac{8}{3} \rho_b V_s \right)^2 * \sigma^2_{Vs}} \quad (6.15)$$

In the above equations, I used an uncertainty of ±5 % in the slowness value computed by the logging tool for acoustic velocities and ±0.025 g/cc as uncertainty in the bulk density at 1σ confidence level.

6.3.3 Computing error in bulk modulus of pore fluid (K_{fluid})

The bulk modulus of the pore fluid can be calculated using the equation

$$K_{fluid} = \left[\sum_{i=1}^{n} \frac{S_i}{K_i} \right]^{-1} \tag{6.16}$$

where K_{fluid} is the bulk modulus of the reservoir fluid, S_i is the saturation of the individual fluid phases and K_i is the bulk modulus of the individual fluid phase. Since I am using a two-component system the above equation can be expanded to read as

$$K_{fluid} = \left[\frac{S_w}{K_w} + \frac{(1 - S_w)}{K_{oil}} \right]^{-1}. \tag{6.17}$$

Although the error values for S_w and K_{fluid} can be computed separately, the exact sources of error sources would need to be known priori and accounted for. As an example, the acoustic velocity is a function of pressure and temperature. Therefore the errors in the these measurements will be required to be included in the computation. In some cases, the exact sources of this error are unknown and therefore it is prudent to use a generic error value for estimating the error of a parameter which is a function of several variables and whose measurement characteristics is unknown. I used the following generic error values for water saturation, the bulk modulus of the fluid phases.

- RMS error in water saturation (σ_{Sw}) = 20 %
- RMS error in fluid bulk modulii (σ_{Koil}, σ_{Kwater}) = 5 %

Using the above values the error in bulk modulus of reservoir fluid was computed as per the equation shown below.

$$\sigma^2_{K_{fluid}} = \left[-\left[\frac{S_w}{K_w} + \frac{(1-S_w)}{K_{oil}} \right]^{-2} * \left[\frac{1}{K_w} - \frac{1}{K_{oil}} \right] \right]^2 * \sigma^2_{Sw} + \left[-\left[\frac{S_w}{K_w} + \frac{(1-S_w)}{K_{oil}} \right]^{-2} * \left[\frac{-S_w}{K_w^2} \right] \right]^2 * \sigma^2_{Kw} + \left[-\left[\frac{S_w}{K_w} + \frac{(1-S_w)}{K_{oil}} \right]^{-2} * \left[\frac{-(1-S_w)}{K_{oil}^2} \right] \right]^2 * \sigma^2_{Koil} \quad (6.18)$$

The equation 6.18 was determined by applying the error propagation equation to the value of bulk modulus of fluid which in turn is a function of three variables namely S_w, K_{oil} and K_{brine}.

6.3.4 Computing error in saturated bulk modulus with substituted fluid (K_{sat2})

The saturated bulk modulus using the substituted fluid was calculated using the equation

$$K_{Sat\,2} = K^* + \frac{\left(1 - \frac{K^*}{K_o}\right)^2}{\frac{\phi}{K_{fl\,2}} + \frac{(1-\phi)}{K_0} - \frac{K^*}{K_o^2}} \quad (6.19)$$

where

K_{Sat2} = Saturated bulk modulus of rock with the substituted fluid,

Φ = Porosity,

K^* = Bulk modulus of porous rock frame,

K_0 = Bulk modulus of the mineral matrix,

K_{fl2} = Bulk modulus of the substituted pore fluid,

K_{Sat} = Saturated bulk modulus of the in-situ rock.

As is apparent from the above equation, K_{Sat2} is a function of K*, K_0, φ and K_{fl2}. Additionally K* itself is a function of K_{Sat1}, K_{fl1}, K_0 and φ. It is also possible to calculate K_{Sat2} by eliminating the term K* as shown earlier in the section 5.3.4. Eliminating the term K*

greatly simplifies the calculation of the error in K_{Sat2} using the error propagation equation by reducing the complexity of calculation involving dependent variables. The form of the error propagation equation for calculating error in saturated bulk modulus with substituted fluid is shown below. By eliminating the term K* we have

$$K_{Sat2} = K_0 \frac{\mathrm{X}}{(1+\mathrm{X})} \quad \text{where, } \mathrm{X} = \frac{K_{Sat1}}{K_0 - K_{Sat1}} - \frac{K_{fl1}}{\varphi(K_0 - K_{fl1})} + \frac{K_{fl2}}{\varphi(K_0 - K_{fl2})}. \qquad (6.20)$$

The error term σ_{KSat2}, for the parameter K_{Sat2} is a result of the error propagated from the logging measurements and is given as

$$\sigma_{Ksat2} = \sqrt{\left[\frac{dK_{Sat2}}{dK_0}\right]^2 * \sigma_{K0}^2 + \left[\frac{dK_{Sat2}}{d\phi}\right]^2 * \sigma_{\phi}^2 + \left[\frac{dK_{Sat2}}{dK_{Sat1}}\right]^2 * \sigma_{KSat1}^2 + \left[\frac{dK_{Sat2}}{dK_{fl2}}\right]^2 * \sigma_{K_{fl2}}^2 + \left[\frac{dK_{Sat2}}{dK_{fl1}}\right]^2 * \sigma_{fl1}^2 + 2\sigma_{KSat1\phi}^2 \left[\frac{dK_{Sat2}}{dK_{Sat1}}\right]\left[\frac{dK_{Sat2}}{d\phi}\right]} \qquad (6.21)$$

The term $2\sigma_{Sat1\emptyset}$ in the above equation represents the covariance between K_{Sat1} and porosity. The bulk modulus of the saturated rock and the porosity are negatively correlated and therefore requires the covariance term in the equation (Broadhead, 2005). This strong negative correlation is commonly observed in the data but is not a result of any inter-dependence of the calculated parameters. As discussed earlier in chapter 1, the objective of this study is to determine the measurement error propagated from the logging instruments and therefore it is not necessary to include the covariance term in the error propagation equation unless both parameters have been derived from a common variable. In this case, both porosity and K_{Sat1} are both functions of density measurement, where density is the independent variable. And therefore when determining the solution to terms such as $\frac{dK_{Sat2}}{d\emptyset}$ *or* $\frac{dK_{Sat2}}{dK_{Sat1}}$ as shown in equation 6.21, the porosity term cannot be considered to be an independent variable

for the purposes of this study. This is due to the fact that the porosity has been computed from the formation density using the standard porosity equation for a constant matrix and fluid density and therefore shows strong negative correlation with density. If the total (or effective) porosity term was measured by an independent instrument (i.e. porosity instrument such as Neutron or NMR) the measurement error in porosity can then be considered to be independent and would have no dependence on the density parameter and vice versa. Additionally, including the covariance term to define relationship for just one pair of variables would be incorrect since several other sets (such as density and velocity or K_0 and velocity etc.) may also show similar correlations and covariance's for such sets would then need to be included in the error propagation equation. Including covariance terms for individual sets of data may be impractical since several other factors such as burial history, age, compaction, shape and sorting of the individual grains, presence of shale, to name a few, play an important role in determining degree and direction of individual correlations. As an example, presence of shale can reduce the density in varying amounts depending whether the shale is present in laminated or dispersed form. Another assumption that is commonly made is that shale has the same properties regardless of how it is distributed in the rock. The solutions to the individual terms in the equation 6.21 as stated by Broadhead (2005) are given below.

$$\frac{dK_{Sat2}}{dK_0} = \frac{X}{1+X} + \frac{K_0}{(1+X)^2}\left(-\frac{K_{Sat1}}{(K_0 - K_{Sat1})^2} + \frac{K_{fl1}}{\varphi(K_0 - K_{fl1})^2} - \frac{K_{fl2}}{\varphi(K_0 - K_{fl2})^2} \right)$$

$$\frac{dK_{Sat2}}{d\phi} = \frac{K_0}{(1+X)^2}\left(\frac{K_{fl1}}{\varphi^2(K_0 - K_{fl1})} - \frac{K_{fl2}}{\varphi^2(K_0 - K_{fl2})} \right)$$

$$\frac{dK_{Sat2}}{dK_{Sat1}} = \frac{K_0}{(1+X)^2}\left(\frac{K_0}{(K_0 - K_{Sat1})^2}\right)$$

$$\frac{dK_{Sat2}}{d_{fl1}} = \frac{K_0}{(1+X)^2}\left(\frac{K_0}{\varphi(K_0 - K_{fl1})^2}\right)$$

$$\frac{dK_{Sat2}}{d_{fl2}} = \frac{K_0}{(1+X)^2}\left(\frac{K_0}{\varphi(K_0 - K_{fl2})^2}\right)$$

In the above equations, the variables K_0, K_{fl1}, and K_{fl2} are considered to be independent and obtaining their solution for the variation of K_{Sat2} with respect to these terms is straightforward. However when determining the solution to the terms $\frac{dK_{Sat2}}{d\emptyset}$ and $\frac{dK_{Sat2}}{dK_{Sat1}}$, Brodhead (2005) considers the porosity term to be an independent variable. However since Wyllie's equation has been used to calculate porosity from the density measurement, the solutions to the terms $\frac{dK_{Sat2}}{d\emptyset}$ and $\frac{dK_{Sat2}}{dK_{Sat1}}$ will require porosity and the density to be considered as dependent variables. The solution to the terms $\frac{dK_{Sat2}}{d\emptyset}$ and $\frac{dK_{Sat2}}{dK_{Sat1}}$ can be easily determined by rewriting K_{Sat1} as

$$K_{Sat1} = 2.65 - 1.65\emptyset\left(V_P^2 - \frac{4}{3}V_S^2\right),$$

where density is expressed by density = 2.65- 1.65 * φ

$$\frac{dK_{Sat2}}{d\phi} = \frac{K_0}{(1+X)^2}\left(\frac{K0}{(K_0 - K_1)^2} * \frac{dK_{Sat1}}{d\varphi} + \frac{K_{fl1}}{\varphi^2(K_0 - K_{fl1})} - \frac{K_{fl2}}{\varphi^2(K_0 - K_{fl2})}\right)$$

where $\frac{dK_{Sat1}}{d\emptyset} = 1.65\left(\frac{4}{3}V_S^2 - V_P^2\right)$

Similarly the term $\frac{dK_{Sat2}}{dK_{Sat1}}$ can be written as

$$\frac{dK_{Sat2}}{dK_{Sat1}} = \frac{K_0}{(1+X)^2} * \left[\frac{K_0}{(K_0 - K_1)^2} + \frac{1}{\varphi^2} * \frac{d\varphi}{dK_{Sat1}} \left\{ \frac{K_{fl1}}{K_0 - K_{fl1}} - \frac{K_{fl2}}{K_0 - K_{fl2}} \right\} \right]$$

where $\frac{d\emptyset}{dK_{Sat1}} = \frac{1}{dK_{Sat1}/d\emptyset}$

The equations shown above have been used to calculate propagated error in the K_{Sat2} term without the need to use the bulk modulus of rock frame (K*) term. This greatly simplifies the calculation. All parameters with the exception of bulk modulus of the new fluid (K_{fl2})have been previously computed. The bulk modulus of new fluid (K_{fl2}) calculation is similar to as described in section 5.3.5. As in the original calculation, a value of 0.7 was used as a cutoff value for water saturation(Sw) to delineate hydrocarbon and water-bearing zones. Therefore minor hydrocarbons present in zones showing computed water saturation > 0.7 are effectively ignored by the fluid substitution process. This helps target the fluid substitution process to the hydrocarbon-bearing intervals. It is important to take care when applying the Wyllies porosity equation in formations that have higher fractions of shale, the porosity is first corrected for the presence of shale the shale fraction.

6.3.5 Computing error in bulk modulus of the porous rock frame (K*)

Although I describe the methodology to calculate the error in the K* term, it is not used in this study since the K* term has been eliminated as per equation 6.20. The paper by Smith et al. (2003) describes the method to compute the bulk modulus of the porous rock frame (K^*) using the equation shown below

$$K^* = \frac{K_{Sat}\left(\frac{\phi K_0}{K_{fl}} + 1 - \phi\right) - K_0}{\frac{\phi K_0}{K_{fl}} + \frac{K_{Sat}}{K_0} - 1 - \phi} \tag{6.22}$$

where

ϕ = Porosity

K_0 = Bulk modulus of the mineral matrix

K_{fl} = Bulk modulus of the pore fluid

K_{Sat} = Saturated bulk modulus of the in-situ rock

The K* parameter is calculated using the logging data representing the rock containing original fluid in the pore space. The error propagation equation for calculating the uncertainty in K* due to error propagation from logging measurements can be written as

$$\sigma_{K^*} = \sqrt{\left[\frac{dK^*}{dK_{Sat}}\right]^2 * \sigma^2_{K_{Sat}} + \left[\frac{dK^*}{d\phi}\right]^2 * \sigma^2_{\phi} + 2\sigma^2_{K_{Sat}\phi}\left[\frac{dK^*}{dK_{Sat}}\right]\left[\frac{dK^*}{d\phi}\right] + \left[\frac{dK^*}{dK_{fl}}\right]^2 * \sigma^2_{K_{flt}} + \left[\frac{dK^*}{dK_0}\right]^2 * \sigma^2_{K_0}} \tag{6.23}$$

where the term $\sigma_{K_{Sat}\phi}$ is the covariance between K_{Sat} and porosity (φ).

I have previously computed variables K_0 and K_{fl} and their respective uncertainties. As described in section 6.3.4, the porosity (φ) and the saturated bulk modulus (K_{Sat}) are both functions of the formation bulk density and the uncertainty calculation for K_{Sat} and φ would include propagated error from the density measurement. When calculating the solution to the term such as $\frac{dK*}{d\emptyset}$ from equation 6.23 implies that a variation (or uncertainty) in the porosity parameter is a result of variation (or uncertainty) in the density parameter for a given matrix

density and pore fluid. The uncertainty in the density term would then result in the uncertainty of the K_{Sat} parameter. This interdependency is due to the fact that the porosity term has been calculated using the standard equation from the density measurement for a constant matrix density. In this study, I uses a constant value to define for uncertainty in the density term. This however is not a requirement and a separate uncertainty curve for density can be used if it is available, which will take into account the variation with depth as a result of changing physical properties and borehole conditions. If the total (or effective) porosity term was measured by an independent porosity instrument (i.e. such as Neutron or NMR instruments) the measurement uncertainty in the porosity term would be independent of the uncertainty in the density term. Therefore using an independent porosity measurement will allow the terms K_{Sat} and ϕ to be considered as independent variables for the purposes of error propagation from logging instruments and greatly simplifies the solution to the terms $\frac{dK*}{d\emptyset}$ or $\frac{dK*}{dK_{Sat}}$.

I state below three methods of calculating the uncertainty in K* by considering the porosity and K_{Sat} to be dependent variables while K_0 and K_{fl} are recognized as independent variables. The suggested methods state the procedures to express φ and K_{Sat} in terms of each other, therefore allowing us to determine $\frac{dK*}{d\emptyset}$ or $\frac{dK*}{dK_{Sat}}$ terms. This calculation is unnecessary for the purposes of achieving objectives of this study, since the error in K_{Sat2} was already determined without the need to calculate the error in K*. Nevertheless the methods to calculate uncertainty in K* are discussed here for completeness.

Method 1:

The bulk modulus of porous rock frame (K*) is expressed by equation 6.22. This equation contains the two dependent variables, namely porosity and K_{Sat}. Therefore, simple partial differential method cannot be used directly since it would require the two variables to be independent. In order to determine solution to the terms such as $\frac{dK*}{dKSat}$ and $\frac{dK*}{d\emptyset}$, the first method would be to express porosity in terms of K_{Sat} using the following set of equations.

Density is expressed in terms of porosity as density = 2.65-1.65*φ for constant matrix and fluid densities by using the standard porosity equation. The relationship between porosity and K_{Sat} can be derived as shown below.

$$K_{Sat} = Density * (V_P^2 - 4/3 V_S^2) .$$

By expressing the density term of K_{Sat} gives the porosity as

$$Porosity = 1.606 - \frac{K_{Sat}}{1.65 * (V_P^2 - 4/3 V_S^2)}$$

By substituting the porosity term in the equation 6.22 gives the following expression.

$$K^* = \frac{K_{Sat}\left(\frac{1.606 - \frac{K_{Sat}}{1.65*(V_P^2 - 4/3 V_S^2)} K_0}{K_{fl}} + 1 - 1.606 - \frac{K_{Sat}}{1.65*(V_P^2 - 4/3 V_S^2)}\right) - K_0}{\frac{1.606 - \frac{K_{Sat}}{1.65*(V_P^2 - 4/3 V_S^2)} K_0}{K_{fl}} + \frac{K_{Sat}}{K_0} - 1 - 1.606 - \frac{K_{Sat}}{1.65*(V_P^2 - 4/3 V_S^2)}} \quad (6.24)$$

By expressing porosity in terms of K_{Sat}, allows us to differentiate K* with respect to K_{Sat} i.e. the term $\frac{dK*}{dK_{Sat}}$. In the equation 6.24, the velocities Vp and Vs can be considered to be

constants because they have been measured by an independent instrument and this allows their uncertainties to remain independent. The above equation appears tedious to solve but has been made much easier by directly expressing porosity in terms of K_{Sat} and allows solving for dependent variables. We can use the similar methodology as used above to determine solution to the term $\frac{dK*}{d\phi}$ by expressing K_{Sat} in terms of density, V_p, and V_s. and then further expressing density in terms of porosity. This allowed me to replace K_{Sat} terms in the equation 6.22 with the alternate form as shown below.

$$K_{Sat} = (2.65 - 1.65 * Porosity)\left(Vp^2 - \frac{4}{3}Vs^2\right)$$

The expression for K* when K_{Sat} is expressed in terms of porosity is shown below.

$$K^* = \frac{(2.65-1.65\phi)*(V_P^2 - 4/3 V_S^2)\left(\frac{\phi K_0}{K_{fl}} + 1 - \phi\right) - K_0}{\frac{\phi K_0}{K_{fl}} + \frac{(2.65-1.65\phi)*(V_P^2 - 4/3 V_S^2)}{K_0} - 1 - \phi} \qquad (6.25)$$

Again the velocity terms are considered to be constants and the above equation allows us to determine $\frac{dK*}{d\phi}$ for the dependent variables K_{Sat} and φ. The co-variance between porosity and K_{Sat} in the equation 6.23 can be determined using the data for the entire log interval. The derivative of K* with respect to remaining two variables namely bulk moduli of the pore fluid (K_{fl}) and the mineral matrix (K_0) is relatively simple to compute since the uncertainties in the two variables are completely independent. The actual expressions for derivative terms are shown below for completeness.

$$\left[\frac{dK^*}{dK_{fl}}\right]=\frac{\left\{\left(\frac{\phi K_0}{K_{fl}}+\frac{K_{Sat}}{K_0}-1-\phi\right)*\left(-\frac{K_{Sat}K_0}{K_{fl}^2}\right)\right\}-\left\{\left(K_{Sat}\left(\frac{\phi K_0}{K_{fl}}+1-\phi\right)-K_0\right)*\left(-\frac{\phi * K_0}{K_{fl}^2}\right)\right\}}{\left[\frac{\phi K_0}{K_{fl}}+\frac{K_{Sat}}{K_0}-1-\phi\right]^2}$$

$$\left[\frac{dK^*}{dK_0}\right]=\frac{\left\{\left(\frac{\phi K_0}{K_{fl}}+\frac{K_{Sat}}{K_0}-1-\phi\right)*\left(\frac{K_{Sat}*\phi}{K_{fl}}-1\right)\right\}-\left\{\left(K_{Sat}\left(\frac{\phi K_0}{K_{fl}}+1-\phi\right)-K_0\right)*\left(\frac{\phi_0}{K_{fl}}\right)\right\}}{\left[\frac{\phi K_0}{K_{fl}}+\frac{K_{Sat}}{K_0}-1-\phi\right]^2}$$

Method 2:

The second suggested method to determine relationship between K_{Sat} and φ involves using the Gassmann equation of the form shown below.

$$\frac{K_{Sat}}{K_0-K_{Sat}}=\frac{K^*}{K_0-K*}+\frac{K_f}{\phi(K_0-K_f)}$$

For a specific value of K*, a relationship between K_{Sat} and porosity can be determined by rearranging the above equation to the form

$$K_{Sat}=\frac{C_1+\frac{C_2K_0}{\phi}}{1+C_1+\frac{C_2}{\phi}}$$

where $C1 = \frac{K*}{K_0 - K*}$ and $C2 = \frac{K_f}{\emptyset(K_0 - K_f)}$

K*= Bulk modulus of porous rock frame.

K_f= Bulk modulus of pore fluid

K_0=Bulk modulus of the mineral matrix

An empirical relationship between K_{Sat} and φ can be determined for specific range of K* values that are observed in the well in order to determine the relationship between K_{Sat} and porosity by using a suitable data fitting function. This method would generate several sets of empirical relationships between K_{Sat} and porosity, each for a specific value of K*. While the relationship between K_{Sat} and porosity can be derived for different values of K*, in reality, a specific well may only have few values of K*.

Method 3:

In another method as suggested by Mavko et al., (1995) allows determining relationship between K_{Sat} and porosity using the equations below.

$$\frac{1}{K_{Sat}} = \frac{1}{K_0} + \frac{\phi}{K_{\tilde{\phi}}}$$

where $K_{\tilde{\phi}} = K_{\phi} + \frac{K_0 K_f}{K_0 - K_f}$

K_f= pore fluid bulk modulus

$K_{\tilde{\Phi}}$=dry pore space stiffness

K_0=Bulk modulus of the mineral matrix

The method described above would require availability of core data in order to determine the pore space stiffness parameter. This data was unavailable and hence the method could not be directly applied for this study. Another method described by, Murphy et al. (1993) uses the contact theory to predict that the frame moduli K* and G that are simple functions of porosity and state that the theory predicts that the modulus ratio K*/G is constant between 0.667 and 1.667. The authors base this on contact theory which predicts that as grain contacts grow in size the porosity decreases. The relationship between K* and porosity can be determined if the contact area between individual grains is known. This method presents a unique problem since elastic properties of both matrix and cement along with an estimate of contact area would need to be known priori in order to determine relationship between K* and porosity. Once the relationship between K* and porosity is known it is possible to determine the relationship between K_{Sat} and porosity.

Although there is no need to calculate the error in K* for determining the error in the fluid substituted velocity, the three methods stated here can assist in determining the relationship between K_{Sat} and porosity if it is desired to use the substitution method as suggested by Smith et al. (2003).

6.3.6 Computing error in shear modulus (G)

Calculation of uncertainty in the shear modulus is relatively simple. As described in section 5.6, the shear modulus is calculated using the equation.

$$G = \rho_b * V_S^2 .$$

where

G = Shear modulus in GPa.

ρ_b = Bulk density of the rock (g/cc)

V_s = Shear velocity (Km/sec)

By applying the error propagation equation we get

$$\sigma_G = \sqrt{V_S^2 * \sigma_b^2 + 4 * V_S^2 * \rho_b^2 * \sigma_{Vs}^2}.$$

where

σ_G = RMS error in shear modulus in GPa

σ_{Vs} = RMS error in shear velocity in Km/sec

Throughout the process of fluid substitution the value of shear modulus of the rock (G) is kept constant. However if the value of G is computed from the logging data then an uncertainty associated with the V_s measurement will be propagated to the shear modulus derived from the logging data.

6.3.7 Computing error in fluid substituted bulk density

The paper by Smith et al. (2003) states that the new bulk density can be computed using the standard porosity equation given as $\rho_b = \rho_g(1 - \varphi) + \rho_{fl}\varphi$. I replaced the term ρ_g with apparent grain density as described in section 5.3.7 to account for variation in the bulk density due to the presence of clay. The apparent grain density calculation is shown below.

$$AGD = \frac{(DenMat * (1 - Porosity - Vsh) + DenShale * Vsh}{1 - Porosity}.$$

where

AGD = Apparent grain density (g/cc) or (ρ_g in the standard porosity equation)

DenMat = Matrix grain density (constant - 2.65 g/cc)

Vsh = Volume of shale in fraction

DenShale = Density of dry shale (constant - 2.60 g/cc)

The uncertainty in the apparent grain density is one of the contributors to the error in bulk density. The calculation of the uncertainty in the fluid substituted bulk density would first require determination of uncertainty in parameters such as the apparent grain density and the density of the substituted fluid. For clean rocks (low shale fraction) a single value can be assigned for the matrix density and a reasonable assumption for uncertainty in the value of density of matrix and the density of fluid can be made. For example, an error in matrix density and density of fluid for clean sandstones can be ±0.01 or ±0.02 g/cc respectively unless an alternate uncertainty value is otherwise available. However when the fraction of shale in the rock matrix increases, it becomes difficult to estimate the error in the apparent grain density, since the error parameters such as Vsh, DenShale etc would have to be known priori. Calculating uncertainty in these parameters would then require several assumptions of its uncertainty values and would therefore make the calculation unreliable. I therefore used a constant uncertainty value of ±0.025 g/cc which is the same as the uncertainty in the input density parameter used in this study.

6.3.8 Computing error in fluid substituted velocity

This is the final step in the calculation of uncertainty in the fluid substituted velocity. The P and S velocities have been calculated using the equations stated below.

$$Vp = \sqrt{\frac{K_{Sat2} + \frac{4}{3}G}{\rho_b}} \quad \text{and} \quad Vs = \sqrt{\frac{G}{\rho_b}}$$

All variables in the above equations are considered to be statistically independent and therefore do not require the use of covariance term in the error propagation equation. This parameter independence with respect to data uncertainty is for the purposes of this study. Therefore the error propagation equation can be solved as per equations below.

$$\sigma_{Vp2} = \sqrt{\left(\frac{dV_{P2}}{dK_{Sat2}}\right)^2 * \sigma_{KSat2}^2 + \left(\frac{dV_{P2}}{dG}\right)^2 * \sigma_G^2 + \left(\frac{dV_{P2}}{d\rho_{b2}}\right)^2 * \sigma_{\rho b2}^2}$$

$$\sigma_{Vs2} = \sqrt{\left(\frac{dV_{S2}}{dG}\right)^2 * \sigma_G^2 + \left(\frac{dV_{S2}}{d\rho_{b2}}\right)^2 * \sigma_{\rho b2}^2}$$

where

$$\frac{dV_{P2}}{dK_{Sat2}} = 0.5 * \left(\frac{K_{Sat2} + \frac{4}{3}G}{\rho_{b2}}\right)^{-0.5} * \frac{1}{\rho_{b2}}, \quad \frac{dV_{P2}}{dG} = 0.5 * \left(\frac{K_{Sat2} + \frac{4}{3}G}{\rho_{b2}}\right)^{-0.5} * \frac{4}{3\rho_{b2}},$$

$$\frac{dV_{P2}}{d\rho_{b2}} = -0.5 * \left(\frac{K_{Sat2} + \frac{4}{3}G}{\rho_{b2}}\right)^{-0.5} * \frac{K_{Sat2} + \frac{4}{3}G}{\rho_{b2}^2}$$

and

$$\frac{dV_{S2}}{dG} = 0.5 * \left(\frac{G}{\rho_{b2}}\right)^{-0.5} * \frac{1}{\rho_{b2}}, \quad \frac{dV_{S2}}{d\rho_{b2}} = -0.5 * \left(\frac{G}{\rho_{b2}}\right)^{-0.5} * \frac{G}{\rho_{b2}^2}$$

The terms σ_{KSat2}, σ_G, and $\sigma_{\rho b2}$ represent the uncertainty in the saturated bulk modulus with substituted fluid, uncertainty in the shear modulus and the uncertainty in the bulk density with substituted fluid respectively.

END OF THESIS

References

1. Batzle, M., Wang, Z., 1992, Seismic properties of pore fluids, Geophysics., **57**, 1396-1408.
2. Berryman, J.G, 1999, Tutorial: Origin of Gassmann's equations, Geophysics, **64**,No 5, 1627-1629
3. Berryman, J.G., Milton, G.W., 1991, Exact results for generalized Gassmann's equation in composite porous media with two constituents., Geophysics., **56**, 1950-1960
4. Biot, M.A., 1956, Theory of propagation of elastic waves in fluid saturated porous solid, J. Acoustic Soc. Am, **28**, 168-191
5. Broadhead, M.K., 2005, Aspects of an analytical uncertainty analysis for Gassmann fluid substitution, EAGE 67th conference, P108
6. Castagna, J., 2009, Personal communication
7. Castagna, J., and Backus, M., 1993, Offset Dependent reflectivity - Theory and Practice of AVO analysis, Investigations in Geophysics No.8., published by SEG.
8. Clifford, A.A.,1973, Multivariate Error Analysis, John Wiley and Sons.
9. Doveton, J.,1994, Geologic Log Analysis using Computer Methods: AAPG Computer applications in Geology No 2.
10. Houck, R., 2002, Quantifying the uncertainty in AVO interpretation, Geophysics, **67**, 117-125
11. Knoll, G., 1979, Radiation Detection and Measurement: John Wiley and Sons
12. Knott, C.G., 1899, Reflection and refraction of elastic waves with seismological applications: Philosophical magazine, 5th series, **48**, 64-97
13. Drosg, M., 2007, Dealing with Uncertainties, A Guide to Error Analysis: Springer

14. Gassmann, F., 1951, Uber die Elastizität Poröser Medien:Vier.der Natur.Gesellschaft in Zűrich,96,895-921
15. Mavko, G., Mukerji, T., Dvorkin, J., 2003, The Rock Physics Handbook, Cambridge University Press
16. Hilterman, F.J, 2001, Seismic Amplitude Interpretation, SEG Distinguished Instructor Short Course, No **4**
17. Mollison, R.A., Schon, J.H., Fanini, O.N., 1999, A model for hydrocarbon saturation determination from an orthogonal tensor relationship in thinly laminated anisotropic reservoirs, SPWLA 40th Annual Symposium, Paper **OO**
18. Mollison, R.A., Ragland, T.V., Schon, J.H., Fanini, O.N., Popta, J., 2006, Reconciliation of Waxman-Smits and Juhasz Normalized Qv models from a tensor petrophysical model approach using field data, SPWLA 40th Annual Symposium, Paper OO
19. Ostrander, W.J., 1984, Plane wave reflection coefficients for gas sands at nonnormal angles of incidence, Geophysics, **49**, 1637-1649
20. Paradowski,L.,1997, Uncertainty Ellipses and Their Application to Interval Estimation of Emitter Position, IEEE Transactions on Aerospace and Electronic systems, **33**,No 1
21. Richard, R.A., 1992, An Introduction to Applied Probability, Addison-Wesley
22. Samake, D., Castagna, J., Mahob, P., 2000, Stochastic fluid substitution and seismic modeling, 70th Annual SEG Meeting Expanded Abstracts
23. Seth, S., Wysession, M., 2003, An Introduction to Seismology, Earthquakes and Earth Structure, Blackwell Publishing.
24. Smith, T., Sondergeld, C., Chandra S.Rai.,2003, Gassmann fluid substitutions: A tutorial, Geophysics, **68**, No 2.

25. Theys, P., Log Data Acquisition and Quality Control, 1999, Published by Editions Technip, Second Edition
26. Thomas, E.C., Steiber, S.J., 1975, The distribution of shales in sandstones and its effect upon porosity, SPWLA, 16th Annual Symposium Transactions
27. Thomsen. L., 1988, Reflection seismology over azimuthally anisotropic media, Geophysics, **53**, 304-313.
28. Timm,N., 2002, Applied Multivariate Analysis, Springer
29. Triola, M., 2006, Elementary Statistics, 9th Edition, Pearson Addison Wesley
30. Vernik.L., 2007, Anisotropic correction of sonic logs in wells with large relative dip, Geophysics, **73**, E1-E5.
31. Worthington, P.F., 1985, The Evolution of shaly-sand concepts in reservoir evaluation, The Log Analyst, **26**, No 1, 23-40.
32. Yardley B., Theory of Error, 1958, Addison Wesley
33. Zoeppritz, K., 1919, Erdbebenwellen VIIIB, On the reflection and propagation of seismic waves, Göttinger Nachrichten,I, 66-84